#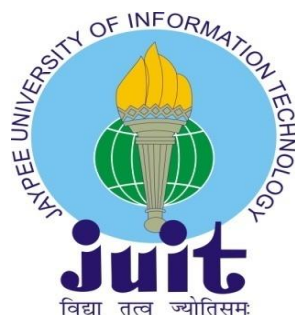 MODULAR DESIGN OF PICROSIDES BIOSYNTHESIS UNRAVELLED THROUGH INTERMEDIATES FLUX DYNAMICS vis-à-vis EXPRESSION ANALYSIS OF PATHWAY GENES IN A MEDICINAL HERB, *Picrorhiza kurroa* Royle ex Benth

Thesis submitted in fulfillment of the requirements for the degree of

DOCTOR OF PHILOSOPHY
IN
BIOTECHNOLOGY

BY
VARUN KUMAR
Enrollment No. 126563

DEPARTMENT OF BIOTECHNOLOGY & BIOINFORMATICS

JAYPEE UNIVERSITY OF INFORMATION TECHNOLOGY

WAKNAGHAT, SOLAN-173234, HP, INDIA

MAY 2017

CERTIFICATE

This is to certify that the thesis entitled, **"Modular design of picrosides biosynthesis unravelled through intermediates flux dynamics vis-à-vis expression analysis of pathway genes in a medicinal herb, *Picrorhiza kurroa* Royle ex Benth"** submitted by **Varun Kumar** to the **Jaypee University of Information Technology, Waknaghat, India** for the award of degree of **Doctor of Philosophy in Biotechnology** is a record of the candidate's own work, carried out by him under my supervision. This work has not been submitted in part or full to any other University or Institute for the award of this or any other degree or diploma.

Supervisor

Date: 01|06|2017

Prof. (Dr.) Rajinder Singh Chauhan

Dean

Department of Biotechnology & Bioinformatics,

Jaypee University of Information Technology,

Waknaghat, Solan-173234, HP, INDIA

Email: rajinder.chauhan@juit.ac.in

IV

DECLARATION

I hereby declare that the work contained in the present PhD thesis entitled **"Modular design of picrosides biosynthesis unravelled through intermediates flux dynamics vis-à-vis expression analysis of pathway genes in a medicinal herb,** *Picrorhiza kurroa* **Royle ex Benth"** submitted at **Jaypee University of Information Technology, Waknaghat, India,** is an authentic record of my original research work, carried out under the supervision of **Dr. Rajinder Singh Chauhan.** This work has not been submitted in part or full for the award of any other degree or diploma in any other university/ Institute.

Signature of the Candidate

Varun Kumar

Enrolment No.:126563

Department of Biotechnology & Bioinformatics,

Jaypee University of Information Technology,

Waknaghat, Solan-173234, HP, INDIA

Date: 01/06/2017

Place: WAKNAGHAT

III

ACKNOWLEDGEMENTS

TABLE OF CONTENTS

LIST OF TABLES

LIST OF FIGURES

	biosynthesis-relevant genes at different time intervals of *P. kurroa* growth; (A) 20 days and, (B) 30 days. The structures were coded with different colors to highlight the genes and steps with important roles in P-I biosynthesis. 1, Glucose; 2, Glucose-6-phosphate; 3, Glyceraldehyde-3-phosphate; 4, Phosphoenolpyruvate; 5, Pyruvate; 6, 6-phosphogluconolactone; 7, Erythrose-4-phosphate; 8, 3-Deoxy-D-arabinoheptulosonate 7-phosphate; 9, Phenylalanine; 10, *trans*-cinnamic acid; 11, Acetyl CoA; 12, Oxaloacetate; 13, Citrate; 14, Isocitrate; 15, α-keto glutarate; 16, Malate; 17, 3-hydroxy-3-methylglutaryl coenzyme A; 18, Mevalonate; 19, Mevalonate phosphate; 20, Mevalonate pyrophosphate; 21, 1-deoxy-D-xylulose-5-phosphate; 22, 2-C-methyl-D-erythritol; 23, 4-(CDP)-2-methyl-D-erythritol; 24, Geranyl pyrophosphate; 25, Geraniol; 26, 10-hydroxy geraniol; 27, Catalpol; A, HK; B, PK; C, G6PDH; D, DAHPS; E, PAL; F, ICDH; G, MDH; H, HMGR; I, PMK; J, DXPS; K, ISPD; L, GS; M, G10H.		
5.2	Influence of different precursors treatment on the fluxes through iridoid/monoterpene and shikimate/phenylpropanoid pathways; (a) CA, (b) CA+CAT, and (c) CAT. The symbols were added and structures were coded with different colors to highlight the effects occurring on the P-I biosynthesis in different treatments. Gene expressions were highlighted with a green circle with arrow pointing up showing up-regulation while a red circle with arrow pointing down showing down-regulation. Orange colored boxes with arrows pointing up and down indicate up-regulation and down-regulation of PAL enzyme, respectively. Red colored loops indicate feedback inhibition effect. Bold arrows indicate the up-regulation of respective steps.	**79**	

	Green colored stars indicate high significant increase.	
5.3	Complete framework of metabolic network depicting P-I and P-II biosynthesis in different tissues of *P. kurroa*. The established routes of P-I and P-II production were presented with different colors to highlight the modulations in shoots and stolons of *P. kurroa*. Up-regulated gene expressions are highlighted with bold and green color.	**82**

LIST OF ABBREVIATIONS

G-6-P	Glucose-6-phosphate
ABA	Abscisic acid
PSY	Pytoene synthase
DHAP	Dihydroxyacetone phosphate
G-3-P	Glyceraldehyde-3-phosphate
SQS	Squalene synthase
OAA	Oxaloacetate
2-PG	2-phosphoglycerate
PEP	Phosphoenolpyruvate
6-PGL	6-phosphogluconolactone
FPP	Farnesyl pyrophosphate
FPPS	Farnesyl pyrophosphate synthase
GGPP	Geranylgeranyl pyrophosphate
GGPPS	Geranylgeranyl pyrophosphate synthase
E-4-P	Erythrose-4-phosphate
DOXP	1-deoxy-D-xylulose-5-phosphate
3-PGA	3-phosphoglycerate
RUBP	Ribulose 1,5-bisphosphate
ENO	Enolase
PDC	Pyruvate dehydrogenase complex
IPP	Isopentenyl pyrophosphate
DSD	Dehydroshikimate dehydratase
DAHP	3-Deoxy-D-arabinoheptulosonate 7-phosphate
PA	Protocatechuate
DHS	3-dehydroshikimate
CHS	Chalcone synthase
Phe	Phenylalanine
CCR	Cinnamoyl CoA reductase
GPP	Geranyl pyrophosphate
VA	Vanillic acid
HK	Hexokinase

TPI	Triosephosphate isomerase
G10H	Geraniol-10-hydroxylase
GS	Geraniol synthase
TCA	Tricarboxylic acid
HMGR	Hydroxymethylglutaryl-CoA reductase
GPPS	Geranyl pyrophosphate synthase
FA	Ferulic acid
F5H	Ferulic acid-5-hydroxylase
5HFA	5-hydroxyferulic acid
4CL	4-coumarate CoA ligase
BA	Benzoic acid
HADH	3-hydroxyacyl CoA dehydrogenase
CMT	Caffeic acid-3-O methyltransferase
ADT	Arogenate dehydratase
PAL	Phenylalanine ammonia lyase
DXPS	1-deoxy-D-xylulose-5-phosphate synthase
p-CA	*p*-coumaric acid
TDC	Tyrosine decarboxylase
C4H	Cinnamic acid-4-hydroxylase
CM	Chorismate mutase
PPA-AT	Prephenate aminotransferase
P-I	Picroside-I
P-II	Picroside-II
CA	*trans*-cinnamic acid
AS	Anthranilate synthase
DAHPS	3-Deoxy-D-arabinoheptulosonate 7-phosphate synthase
Trp	Tryptophan
ADH	Arogenate dehydrogenase
SD	Shikimate dehydrogenase
Tyr	Tyrosine
10HG	10-hydroxygeraniol
PK	Pyruvate kinase

ICDH	Isocitrate dehydrogenase
MDH	Malate dehydrogenase
AKG	α-keto glutarate
G6PDH	Glucose-6-phosphate dehydrogenase
MVA	Mevalonate
MEP	Methyl erythritol phosphate
qRT-PCR	Quantitative Real Time Polymerase Chain Reaction
DMAPP	Dimethylallyl pyrophosphate
NGS	Next Generation Sequencing
KEGG	Kyoto Encyclopedia of Genes and Genomes
DXPR	1-deoxy-D-xylulose-5-phosphate reductoisomerase
ISPD	4-diphosphocytidyl-2C-methyl-D-erythritol synthase
ISPE	4-diphosphocytidyl-2C-methyl-D-erythritol kinase
MECPS	2-C-methyl-D-erythritol 2,4-cyclopyrophosphate synthase
HDS	1-hydroxy-2-methyl 2-(E)-butenyl-4-pyrophosphate synthase
ISPH	1-hydroxy-2-methyl 2-(E)-butenyl-4-pyrophosphate reductase
IPPI	Isopentenyl pyrophosphate delta-isomerase
HMGS	Hydroxymethylglutaryl-CoA synthase
PMK	Phosphomevalonate kinase
MVK	Mevalonate kinase
PMD	Diphosphomevalonate decarboxylase
DQS	Dehydroquinate synthase
SK	Shikimate kinase
DQD	Dehydroquinate dehydratase
EPSPS	5-enolpyruvylshikimate-3-phosphate synthase
SQM	Squalene monooxygenase
TAT	Tyrosine aminotransferase
UPD	Uroporphyrinogen decarboxylase
UGD	Uridine diphosphate glucuronic acid decarboxylase
ACT	Anthocyanin acyltransferase
ALD	Aldehyde dehydrogenase
APD	Arogenate/Prephenate dehydratase

CPM	Cytochrome P450 monooxygenase
F3D	Flavanone 3-dioxygenase
2HFD	2-hydroxyisoflavanone dehydratase
DCH	Deacetoxycephalosporin-C hydroxylase
CHA	Chalcone
PCA	Principal Component Analysis
PCC	Pearson's Correlation Coefficient
cDNA	Complementary DNA
FPKM	Fragments Per Kilobase Per Million
DGE	Differential Gene Expression
BSA	Bovine Serum Albumin
PMSF	Phenylmethane sulfonyl fluoride
LDH	Lactate dehydrogenase
ADP	Adenosine diphosphate
ATP	Adenosine triphosphate
NAD^+/NADH	Nicotinamide adenine dinucleotide
NADPH/$NADP^+$	Nicotinamide adenine dinucleotide phosphate
ME	Malic enzyme
BHT	Butylated hydroxytoluene
UV	Ultraviolet
TFA	Trifluoroacetic acid
RT	Room Temperature
HPLC	High Performance Liquid Chromatography
CAT	Catalpol
KN	Kinetin
IBA	Indole-3-butyric acid
C18 column	Octadecyl carbon chain (C18)-bonded silica
PKS	*Picrorhiza kurroa* shoots
PKR	*Picrorhiza kurroa* roots
PKST	*Picrorhiza kurroa* stolons

ABSTRACT

Picroside-I (P-I) and Picroside-II (P-II) are the iridoid glycosides in *Picrorhiza kurroa* having therapeutic potential against numerous neurological and hepatic disorders. These are also used as active ingredients in various commercial herbal drugs formulations available for the treatment of liver ailments. P-I and P-II are biosynthesized in a tissue specific manner i.e. shoots synthesize P-I, roots produce P-II and stolons/rhizomes produce both P-I and P-II. Nevertheless, mass propagation of *P. kurroa* shoots through *in vitro* culture has been optimized but with lower yields of only P-I. In contrast, P-II was not detected in *P. kurroa* plants grown *in vitro*. Thus, to enhance the contents of P-I and P-II in tissue specific manner in *P. kurroa*, it is a necessity to engineer metabolic carbon flux towards picrosides production. However, metabolic engineering of picrosides production remains a challenge considering the fact that biosynthetic architecture of picrosides is complex and non-linear with poorly understood fluxes dynamics. Consequently, it is hard to decide a particular strategy for enhancing the contents of P-I and P-II in *P. kurroa* through metabolic engineering. Therefore, in this research work, we have applied metabolic flux analysis to elucidate the mechanism behind P-I and P-II biosynthesis in *P. kurroa*. To address this, the interconnections between primary and secondary metabolism for enhanced P-I production were investigated on the basis of temporal effects on expression patterns of genes catalyzing rate limiting steps in both primary and secondary metabolic pathways. The results revealed associations of *DXPS*, *PMK*, *HMGR*, *ISPD* and *HK* genes with P-I content for the first 20 days of *P. kurroa* growth at $15°C$ *in vitro*, whereas *G10H* and *DAHPS* showed highest expression levels in 30 days grown shoots where the P-I content was also maximum. This indicates that *G10H* (iridoid pathway) and *DAHPS* (shikimate/phenylpropanoid pathway) act in conjunction for increased P-I production in *P. kurroa*. Further, the *in vitro* feeding of cinnamic acid (CA) and catalpol (CAT); the immediate biosynthetic precursors of P-I produced from shikimate/phenylpropanoid and iridoid pathways, respectively, showed 4.2-fold increase in P-I production. This analysis confirmed that CA and CAT stimulated the production of P-I due to synergistic effect. Moreover, from the results of elucidation of metabolic basis of the P-I production, it was concluded that both CA+CAT stimulated P-I biosynthesis while their individual feeding limited P-I production due to feedback inhibition effect.

The investigation of metabolic basis of P-II biosynthesis on the other hand, faced challenges since it was not produced in *P. kurroa* plants grown *in vitro* which was a major impediment in elucidating the biosynthetic route of P-II. Therefore, in this study, we have utilized natural variation for P-II content in stolon tissues of different *P. kurroa* accessions and deciphered its metabolic route by integrating metabolomics of intermediates with differential NGS transcriptomes. Upon navigating through high *vs* low P-II content accessions (1.3-2.6%), we have established that P-II is biosynthesized *via.* degradation of ferulic acid to produce vanillic acid which acts as its immediate biosynthetic precursor. Moreover, the ferulic acid treatment *in vitro* at 150 μM concentration provided further confirmation with 2-fold increase in vanillic acid content. Interestingly, the cross-talk between different tissues of *P. kurroa* i.e. shoots and stolons, resolved spatial complexity of P-II biosynthesis and consequently speculated the burgeoning necessity to bridge gap between vanillic acid and P-II production in *P. kurroa* shoots. This work thus, offers a forward looking strategy to enhance contents of P-I and P-II in tissue specific manner so as to provide a sustainable production platform for these medicinal compounds vis-à-vis relieving pressure from natural habitat of *P. kurroa*.

INTRODUCTION

Picrorhiza kurroa Royle ex Benth, locally known as Kutki or Karu, is a medicinal herb included in the family Plantaginaceae (earlier recognised as Scrophulariaceae). It is found in the high altitude regions (3000-5000 m) of North-Western Himalayas [1]. From ancient times, *P. kurroa* has been used as a traditional medicine by local communities for the treatment of respiratory, allergic, stomach and liver disorders because of its bioactivities such as hepatoprotective [2], antioxidative [3], anti-allergic [4], anti-asthmatic [4], anti-cancerous [5] and immunomodulatory activity [6]. The pharmacological potential of *P. kurroa* is ascribed to the presence of two iridoid glycosides i.e. picroside-I (P-I) and picroside-II (P-II). In *P. kurroa*, picrosides (P-I and P-II) are biosynthesized in a tissue specific manner i.e. shoots synthesize P-I, roots produce P-II and stolons/rhizomes produce both P-I and P-II [7]. Therefore, mature stolons/rhizomes of *P. kurroa* (which contained both P-I and P-II) are used as an ingredient in various herbal drug formulations such as katuki, arogya, livocare, vimliv and livplus, available in the market for treatment of liver disorders [2, 7].

Among numerous medicinal herbs existing in India, *P. kurroa* is registered as one of the top 15 with respect to revenues generated by the traded material. The consumption and demand of *P. kurroa* by herbal drug industries has reached to 415 MT/year which is ~40 times higher as compared to its requirement in 1990 [8]. This figure gives only a sign of its consumption as most of its collection and trade is illegal from wild/natural sources, the major resource base of *P. kurroa*. The extensive and unorganized collection of *P. kurroa* raised serious socio-economic concerns among farmers, herbal industries and policy makers due to its reduced population in the natural habitat. *P. kurroa* propagates vegetatively in natural habitat where it arises in the form of a young bud on mature stolons which subsequently produce a complete plant with roots, shoots and stolons (Figure 1.1). Therefore, during illegal procurement and lack of knowledge on harvesting, complete plants get uprooted and then rhizomes are separated and sold in the market while rest of the plant material is thrown away. This has resulted in the loss of young buds which arouse on the mature stolons thereby obstructing its propagation in wild. Owing to a heavy extraction of *P. kurroa* from wild (entire Himalayan range), it is listed

in the "Negative List of Export (GOI), Appendix II of Cities, Red Data Book of Indian Plants and Prioritized List of Medicinal Plants for Conservation" by International Union for Conservation of Nature, IUCN [9].

Figure 1.1. Growth and development stages of *P. kurroa*

The imposition of legal restrictions on the collection of raw material from wild led to the adulteration of *P. kurroa* which has reduced its quality in terms of active constituents composition i.e. P-I and P-II thereby posing concerns over the efficacy of resulting herbal drugs. One such poor quality herbal raw material of *P. kurroa* from China is sold in the markets of India at a cost of Rs 700 per Kg compared to Rs 350 per Kg from H.P., with ~4 times lower levels of total P-I and P-II [10].

Therefore, there is an urgent need to develop mass production platform for quality herbal raw material of *P. kurroa* with improved levels of major chemical constituents i.e. P-I and P-II. Nevertheless, mass propagation of *P. kurroa* shoots through *in vitro* culture has been optimized but with lower yields of P-I [11]. Moreover, various strategies have also been employed to enhance P-I content in *P. kurroa* shoot cultures including optimization of media compositions and use of various elicitors (methyl jasmonate, abscisic acid, sodium nitroprusside and seaweed extract), but P-I level in tissue cultured grown *P. kurroa* shoots was ~4-5 times less as compared to plants grown in natural habitat [11-13]. Moreover, P-II has not been produced in *P. kurroa* plants grown *in vitro* [7]. Therefore, it would be of paramount importance if P-II can be produced in shoots, which will not only relieve pressure from natural habitat of *P. kurroa* for uprooting rhizomes/roots but will also provide a continuous supply of herbal raw material through shoot cultures with desired levels of P-I and P-II.

Therefore, the engineering of metabolic carbon flux towards picrosides production is the only sustainable way to improve the quality of *P. kurroa*. However, non-existence of thorough knowledge on biosynthetic machineries of P-I and P-II and associated key steps in *P. kurroa* have precluded implementing any genetic intervention strategy either towards the production of quality herbal raw material and/or developing their alternate production technologies.

The proposed biosynthetic pathways for P-I and P-II include non-mevalonate (MEP), mevalonate (MVA), shikimate/phenylpropanoid and iridoid pathways [14]. Moreover, key/candidate genes associated with the biosynthesis of P-I and P-II have also been shortlisted through various genomic approaches [15-16]. However, metabolic engineering of picrosides production remains a challenge considering the fact that biosynthetic architecture of picrosides is complex and non-linear with poorly understood fluxes dynamics. Till date, no information is available on what mechanism controls the flux of P-I and P-II biosynthesis in *P. kurroa* and which out of the different modules are limiting for their supply? Further, why P-II is not produced in *P. kurroa* shoots and how it is produced in stolons? It is, therefore, crucial to understand the mechanism behind P-I and P-II biosynthesis in *P. kurroa* prior to designing a suitable metabolic engineering approach.

In previous studies, the secondary metabolic pathways (MVA, MEP, iridoid/monoterpene and shikimate/phenylpropanoid) have only been taken into consideration for P-I and P-II biosynthesis in *P. kurroa* [14-16]. Since secondary metabolism gets stimulus from primary metabolic precursors for their activation, therefore, integration of both primary and secondary metabolic pathways must be executed to understand complete biosynthesis of picrosides in *P. kurroa*. However, it further poses a challenge to shortlist key steps involved in both primary and secondary metabolic pathways with respect to picrosides content. To address this, tracking transcripts levels through quantitative real time polymerase chain reaction (qRT-PCR) has become a prime focus in modern molecular biology [17]. The qRT-PCR has been preferred as it can determine precise changes in expression levels of genes between different tested conditions with high accuracy and sensitivity [18].

The mechanism controlling secondary metabolites biosynthesis has been elucidated through radioactive/stable isotopes labelled metabolic flux analysis in various plant species [19-20] but concurrently accompanied with cost intensive and time consuming experiments [21]. Conversely, the exogenous feeding of key intermediate metabolites as precursors in tissue culture conditions has been reported to trigger the biosynthesis of target secondary metabolites *in vivo* [22]. For example, tryptamine and loganin supplied as exogenous precursors in transgenic cell lines of *Catharanthus roseus* have been reported to increase the secologanin levels along with metabolic flux determination through the pathway intermediates [23]. In addition, the exogenous feeding of tryptamine, tryptophan, geraniol, loganin and 10-hydroxygeraniol in hairy root cultures of *C. roseus* not only increased the accumulation of indole alkaloids but also determined the metabolic flux limitations in their biosynthesis [24].

Therefore, we fed different precursors in *P. kurroa* shoot cultures to elucidate the mechanism behind P-I biosynthesis. Despite the potential of precursor feeding in the elucidation of metabolic routes of P-I production, this is not yet applicable for P-II biosynthesis as P-II has not been produced under *in vitro* conditions. Therefore, it is a challenge to resolve the complexity of P-II biosynthesis as both protocatechuate and ferulic acid (the metabolites of shikimate/phenylpropanoid pathway) are plausible to produce vanillic acid, the immediate precursor of P-II (Figure 1.2) [14, 25].

4
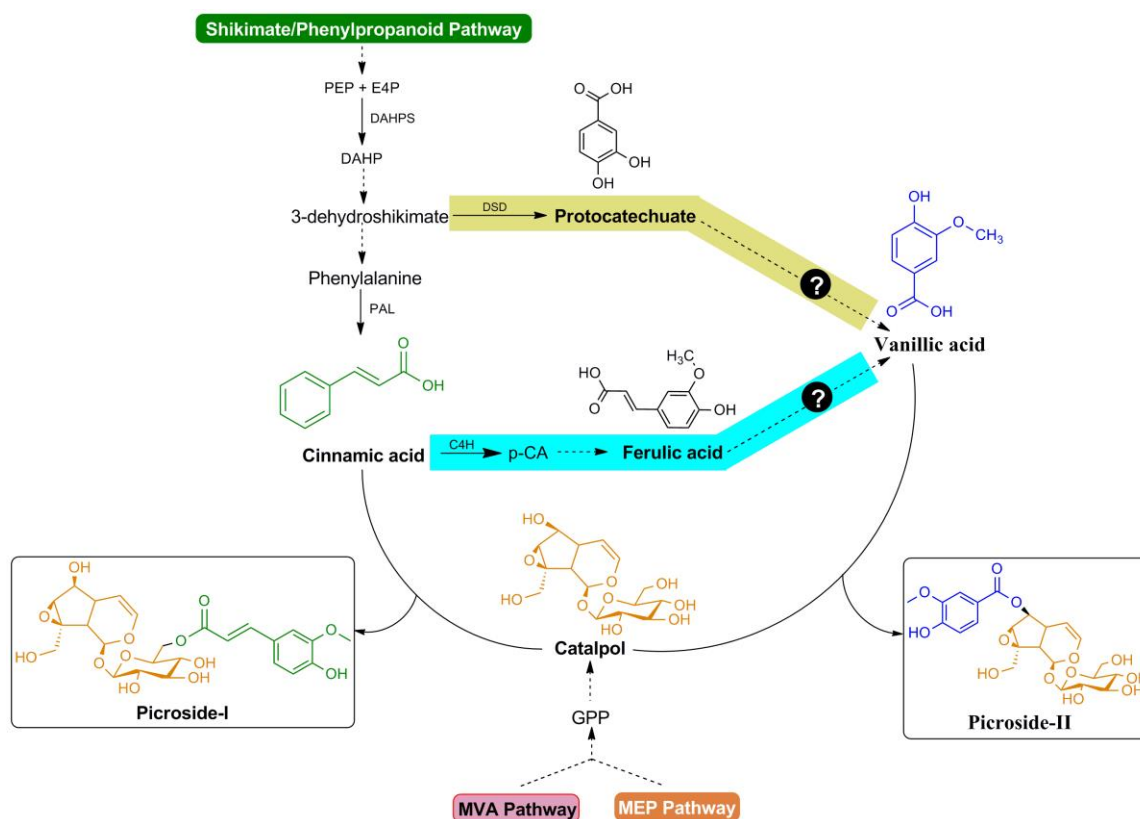
Figure 1.2. Modular design of P-I and P-II biosynthetic pathways. The structures of P-I and P-II are linked to cinnamic acid/vanillic acid (green/blue color) moieties and catalpol (orange color). Question marks indicate plausible routes for vanillic acid production.

The mature stolons were proposed to be the independent biosynthetic organs as evident by the analysis of P-I and P-II contents in different developmental stages of *P. kurroa* [7]. Therefore, we have selected mature stolons to elucidate the mechanism controlling P-II biosynthesis in *P. kurroa*. We have utilized natural variations in P-II content among different accessions of *P. kurroa* so as to guide us in discerning the route and flux of intermediates leading to the P-II biosynthesis. Moreover, the integration of metabolites contents data with the corresponding transcriptomes would enable us to understand the flux of intermediates vis-à-vis gene transcripts controlling P-II biosynthesis in *P. kurroa*. The natural variants of medicinal herbs for target secondary metabolites have not been previously employed directly for the elucidation of biosynthetic pathways. However, natural variations were exploited to elucidate genetic control of glucosinolate production in Arabidopsis [26]. In addition, metabolomics using MS/MS mapped natural variations in *N. attenuata* populations and guided herbivory-induced variations in secondary metabolism [27]. This is the first study which utilized natural variations of picrosides production to elucidate their biosynthetic routes in *P. kurroa*.

Therefore, in the light of immense need to elucidate contributions of different modules in picrosides biosynthesis to enable their future rational metabolic engineering in *P. kurroa*, the present research work was designed with the following objectives:

- Elucidation of connecting links between primary and secondary metabolism in the context of picrosides biosynthesis in *P. kurroa*

- Elucidation of key steps contributing to P-I biosynthesis through intermediates flux dynamics in *P. kurroa*

- Elucidation of metabolic route and associated key steps for P-II biosynthesis in *P. kurroa*

REVIEW OF LITERATURE

Picrorhiza kurroa is a critically endangered medicinal herb which has been utilized in the formulation of various herbal drugs commercially used for the treatment of liver ailments. The pharmacological importance of this herb is ascribed to the exhibition of diverse iridoid glycosides fraction. Considering the enormous bioactivities of iridoid glycosides from *P. kurroa*, it is essential to perform an exhaustive compilation of research published on this herb in the past years. It could provide useful insights into the areas which are yet to be explored. Therefore, in this section, we have summarised the existing knowledge on major iridoid glycosides from *P. kurroa*, their commercial herbal drug formulations, pharmacological activities, and current status of biosynthetic machinery.

2.1. Prevalence of liver infections and mortality rates – WHO latest statistics in Indian perspective

The incidences of chronic liver disorders are rising throughout the world and have also been seen in India irrespective of sex, race and age. Liver diseases are considered to be silent killers as persons wouldn't realize about this problem until it becomes serious. Liver cirrhosis is an end result of various liver diseases which in worst conditions affects the functioning of liver by increasing resistance to blood flow through the liver. Globally, the cirrhosis of liver is caused by alcohol consumption, non-alcoholic fatty liver and viral hepatitis. The non-alcoholic fatty liver disease can be further caused due to accumulation of fats or Non-Alcoholic Steato-Hepatitis (NASH), a condition in which liver cells face fat accumulation, inflammation and damage. Dr S.H. Kayamkhani, a gastroenterologist, said that "*Alcohol abuse continues to cause maximum cases of liver cirrhosis. But in recent years, viral hepatitis infections as well as non-alcoholic fatty liver disease (NAFLD) associated with diabetes, obesity and sedentary lifestyle too are on the rise*". According to the latest data published by WHO (World Health Organization), 216,865 deaths occur in India due to liver diseases which is 2.44% of the total deaths caused (http://www.worldlifeexpectancy.com/india-liver-disease).

2.2. Drugs used for the treatment of liver disorders – rise of market for herbal remedies

Over the years, synthetic and recombinant drugs *viz.* corticosteroids and interferons, have been used for the treatment of various liver disorders but simultaneously associated with harmful side effects including; agitation, depression, retinal ischemia, anxiety and nephrotic syndrome [28]. Therefore, plant based remedies came into spotlight for the treatment of liver disorders. The various herbal drugs such as colchicine, glycyrrhizin, silymarin and curcumin were obtained from medicinal plants and are considered as potent hepatoprotective agents [28]. Among these herbal drugs, high doses of colchicine induced toxic effects and therefore, prescribed at very low doses [29]. Further, the majority of reports showed association of curcumin with the treatment of liver cirrhosis but only a limited number of researchers have suggested its role in the prevention of virus induced hepatic injury [28]. In contrast, glycyrrhizin has been reported to be effective against chronic hepatitis [28]. However, silymarin has been considered as one of the favored drugs for the treatment of liver disorders; though, simultaneous screening of other medicinal herbs revealed *P. kurroa* based herbal drugs to be highly effective against various liver disorders [1]. The herbal drugs prepared from the *P. kurroa* are commercially available in the market and the demand of raw material has raised to 415 MT/year which is ~40 times higher as compared to its requirement in 1990 [8]. The list of herbal drugs prepared from *P. kurroa* is provided in Table 2.1.

Table 2.1. Commercial herbal drugs formulations from *Picrorhiza kurroa* [30]

S. No.	Herbal drug	Manufacturer
1	Arogya	Zhandu Pharma Works Ltd., Vapi, Gujarat
2	Katuki	Zhandu Pharma Works Ltd., Mumbai
3	Livocare	Dindayal Aushdi Pvt. Ltd., Gwalior
4	Kutaki	Tansukh Herbal Pvt. Ltd., Lucknow
5	Livomap	Maharishi Ayurveda Pvt. Ltd., New Delhi
6	Livplus	BACFO Pharmaceuticals Ltd., Noida
7	Livomyn	Charka Pharma Pvt. Ltd., Mumbai
8	Vimliv	OM Pharma Ltd., Bangalore
9	Pravekliv	Pravek Kalp Herbal Products Pvt. Ltd., Noida

2.3. Chemical constituents of *P. kurroa* with pharmacological potential

The two main chemical constituents (picrosides-I and II) of *P. kurroa*, reported as major bioactive compounds, are tamed in this section to overview their pharmacological potential. The bioactivities of individual compounds are listed in Table 2.2 and explained in the following sections:

Table 2.2. Bioactivities of P-I and P-II from *Picrorhiza kurroa*

S. No.	Treatments	Conc. of active compound	Model used	Iridoid glycoside	Reference
1	Neuritogenesis	60 μM	*In vitro*	P-I; P-II	[31-32]
2	Anticancer	5 μM and 10 μM	*In vitro*	P-I	[33]
3	Neuroprotective	10 mg/kg intravenously at 2 h ischemia before reperfusion 22 h	*In vivo*	P-II	[34-35]
		20 mg/kg, intraperitoneally at ischemia 1.5 h	*In vivo*		[36]
		10-20 mg/kg, intraperitoneally at ischemia 1.5-2 h	*In vivo*		[37]
		10 mg/kg, intraperitoneally at ischemia 1.5-2 h	*In vivo*		[38]
		20 mg/kg, intraperitoneally at ischemia 2 h	*In vivo*		[39]
4	Hepatoprotective	5, 10, 20 mg/kg for 7 days, intragastrically	*In vivo*	P-II	[40-41]
		12 mg/kg for 7 days, oral	*In vivo*	P-I	[2]
5	Hypoxia/reoxygenation induced cardiomyocytes injury	50-200 μg/ml for 48 h	*In vitro*	P-II	[42-43]
6	Myocardial ischemia reperfusion injury	1 μM, 10 μM and 100 μM	*In vitro*	P-II	[44]
7	Hind limb ischemia reperfusion injury	10 mg/kg, intraperitoneally 30 min before ischemia	*In vivo*	P-II	[45]
8	Renal ischemia reperfusion injury	10 mg/kg, through tail vein at the end of the 45 min of ischemia and prior to reperfusion	*In vivo*	P-II	[46]

2.3.1. Picroside-I

P-I is an iridoid glycoside obtained from *P. kurroa* which has been reported to prevent Alzheimer's disease by inducing neurite outgrowth, a phenomenon known as neuritogenesis. The neurites outgrowth has been stimulated from PC12D cells (a cell line derived from rat pheochromocytoma) in the presence of nerve growth factor [31] and other neuritogenic substances including staurosporine, basic fibroblast growth factor and dibutyryl cyclic AMP [32]. The application of both P-I and P-II in a concentration dependent manner *viz.* >0.1 μM activated these neuritogenic substances and consequently prevented the loss of neurons through their enhanced differentiation leading to the cure of neurodegenerative disorders [31-32].

The P-I has also been documented to treat hepatic injuries induced by D-galactosamine in rats. The administration of P-I for 7 days at a concentration of 12 mg/kg per day significantly inhibited the D-galactosamine induced accumulation of phospholipids and lipid peroxides along with acid phosphatase activity in liver possibly due to its antioxidant effect [2]. Moreover, the anticancer potential of P-I was revealed by inhibited migration of a breast cancer cell line i.e. MCF-7 upon its introduction at a concentration of 5 μM and 10 μM *in vitro* [33].

2.3.2. Picroside-II

P-II, an iridoid glycoside obtained from *P. kurroa*, has been reported to prevent various disorders including hepatic injuries, ischemia reperfusion injury, cardiomyocytes injury and asthma (Table 2.2). The potential of P-II in the treatment of hepatic disorders was revealed by Gao and Zhou [40] who observed elevated levels of superoxide dismutase and glutathione peroxidase activities (known as antioxidant enzymes) upon administration of different doses of P-II for 7 days at a concentration of 5, 10 and 20 mg/kg per day in rat models with induced liver damage by treatment of D-galactosamine, acetaminophen and carbon tetrachloride. This study suggested that prevention of hepatotoxicity by P-II might be due to its antioxidative effect. Further, this was confirmed by Gao and Zhou [41] who showed that administration of P-II at a concentration of 10 mg/kg caused reduction of malonic dialdehyde levels and up-regulated superoxide dismutase activity in rat liver along with increased expression levels of *bcl-2* gene. The elevated levels of *bcl-2* gene play a critical role in resistance to hepatocyte apoptosis.

Further, the prevention of various ischemic reperfusion injuries such as hind limb, renal, myocardial and cerebral was also observed after treatment with P-II. In hind limb ischemia reperfusion injury, reduced deformability of erythrocytes has been observed but the administration of P-II at a concentration of 10 mg/kg maintained the erythrocytes deformability during the injury [45]. In contrast, renal ischemia reperfusion injury was characterized by reduced expressions of *caspase-3* and *bcl-2* genes, while *poly (ADP-ribose) polymerase-1* and *Bax* genes got up-regulated. These genes are involved in apoptosis induced by the injury and *in vivo* treatment with P-II at a concentration of 10 mg/kg significantly inhibited the modulations occurred in these genes and thereby prevented the apoptosis [46]. The role of P-II in the prevention of myocardial ischemia reperfusion injury was explored by Wu et al. [44]. This study showed that *in vitro* treatment with P-II up-regulated nitric oxide levels, *bcl-2* gene expression and phosphoinositide 3-kinase/Akt/endothelial NOS pathway to prevent apoptosis induced by myocardial ischemia reperfusion injury (Table 2.2). Further, the neuroprotective potential of P-II was investigated against cerebral ischemia reperfusion injury by observing its influence on apoptosis of neurons, oxidative stress and inflammation. Li et al. [35] showed reduced expressions of (ADP-ribose) polymerase-1 and caspase-3 proteins after P-II treatment which indicated the prevention of neuronal apoptosis. However, Guo et al. [34] observed that P-II treatment significantly reduced expression levels of nuclear transcription factor κB, toll-like receptor 4 and tumor necrosis factor α to induce anti-inflammatory effect and subsequently inhibited the neuronal apoptosis. Later on, down-regulation of ERK1/2 (extracellular signal regulated kinase) pathway upon P-II treatment was observed to be the reason behind reduced neuronal apoptosis [39]. Moreover, the dose and time of P-II treatment were optimized for their neuroprotective effects and maximum response was observed with administration of P-II at a concentration of 20 mg/kg body weight at 1.5 h ischemia [36]. Further, Liu et al. [38] and Zhao et al. [37] observed maximum therapeutic effect against cerebral ischemia reperfusion injury after P-II injection with a dose of 10 mg/kg body weight at 1.5-2.0 h ischemia and 10-20 mg/kg body weight at 1.5-2.0 h ischemia, respectively.

The administration of P-II has also been reported to prevent hypoxia/reoxygenation injury induced by oxidative stress. Meng et al. [42] revealed that P-II treatment significantly reduced the levels of reactive oxygen species by stimulating antioxidant response through up-regulation of superoxide dismutase and glutathione peroxidase activities which

prevented the cardiomyocytes from oxidative stress induced hypoxia/reoxygenation injury. Further, it has been observed that P-II treatment prevented apoptosis induced by hypoxia/reoxygenation injury through up-regulation of CREB (cAMP response element-binding protein) and PI3K/Akt, pathways along with bcl-2 expression in cardiomyocytes [43].

2.4. Biosynthesis of iridoid glycosides in *P. kurroa*

Iridoid glycosides constitute one of the classes of natural products in *Picrorhiza* genus that may serve roles in plant defence and communication. These are simply monoterpenes i.e. C_{10} compounds, which are biosynthesized from 10-oxogeranial through the formation of iridoid ring in iridodial. The reaction was catalyzed by an enzyme, iridoid synthase [47]. The attachment of glucose moiety to these iridoids leads to the formation of iridoid glycosides. In *P. kurroa*, various iridoid glycosides have been reported in addition to picrosides as shown in Figure 2.1. Among all iridoid glycosides fraction, picrosides constitute the major portion with pharmacological potential and therefore, the biosynthetic machinery of picrosides needs to be comprehended in *P. kurroa*.

2.4.1. Picrosides biosynthesis architecture

Picrosides (P-I, P-II, P-III and P-IV) along with other iridoid glycosides such as, kutkoside and 6-feruloylcatalpol, are biosynthesised from catalpol; a basic skeletal backbone required for their formation. The esterification of catalpol backbone with different aromatic acids (CA, VA, FA, p-CA and caffeic acid) at one of the three positions i.e. group 1 (R1), group 2 (R2) and group 3 (R3) leads to the formation of picrosides and other iridoid glycosides as shown in Figure 2.2. Among various iridoid glycosides present in *P. kurroa*, only the biosynthesis of P-I and P-II has been well studied, which is perhaps due to the fact that herbal drugs derived from *P. kurroa* contain both P-I and P-II as major active constituents [7]. The complete biosynthetic pathway leading to the formation of P-I and P-II has been recently deciphered by using a retro-biosynthetic approach in which different pathways were assembled and optimized progressively from earlier to later steps supported by literature survey and fragmentation or dissecting the parent compound (Figure 2.2) [14].
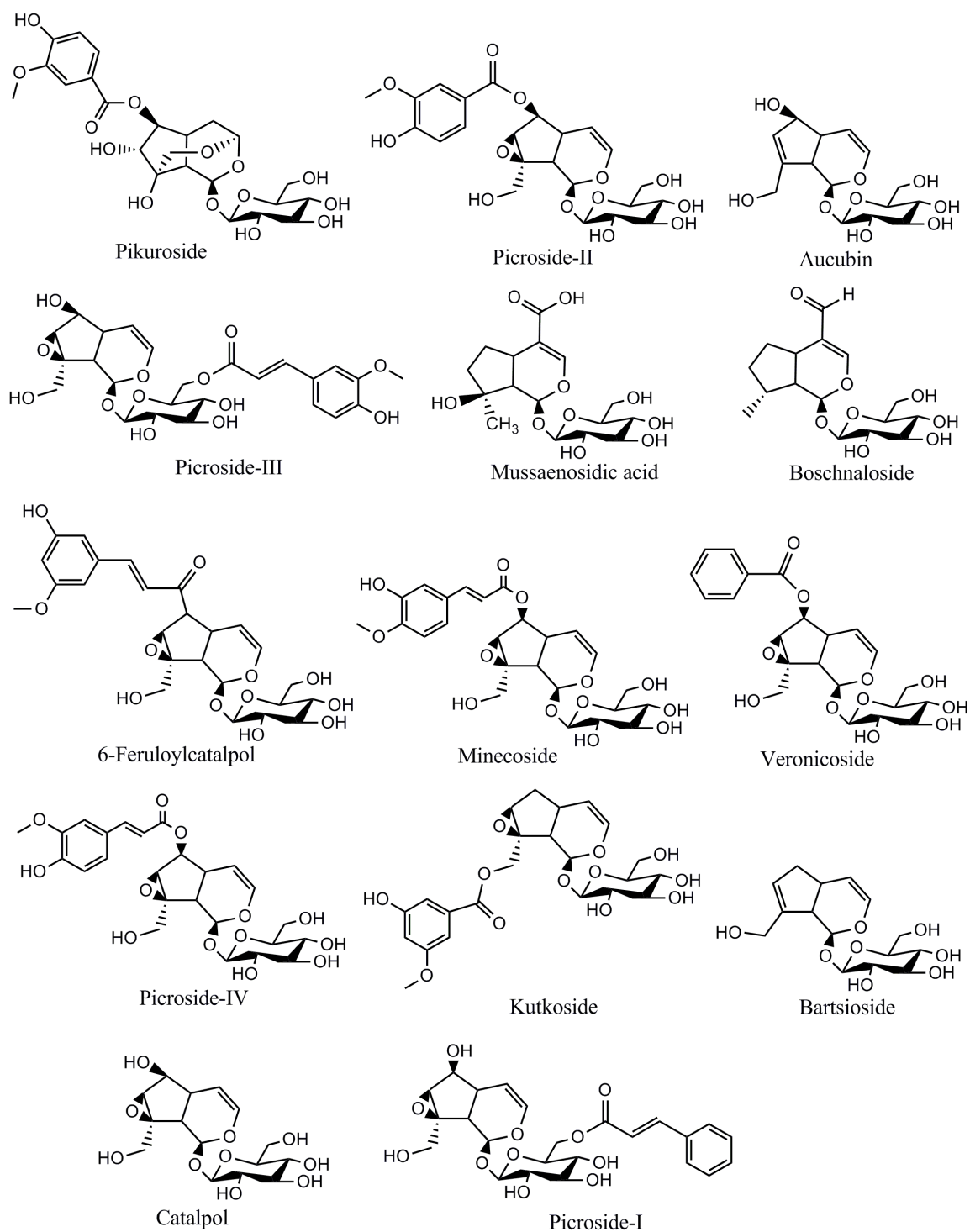
Figure 2.1. Iridoid glycosides present in *P. kurroa*

Pikuroside

Picroside-II

Aucubin

Picroside-III

Mussaenosidic acid

Boschnaloside

6-Feruloylcatalpol

Minecoside

Veronicoside

Picroside-IV

Kutkoside

Bartsioside

Catalpol

Picroside-I
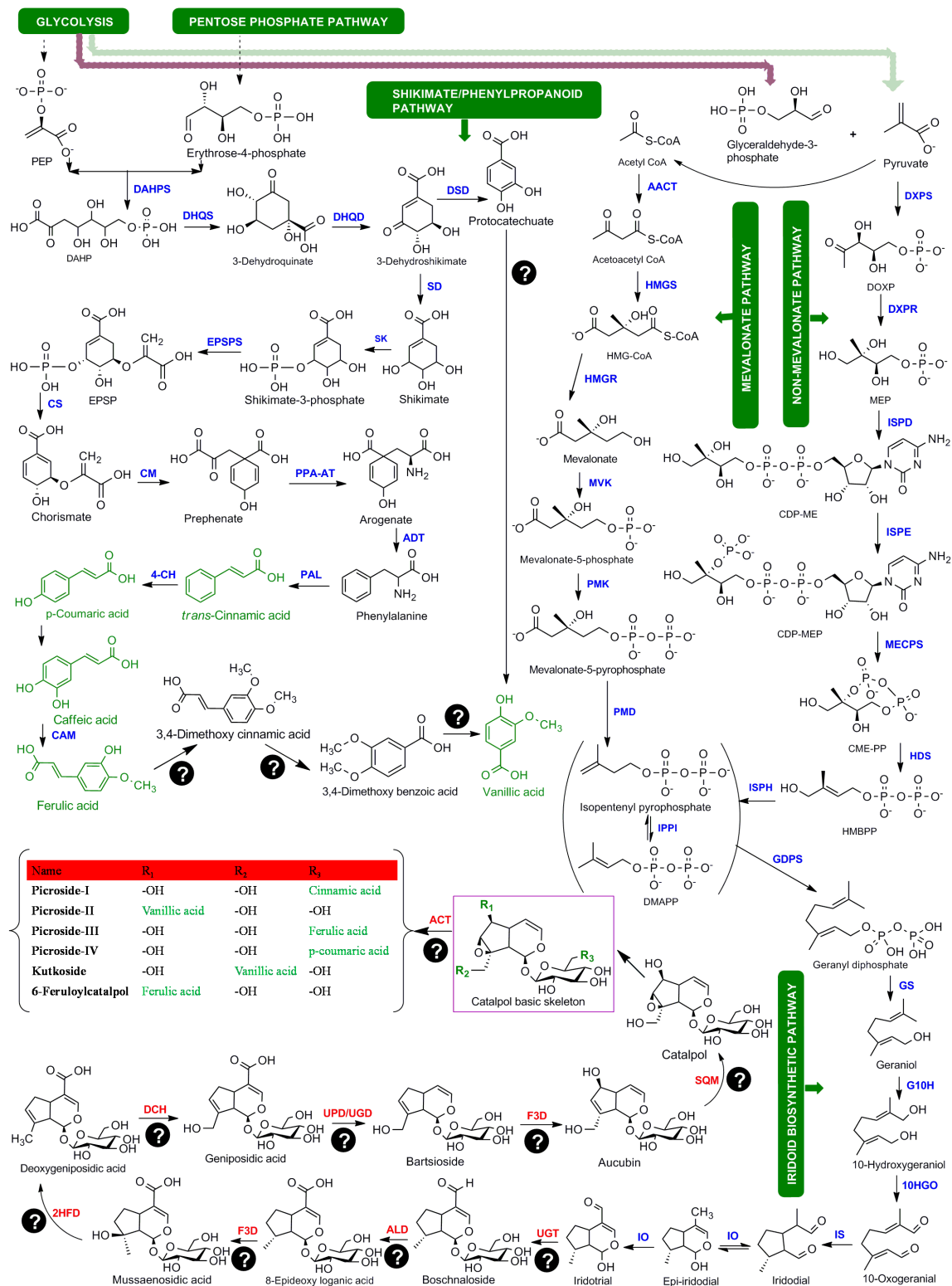
Figure 2.2. Biosynthesis of iridoid glycosides in *P. kurroa*. The metabolic network has been reconstructed including MVA/MEP, shikimate/phenylpropanoid and iridoid pathways. Single and multiple steps are represented with solid and dotted arrows, respectively. Question marks indicate proposed enzymes which are yet to be validated [14, 16].

It has been proposed that the biosynthesis of both P-I and P-II starts with mevalonate and non-mevalonate pathways, which are also considered as common pathways for terpenoid biosynthesis [48]. The mevalonate pathway which occurs in cytosol was discovered in 1950s. It is also known as MVA pathway and involves six reactions starting from acetyl CoA to finally produce isopentenyl pyrophosphate (IPP), a C5 compound acts as a precursor for terpenes biosynthesis [49]. In addition, the non-mevalonate pathway has been recently discovered in 1990s and occurs in plastids [50]. It is also known as MEP or DXS pathway and provides an alternative route for production of IPP and dimethylallyl pyrophosphate (DMAPP); an allelic isomer of IPP [51]. The MEP pathway involves a series of seven enzyme catalyzed reactions and originates with the formation of 1-deoxy-D-xylulose 5-phosphate (DXS) from pyruvate and glyceraldehyde 3-phosphate. The reaction is catalyzed by an enzyme, 1-deoxy-D-xylulose 5-phosphate synthase (DXPS) [52]. The IPP produced from both MVA and MEP pathways fuses with DMAPP to produce geranyl pyrophosphate (GPP), the starting compound for the formation of monoterpenes. Beyond GPP, the P-I and P-II are biosynthesised *via.* monoterpene biosynthesis/Iridoid pathway [14].

The first reaction of monoterpene biosynthesis i.e. formation of geraniol from dephosphorylation of GPP, is catalyzed by the enzyme geraniol synthase [53]. The geraniol is then hydroxylated through geraniol-10-hydroxylase and the reaction product i.e. 10-hydroxygeraniol is further converted to 10-oxogeranial in a reaction catalyzed by 10-hydroxygeraniol oxidoreductase [54-55]. The 10-oxogeranial then undergoes subsequent reduction and cyclization to form iridoid ring in iridodial followed by the conversion to iridotrial. The reactions are catalyzed by iridoid synthase and iridoid oxidase, respectively [47, 56]. The next steps of iridoid pathway involve glucosylation, hydroxylation, dehydration, decarboxylation, epoxidation and esterification reactions (Figure 2.2). The biosynthesis of 8-epi-deoxyloganic acid from iridotrial was reported by Isabel and Kaplan [57]. Damtoft et al. [58] showed that catalpol was synthesised from aucubin on the basis of high incorporation from 8-epi-deoxyloganic acid through a series of intermediates in *Scrophularia* (family; Scrophulariaceae). Nevertheless, enzyme information for these biosynthetic steps have been proposed on the basis of reaction types and groups transfer followed by gene expression analysis vis-à-vis picrosides content, but these steps are yet to be characterized at enzyme level [16, 59]. Further, the proposed biosynthetic route of P-I and P-II i.e. iridoid pathway was also validated through

15

detection of five intermediate metabolites i.e. boschnaloside, bartsioside, mussaenosidic acid, aucubin and catalpol, in *P. kurroa* by using LC/ESI-MS/MS method [14]. Therefore, catalpol biosynthesis included a total of 14 steps after GPP followed by one additional step which involved the esterification of catalpol and aromatic acids from shikimate/phenylpropanoid pathway as shown in Figure 2.2.

For P-I biosynthesis, *trans*-cinnamic acid has been proposed to modify catalpol and the former is known to be biosynthesized *via.* shikimate/phenylpropanoid pathway [14]. The shikimate/phenylpropanoid pathway originates with the formation of 3-Deoxy-D-arabinoheptulosonate 7-phosphate (DAHPS) from erythrose-4-phosphate and phosphoenolpyruvate by an enzyme, 3-Deoxy-D-arabinoheptulosonate 7-phosphate synthase (DAHPS) and produced *trans*-cinnamic acid through a series of eleven enzyme catalyzed reactions [1]. The formation of *trans*-cinnamic acid is catalyzed by phenylalanine ammonia lyase, which utilizes phenylalanine as a substrate [60]. In contrast to P-I, P-II is proposed to be biosynthesized *via.* esterification of catalpol with vanillic acid [14]. In *P. kurroa*, vanillic acid has been proposed to be produced by two different routes, first is the transformation of protocatechuic acid to vanillic acid [14], and second is through transformation of ferulic acid to vanillic acid [25]. However, none of the proposed routes for vanillic acid biosynthesis has been confirmed as yet in *P. kurroa*.

2.4.2. Strategies used for shortlisting key/candidate genes involved in picrosides biosynthesis

The complete biosynthetic pathway for P-I and P-II involves four integrating pathways; MVA, MEP, shikimate/phenylpropanoid and iridoid/monoterpene pathways in *P. kurroa* [14]. Therefore, a total of 42 and 48 steps are proposed to be involved in the biosynthesis of P-I and P-II, respectively [14, 16]. To shortlist key/candidate genes/enzymes involved in the biosynthesis of P-I and P-II, combination of approaches were used in the past as outlined in Figure 2.3 and described in the following sections.
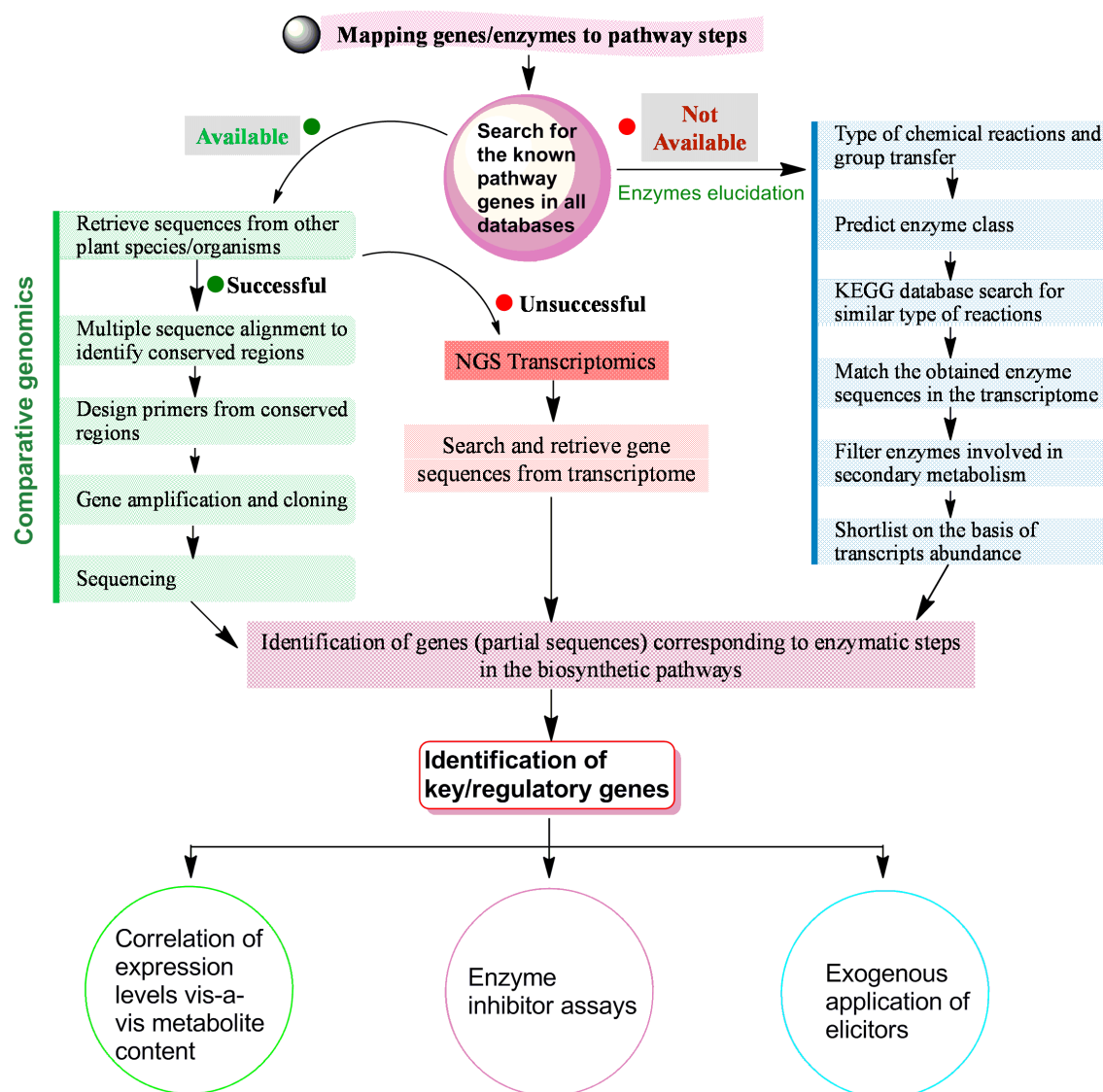
Figure 2.3. Overview of strategies used for the shortlisting of key picrosides biosynthetic genes in *P. kurroa*.

2.4.2.1. Comparative genomics and differential NGS transcriptomics

Comparative genomics refers to the comparison of genome characteristics of different organisms/species. In *P. kurroa*, genes/enzymes, which are involved in the biosynthesis of picrosides and also catalyzing similar enzymatic reactions in other plant species, were retrieved and the corresponding genes were cloned through comparative genomics approach. Pandit et al. [15] cloned two genes of MVA pathway i.e. *HMGS* and *PMK*, while three genes of MEP pathway *viz. MECPS*, *HDS* and *ISPD*, in *P. kurroa*. Moreover, the expression analysis of all 15 genes belonging to MVA/MEP pathways vis-à-vis P-I and P-II contents in *P. kurroa* revealed 57-166-fold up-regulation of *PMK*, *DXPS*, *ISPE*,

17

MECPS and *ISPD* vis-à-vis P-I content, while increased expression of *DXPR* and *HDS* with ~9-12-fold was observed in congruence with P-II content [15]. This study showed that the genes up-regulated with respect to P-I and P-II contents belong to MEP pathway, except *PMK* which belongs to MVA pathway, thereby indicating the major role of MEP pathway in picrosides biosynthesis. Nevertheless, comparative genomics approach has been successfully employed to shortlist key genes in MVA/MEP pathways, but it is limited to only conserved and known pathway steps. Therefore, genes/enzymes information for most of the enzymatic steps has been obtained through generating and mining NGS transcriptomes from differential content phenotypes of *P. kurroa*. In previous studies, a total of six transcriptome datasets were generated from differential picrosides content phenotypes of *P. kurroa* i.e. shoot tissues grown in field (2.7% P-I) as well as *in vitro* at 15°C (0.6% P-I) and 25°C (0.01% P-I); root tissues grown in field (0.4% P-II) and *in vitro* at 25°C (P-II not produced); and stolons of field grown plants with 1.7% P-I and 0.99% P-II contents [16, 25]. These differential transcriptomes provided greater insights not only into the genes involved in biosynthetic pathways but also molecular mechanisms that regulate the contents of picrosides in *P. kurroa*. The partial gene sequences for majority of pathway genes obtained from NGS transcriptomes were retrieved, validated and associated with the contents of picrosides through qRT-PCR on differential content phenotypes. The expression analysis of picrosides biosynthetic pathway genes was carried out between *P. kurroa* plants collected from field and those grown *in vitro* [16]. This analysis has shortlisted 19 genes of MVA/MEP, shikimate/phenylpropanoid and iridoid/monoterpene pathways *viz. HMGS*, *HMGR*, *PMK*, *MVK*, *MVDD*, *GDS*, *DXPS*, *ISPD*, *ISPE*, *MECPS*, *HDS*, *ISPH*, *DQS*, *TAT*, *GS*, *UPD*, *DCH*, *SQM* and *2HFD* which showed higher expression levels vis-à-vis P-I content in *P. kurroa* [16]. In contrast, 7 genes of shikimate/phenylpropanoid and iridoid/monoterpene pathways *viz. SK*, *EPSPS*, *PAL*, *DQD*, *QSD*, *ACT* and *F3D* showed higher expression levels vis-à-vis P-II content; while *CAM*, *UGD*, *CPM*, *CM*, *APD*, *ALD* and *G10H* genes showed higher transcript levels vis-à-vis both P-I and P-II contents [16]. Moreover, the expression levels of all these shortlisted genes were also tested between high *vs* low picrosides contents accessions (genotypes) of *P. kurroa* i.e. PKS-1 (2.7% P-I) and PKS-4 (0.3% P-I); which further reduced the number of candidate genes important for P-I production to seven i.e. *SK*, *EPSPS*, *ISPD*, *DXPS*, *2HFD*, *ISPE* and *PMK* [16]. However, the shortlisting with respect to P-II content was not performed between *P. kurroa*

18

accessions as P-II is not detected in the shoots [16]. Though these studies provided key genes which might be playing a critical role in picrosides biosynthesis but lack in discerning the interconnections among different pathways channelling intermediates into picrosides biosynthesis in *P. kurroa*.

2.4.2.2. Exogenous application of different inhibitors and elicitors

The key/candidate genes for picrosides biosynthesis were also shortlisted through addition of various inhibitors and elicitors into the culture media in order to observe their effects on P-I production in *P. kurroa*. A study conducted by Shitiz et al. [16] revealed that inhibition of MEP pathway with fosmidomycin (an inhibitor of DXPR enzyme) reduced P-I content by 90% which was much higher as compared to mevinolin (an inhibitor of HMGR enzyme) that reduced P-I by only ~12%. The expression analysis of *DXPR* and *ISPD* genes showed reduced levels in shoots treated with fosmidomycin when compared to untreated control shoots, which indicated that MEP pathway contributes more towards P-I biosynthesis and DXPR and ISPD catalyzed the possible rate limiting steps. Moreover, the exogenous application of various elicitors *viz.* seaweed extract, hydrogen peroxide, abscisic acid and sodium nitroprusside significantly increased P-I content *in vitro* [13, 61]. Further, the expression analysis of genes in samples treated with hydrogen peroxide and abscisic acid revealed up-regulation of *PkDXS*, *PkIPPI* and *PkHDR* genes involved in MEP pathway [61]; while seaweed extract and sodium nitroprusside up-regulated the genes of both MVA and MEP pathways for increased P-I production [13]. Though the key genes involved in P-I biosynthesis have been shortlisted by using elicitors yet this approach is not suitable to understand the mechanism behind the *in vivo* production of P-I. The reason is that elicitors would not directly stimulate the production of target secondary metabolites but rather are known to activate the transcription factors which might influence the global expression of biosynthetic pathway genes [62].

2.5. Methods employed for the elucidation of metabolic fluxes in various plant species

Metabolic flux is referred as the rate at which molecules are converted to products in a biochemical pathway. In case of specialized plant metabolites, since multiple pathways contribute to their biosynthesis, it is necessary to decipher metabolic flux through

individual pathways, modules or the intermediates to engineer biosynthesis of a target metabolite. To determine the metabolic flux through a pathway, various approaches used in other plant species are described in the following sections:

2.5.1. Radiotracer approach

In this approach, a metabolite which acts as a precursor to target secondary metabolite is labelled with stable or radioactive isotopes and then isotope signatures are traced in the intermediates and end metabolites [63]. This approach has been considered as one of the most effective method to elucidate biosynthetic pathways in plants and other organisms. Glawischnig et al. [64] reported that biosynthesis of camalexin proceeded *via.* tryptophan rather glucosinolates in *Arabidopsis thaliana* through use of ^{14}C labelled tracers. Moreover, the feeding of deuterium labelled phenylalanine i.e. ^{2}H$_5$-Phe to the petals of *Petunia hybrida* showed benzyl benzoate as an intermediate metabolite in the benzoic acid biosynthesis from L-Phenylalanine [65]. The biosynthetic route of steviol precursors was also deciphered through ^{13}C- labelled glucose and established that it proceeded *via.* MEP pathway in plastids of *Stevia rebaudiana* [66]. Further, Gallage et al. [67] revealed that vanillin was formed in *Vanilla planifolia* from ferulic acid as demonstrated by the administration of ^{14}C- radiolabelled phenylalanine and cinnamic acid to the developing pods. Recently, the flux of TCA cycle towards ethylene production was revealed through the analysis with ^{13}C isotope tracer coupled with liquid chromatography mass spectrometry (LC-MS) in cyanobacteria [20]. Though this approach delivered huge success in the deciphering of plant secondary metabolic pathways yet the reports on quantitative metabolic flux analysis by using this approach are scarce. This approach is complicated considering the experimental design, introduction of tracer, complexity in evaluation of generated data, cost intensive and time consuming experiments [21, 63]. Moreover, due to the complexity of plant metabolomes, and occurrence of large number of structurally unidentified metabolites relying only on metabolomics for metabolic flux analysis, is rather unconventional [68].

2.5.2. Precursor feeding

Precursor feeding is an approach in which various compounds, which act as intermediate metabolic precursors for target secondary metabolites, have been supplied to the culture media in order to observe their effect either on the production of target metabolites or to

determine the flux through respective pathways. This approach is only applicable if the endogenous level of supplied precursors is a limiting factor for the biosynthesis of target secondary metabolites [22]. *In vitro* feeding of phenylalanine has been reported to stimulate the production of taxol in *Taxus cuspidata* cultures [69]. Further, the increased accumulation of vanillin was observed in *Vanilla planifolia* cultures after exogenous treatment with ferulic acid [70]. The elevated accumulation of monoterpenoids i.e. nerol and citronellol was observed after feeding rose cell cultures with a precursor, geraniol [71]. Moreover, the exogenous feeding of tryptophan, tryptamine, geraniol, 10-hydroxygeraniol and loganin in hairy root cultures of *C. roseus* not only increased the accumulation of indole alkaloids, but also determined the metabolic flux limitations in their biosynthesis [24]. These studies established precursor feeding as a reliable method to determine metabolic fluxes leading to the biosynthesis of target secondary metabolites but must be supplemented with transcripts/proteins datasets in order to perform exhaustive flux analysis.

2.6. Natural variants for pathways discovery and cloning genes

Deciphering of biosynthetic pathways for plant secondary metabolites is a highly cumbersome process considering the complexity of their genetic architecture and low levels of metabolic intermediates and corresponding enzymes catalyzing the steps *in planta* [72]. Moreover, the secondary metabolites are mostly synthesized in a tissue specific manner [73-74] which further add complications in elucidation of their biosynthetic routes and associated genes information. With the advent of modern high throughput technologies such as transcriptomics, proteomics and metabolomics, it became comparatively easier to get insight into molecular mechanisms underlying the biosynthesis of target secondary metabolites [75]. However, these technologies fail to explain the genetic control of secondary metabolic pathways. Therefore, the utilization of genetic diversity existing in a plant species, for the production of secondary metabolites, has become a revolutionary approach to track target secondary metabolites biosynthesis through the use of omics [76].

One such example was the identification of an enzyme, salutaridine reductase, from *Papaver somniferum* that catalyzed intermediate step in the biosynthesis of morphine [77]. This study has investigated the correlations between alkaloids and genes expression patterns among sixteen *Papaver* species and one expressed sequence tag out of 2000 up-

regulated in relation to morphine accumulation was then functionally characterized and identified as a novel salutaridine reductase [77]. Further, the accumulation of glucosinolate was observed among 39 ecotypes of *Arabidopsis*, which revealed that 5 polymorphic loci were responsible for generating 14 different glucosinolate profiles in leaves of *Arabidopsis* [26]. A study conducted by Mönchgesang et al. [78] showed the integration of metabolomics and genomics data of 19 genetically different accessions of *A. thaliana* root exudates which revealed polymorphic genetic clustering of coding sequences. In addition, metabolomics using MS/MS mapped natural variations in *Nicotiana attenuata* populations and guided herbivory-induced variations in secondary metabolism [27].

Though natural variants have been successfully used for the elucidation of biosynthetic genes yet these have not been utilized till date for the elucidation of biosynthetic routes leading to the production of target secondary metabolites.

The review of literature has thus opened up following research gaps in the biosynthetic routes of P-I and P-II in *P. kurroa*:

- Interconnections between primary and secondary metabolic pathways are not explored for picrosides biosynthesis in *P. kurroa*

- Partial knowledge available on the biosynthetic route of P-II in *P. kurroa*

- Lack of knowledge on mechanisms controlling biosynthesis of P-I and P-II in *P. kurroa*

MATERIALS AND METHODS

3.1. Collection of plant material

The field grown plants along with 10 accessions (genotypes) of one year old *P. kurroa* were collected from nursery established in Jagatsukh, H.P. (2193 m, altitude; $32^{°}12'0N$ and $77^{°}12'0E$) and established in the greenhouse of Jaypee University of Information Technology, Waknaghat, H.P., India ($31^{°}0'58.55"$ N and $77^{°}4'12.63"$ E; 1700 m, altitude). The details of *P. kurroa* accessions are provided in Table 3.1. The plants maintained in greenhouse were harvested, washed with tap water, and segregated into shoots, mature stolons and roots. The shoots were coded with PKS and mature stolons with PKST whereas roots were labelled as PKR. All the samples were stored at $-80^{°}C$ for their use in further experiments.

Table 3.1. Details of *P. kurroa* accessions collected from different geographic locations of North-Western Himalayas, India [30]

S. No.	Accession	Location/District	Altitude	Latitude	Longitude
1	PK-1	Hudan Bhatori/Chamba	3620	33006'27.1" N	76029'171.1" E
2	PK-2	Bhuri/Kinnaur	3330	31030'01.3" N	78056'34.5" E
3	PK-3	Dhel/Kullu	3597	31045.412" N	77027.680" E
4	PK-4	Teita/Chamba	3590	32°31'28" N	76°31'01" E
5	PK-5	Moral Danda/Shimla	3354	31018'23.6" N	77045'02.1" E
6	PK-14	Yungpa/Kinnaur	3440	34040'5.1" N	78001'12.0" E
7	PK-16	Salam Tith/Chamba	3440	33059.142" N	77011.173" E
8	PK-18	Sural Bhatori/Chamba	3323	33008'41.6" N	76027'49.4" E
9	PK-21	Pattal/Chamba	3245	32057.321" N	76018.417" E
10	PK-26	Shringul Tung/Shimla	3307	32°14'59" N	78°06'48" E

3.2. *In vitro* culturing of *P. kurroa* shoots

The shoot apices of field grown *P. kurroa* plants were nicked and surface sterilized with 0.1% mercuric chloride ($HgCl_2$) in the presence of a fungicide i.e. bavistin (0.5%). The shoot apices were then thoroughly washed (4-5 times) with sterile distilled water and aseptically cultured in flasks containing optimized Murashige and Skoog (MS) medium

[79] appended with 3 and 1mg/L indole 3-butyric acid (IBA) and kinetin (KN), respectively. These flasks were kept at $25\pm1^{\circ}$C (this temperature does not support the production of P-I) in a chamber maintained for tissue culture of plants by providing a 16h photoperiod through 3000 lux, cool white fluorescent light. The cultures were allowed to grow for 30 days at $25\pm1^{\circ}$C. The shoot apices of these cultured plants were used as explants which were cultured and kept in a plant tissue culture chamber maintained at $15\pm1^{\circ}$C (a temperature condition which supports the production of P-I) as reported by Sood and Chauhan [11]. The shoot apices left after culturing were stored at -80°C and labelled as zero day sample. The *in vitro* grown *P. kurroa* shoot samples at $15\pm1^{\circ}$C were then collected at different time intervals (10, 20, 30 and 40 days) of plant growth. For each time interval, shoot samples were collected from three independent flasks and immediately stored at -80°C for the estimation of picrosides and gene expression analyses.

3.3. Precursors feeding experiments

3.3.1. Precursors added *in vitro* for their effects on P-I biosynthesis

The effect of supplementation of two compounds *viz.* cinnamic acid (CA) and catalpol (CAT), considered as the immediate biosynthetic precursors of P-I, in the culture medium was investigated on P-I biosynthesis in *P. kurroa* shoot cultures grown *in vitro*. The stock solutions of three different concentrations of CA (70, 150 and 230 µM) and CAT (30, 70 and 150 µM) were prepared using water (HPLC grade; Merck, USA) along with absolute methanol (used to completely dissolve all the aqueous stocks). In addition, neutral aqueous stock solutions were also prepared from different combinations of CA+CAT i.e. 70 µM CA+30 µM CAT, 150 µM CA+70 µM CAT and 230 µM CA+150 µM CAT. All these aqueous stocks solutions were sterilized by using 0.22 µm syringe filter (Millipore) and added into the culture tubes (three tubes for each treatment) containing optimized MS medium appended with IBA and KN in the ratio of 3:1. The *P. kurroa* shoot cultures already established at $25\pm1^{\circ}$C *in vitro* were used as explant (having negligible P-I content) which were cultured in tubes containing the above prepared media followed by their incubation at $15\pm1^{\circ}$C in a plant tissue culture chamber (temperature that supports P-I production). The shoot cultures of *P. kurroa* kept at $15\pm1^{\circ}$C without the addition of precursors were considered as controls. The *in vitro* culturing for each precursor treatment was carried out in triplicates. The shoots were collected from each treatment as

well as control tubes after 30 days of growth and immediately stored at -80°C for further analyses.

3.3.2. Precursors added *in vitro* for their effects on P-II biosynthesis

The solutions of different precursors including *p*-coumaric acid (p-CA), protocatechuate (PA) and ferulic acid (FA) (Sigma-Aldrich, USA) were prepared as neutral aqueous stocks at 150 µM concentrations. Conversely, 150 µM aqueous solution of vanillic acid (VA) (Sigma-Aldrich, USA) was mixed with 70 µM CAT (Sigma-Aldrich, USA) and used for the feeding of *in vitro* grown *P. kurroa* shoots. These concentrations were selected based on their effects on P-I production in *P. kurroa* when applied alone and in combination under tissue culture conditions as mentioned above. Following this, the solutions of different precursors were added into the culture tubes containing optimized MS medium (containing 3 mg/L IBA and 1 mg/L KN) after filter sterilization through 0.22 µm syringe filter (Millipore). In each culture tube, the shoot explant of *P. kurroa* grown at 25±1°C (having negligible P-I content) was aseptically transferred and all the cultures were kept in a plant tissue culture chamber maintained at 15±1°C (this temperature favours P-I production). The *P. kurroa* shoots without the precursor treatment were referred to as controls. The precursor feeding experiment was executed in triplicates. The sampling of shoots was performed after 30 days of growth and instantly kept at -80°C for further analyses.

3.3.2.1. Culturing of *P. kurroa* shoots grown *in vitro* with different concentrations of VA+CAT mixture and P-II

The effect of different concentrations of VA+CAT mixture *viz.* 25 µM VA+25 µM CAT, 70 µM VA+70 µM CAT, 70 µM VA+150 µM CAT, 150 µM VA+150 µM CAT and 230 µM VA+230 µM CAT was also determined on P-II content in shoot cultures fed with p-CA, PA, FA and VA+CAT (150+70 µM). Moreover, P-II at a concentration of 25 µM was also introduced separately in the MS medium to check the accumulation of P-II in *P. kurroa* shoots. The culturing of *P. kurroa* shoots was performed in triplicates according to the same protocol as mentioned above. The untreated shoots were labelled as controls. The harvesting of shoots was performed after 30 days and immediately kept at -80°C for the analysis of P-I and P-II contents.

3.3.2.2. Treatment of *in vitro* grown *P. kurroa* shoots with VA+CAT mixture and P-II under liquid culture conditions

The solutions of VA+CAT mixture and P-II were prepared at concentrations of 70 μM (each of VA+CAT) and 25 μM, respectively to check the intake of precursors by the plant. These solutions were then incorporated into the culture tubes having optimized liquid MS medium (containing 3 mg/L IBA and 1 mg/L KN) after filter sterilization through 0.22 μm syringe filter (Millipore). The culturing of *P. kurroa* shoots was performed in triplicates under the same conditions as mentioned above. The untreated shoots were labelled as controls. The harvesting of shoots was performed after 30 days and straightway kept at -80°C for further analyses. The analysis of VA and P-II contents was performed in both shoots and liquid media left after the harvesting and carried out in triplicates.

3.4. Extraction and quantification of picrosides

Each sample was weighed to 100 mg and homogenized in a prechilled mortar and pestle with liquid nitrogen. To each homogenized sample, 10 mL of 80% methanol was added and samples were vortexed for 10 min at room temperature (RT). The samples were then allowed to stand at RT for overnight followed by centrifugation at 10,000 rpm for 15 min. The supernatants were collected and filtered through 0.22 μm filter (Millipore). Each filtered sample was then diluted 10-fold with 80% methanol and used for the quantification of P-I and P-II through HPLC. We have used reverse phase HPLC (Waters 515) system containing C18 column (4.6×250 mm, 5 μm) and photodiode array detector (PDA; Waters 2996) for the separation of compounds. The mobile phase was made up of distilled H_2O, methanol (Merck, USA) and acetonitrile (Merck, USA) in the ratio of 70:15:15, respectively. To the mobile phase, 0.03% trifluoroacetic acid (TFA) was added and used for the isocratic elution from column at a flow rate of 1.0 mL min^{-1}. The injection volume was 20 μL and cycle time of HPLC analysis was 30 min at 30°C. The picrosides were detected at a wavelength of 280 nm and identified by comparing their retention time and UV spectra with authentic P-I and P-II standards (ChromaDex).

3.5. Extraction and quantification of intermediate metabolites in shikimate/ phenylpropanoid pathway

The samples were subjected to extraction of intermediate metabolites *viz.* CA, p-CA, FA, PA and VA. The extraction was performed as per the method described in Mattila and Kumpulainen [80] with some modifications. The samples (200mg each) were weighed and homogenized with liquid N_2 in prechilled pestle and mortar. To each homogenized sample, 7 mL of a mixture of methanol (containing 2g/L butylated hydroxytoluene, BHT) and 10% acetic acid in a ratio of 85:15 was added and vortexed for 10 min at room temperature (25°C). The volume of each extract was made up to 10 mL with distilled water and mixed properly. Each extract was then transferred to 100 mL reagent bottle and suspended with 12 mL of distilled water and 5 mL of 10M sodium hydroxide. The extracts were then bubbled with N_2 gas, sealed and kept on a magnetic stirrer for overnight at room temperature. On the following day, the pH of extracts was adjusted to 2.0 with concentrated hydrochloric acid. The metabolites released in the solution were then extracted three times with 15 mL of a mixture of cold diethyl ether and ethyl acetate in a ratio of 1:1 by shaking and centrifuging for 10 min at 7000 rpm and 4°C. The diethyl ether/ethyl acetate layers thus obtained were evaporated in rotary evaporator to dryness and reconstituted in 1.5 mL of absolute methanol. The reconstituted samples were passed through 0.22 μm filter (Millipore) and subjected to quantification of selected metabolites by using reverse phase HPLC as per the method described by Nour et al. [81]. The HPLC system (Waters 515) was equipped with C18 column (4.6×250 mm, 5 μm) and photodiode array detector (PDA; Waters 2996). The gradient elution was used for separation of compounds with 1% acetic acid solution in distilled water (mobile phase A) and absolute methanol (mobile phase B) according to the programme as follows: isocratic 90% A/10% B, 0-27 min; linear gradient from 90% A/10% B to 60% A/40% B, 27-28 min; isocratic 60% A/40% B, 28-33 min; linear gradient from 60% A/40% B to 56% A/44% B, 33-35 min; isocratic 56% A/44% B, 35-43 min; linear gradient from 56% A/44% B to 90% A/10% B, 43-44 min and isocratic 90% A/10% B, 44-48 min. The flow rate of mobile phase was adjusted to 1.0 mL min^{-1}. The injection volume was 10 μL and the selected compounds *viz.* CA, p-CA and FA were detected at a wavelength of 290±4 nm, 310±4 nm and 330±4 nm, respectively while PA and VA were detected at a wavelength of 260±4 nm. All the selected compounds were identified through comparison of their retention time and UV spectra with authentic standards (Sigma-Aldrich, USA). The extraction and quantification experiments were performed in triplicates.

3.6. Extraction and determination of enzyme activities

3.6.1. Hexokinase (HK)

For extraction of HK, one gram of each sample was weighed and homogenized with liquid N_2 in a prechilled mortar and pestle followed by addition of 5 mL of 0.1 M Tris-Cl buffer (pH 7.5) containing magnesium chloride, 5 mM; Triton X-100, 1%; β-mercaptoethanol, 50 mM; sucrose, 50 mM and polyvinylpyrrolidone (insoluble), 1% (*w/v*). The homogenized samples were then centrifuged for 30 min at 10,000xg and $4°C$. The supernatant of each sample was collected and dialyzed for overnight at $4°C$ against extraction buffer diluted ~10-fold with distilled water and without polyvinylpyrrolidone. On the following day, each dialyzed sample was centrifuged for 20 min at 10,000xg and $4°C$. The supernatant was collected and labelled as crude extract for determination of HK activity. The extraction of HK from each sample was performed in triplicates.

HK enzyme activity was determined using a coupled assay as shown in Figure 3.1. The total volume of reaction mixture prepared for the estimation of HK activity was 3.0 mL. It contained 50 mM Tris-Cl buffer (pH 7.5), magnesium chloride (5 mM), glucose (5 mM), $NADP^+$ (1 mM), ATP (2.5 mM), 2.25 U of glucose-6-phosphate dehydrogenase and 200 μL of crude extract. The reaction was initiated by ATP addition at $30°C$ in a water bath and increase in absorbance at 340 nm per 30s was recorded in a UV-VIS spectrophotometer. The activity of HK enzyme was expressed as μmol $NADP^+$ reduced min^{-1} at 340 nm under the specified conditions. The assay for HK enzyme was performed in triplicates.
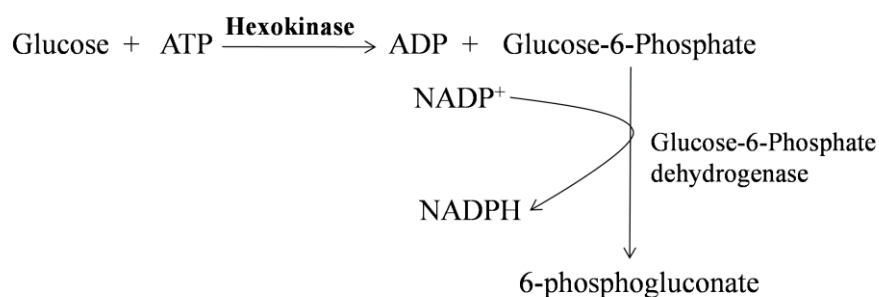
Figure 3.1. Principle of coupled assay for the determination of HK activity

3.6.2. Pyruvate kinase (PK)

One gram of each sample was weighed and homogenized with liquid N_2 in a prechilled mortar and pestle. For the extraction of PK, 5 mL of 0.05 M Tris-Cl buffer (pH 7.5)

containing magnesium sulphate, 10 mM; β-mercaptoethanol, 5 mM; ethylene glycol, 20% (*v/v*); and polyvinylpyrrolidone (insoluble), 1% (*w/v*) was added. The homogenized samples were centrifuged for 30 min at 10,000xg and 4°C. The supernatant of each sample was collected and dialyzed for overnight at 4°C against the extraction buffer diluted ~10-fold with distilled water and without polyvinylpyrrolidone. On the following day, each dialyzed sample was centrifuged for 20 min at 10,000xg and 4°C. The supernatant was collected and labelled as crude extract for the determination of PK activity. The extraction of PK from each sample was performed in triplicates.

For the determination of PK activity, a coupled assay was used as shown in Figure 3.2. The total volume of reaction mixture prepared for the estimation of PK enzyme activity was 1.0 mL. It contained 50 mM Tris-Cl buffer (pH 7.2), magnesium sulphate (10 mM), potassium chloride (50 mM), NADH (0.1 mM), ADP (1.8 mM), PEP (1.2 mM), 2.0 U of lactate dehydrogenase and 50 µL of crude extract. The reaction was initiated by PEP addition at 30°C in a water bath and decrease in absorbance at 340 nm per 30s was recorded in a UV-VIS spectrophotometer. The activity of PK enzyme was expressed as µmol NADH oxidized min^{-1} at 340 nm under the specified conditions. The assay for PK enzyme was performed in triplicates.
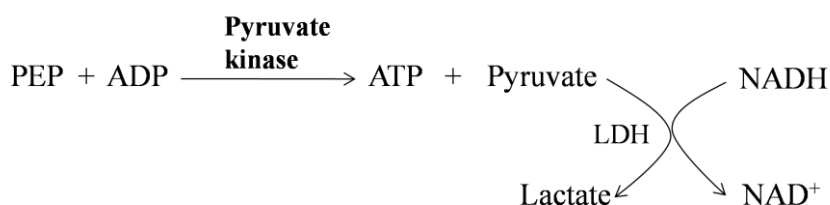
Figure 3.2. Principle of coupled assay for the determination of PK enzyme activity

3.6.3. Isocitrate dehydrogenase (ICDH)

One gram of each sample was weighed and homogenized by using liquid N_2 in a prechilled mortar and pestle. For extraction of ICDH from each sample, 5 mL of 0.05 M sodium phosphate buffer (pH 7.5) containing magnesium chloride, 5 mM; and polyvinylpyrrolidone (insoluble) at a concentration of 1% (*w/v*). The homogenized samples were then centrifuged for 30 min at 10,000xg and 4°C was added. The supernatant of each sample was collected and dialyzed for overnight at 4°C against extraction buffer diluted ~10-fold with distilled water and lacking polyvinylpyrrolidone. On the following day, each dialyzed sample was centrifuged for 20 min at 10,000xg and

4°C. The supernatant was collected and labelled as crude extract for determination of ICDH activity. The extraction of ICDH from each sample was performed in triplicates.

The activity of ICDH enzyme was determined using an assay as shown in Figure 3.3. The total volume of reaction mixture prepared for the estimation of ICDH enzyme activity was 3.0 mL. It contained Tris-Cl buffer (50 mM) pH 7.5, magnesium chloride (5 mM), $NADP^+$ (1 mM), isocitrate (10 mM) and 100 μL of crude extract. The reaction was initiated by the addition of isocitrate at 30°C in a water bath and increase in absorbance at 340 nm per 30s was recorded in a UV-VIS spectrophotometer. The activity of ICDH enzyme was expressed as μmol $NADP^+$ reduced min^{-1} at 340 nm under the specified conditions. The assay for ICDH enzyme was performed in triplicates.
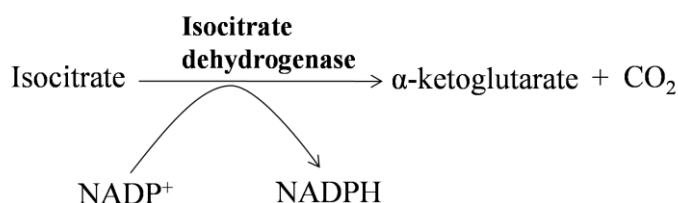
Figure 3.3. Principle of assay used for the determination of ICDH enzyme activity

3.6.4. Malate dehydrogenase (MDH)

One gram of each sample was weighed and homogenized with liquid N_2 in a prechilled mortar and pestle. For extraction of MDH from each sample, 5 mL of 0.1 M Tris-Cl buffer, pH 7.5, which contained magnesium chloride, 5 mM; Triton X-100, 1%; β-mercaptoethanol, 50 mM; sucrose, 50 mM and polyvinylpyrrolidone (insoluble), 1% (*w/v*) was added. The homogenized samples were then centrifuged for 30 min at 10,000xg and 4°C. The supernatant of each sample was collected and dialyzed for overnight at 4°C against extraction buffer diluted ~10-fold with distilled water and without polyvinylpyrrolidone. On the following day, each dialyzed sample was centrifuged for 20 min at 10,000xg and 4°C. The supernatant was collected and labelled as crude extract for determination of MDH activity. The extraction of MDH from each sample was performed in triplicates.

The activity of MDH enzyme was determined using an assay as shown in Figure 3.4. The total volume of reaction mixture prepared for the estimation of MDH enzyme activity was 3.0 mL. It contained potassium 50mM phosphate buffer (pH 7.0), NADH (0.15 mM), oxaloacetate (1 mM) and 100 μL of crude extract. The reaction was initiated by the

addition of oxaloacetate at 30°C in a water bath and decrease in absorbance at 340 nm per 30s was recorded in a UV-VIS spectrophotometer. The activity of MDH enzyme was expressed as μmol NADH oxidized min^{-1} at 340 nm under the specified conditions. The assay for MDH enzyme was performed in triplicates.

$$\text{Oxaloacetate} \xleftrightarrow{\textbf{Malate dehydrogenase}} \text{Malate}$$

NADH NAD^{+}
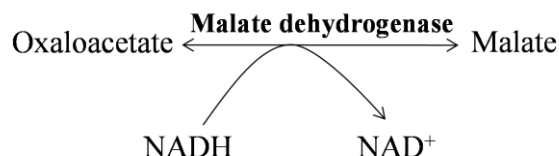
Figure 3.4. Principle of assay used for the determination of MDH enzyme activity

3.6.5. Malic enzyme (ME)

One gram of each sample was weighed and homogenized with liquid N_2 in a prechilled mortar and pestle. For extraction of ME from each sample, 5 mL of 0.1 M Tris-Cl buffer, pH 7.5, which contained magnesium chloride, 5 mM; glycerol, 10% (*v/v*); β-mercaptoethanol, 10 mM; phenylmethane sulfonyl fluoride (PMSF), 1 mM and polyvinylpyrrolidone (insoluble), 1% (*w/v*) was added. The homogenized samples were then centrifuged for 30 min at 10,000xg and 4°C. The supernatant of each sample was collected and dialyzed for overnight at 4°C against extraction buffer diluted ~10-fold with distilled water and without polyvinylpyrrolidone. On the following day, each dialyzed sample was centrifuged for 20 min at 10,000xg and 4°C. The supernatant was collected and labelled as crude extract for the determination of ME activity. The extraction of ME from each sample was performed in triplicates.

The activity of ME enzyme was determined by using an assay as shown in Figure 3.5. The total volume of reaction mixture prepared for the estimation of ME enzyme activity was 3.0 mL. It contained Tris-Cl buffer (50 mM, pH 7.5), magnesium chloride (10 mM), $NADP^{+}$ (0.5 mM), L-malate (10 mM) and 100 μL of crude extract. The reaction was initiated by the addition of L-malate at 30°C in a water bath and increase in absorbance at 340 nm per 30s was recorded in a UV-VIS spectrophotometer. The activity of ME enzyme was expressed as μmol $NADP^{+}$ reduced min^{-1} at 340 nm under the specified conditions. The assay for ME enzyme was performed in triplicates.

$$\text{Malate} \xrightarrow{\text{\textbf{Malic enzyme}}} \text{Pyruvate}$$
$$\text{NADP}^+ \qquad \text{NADPH}$$
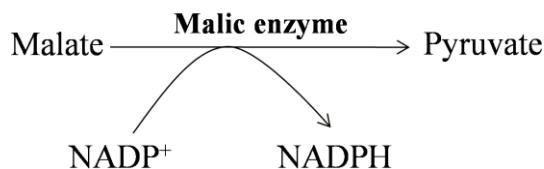
Figure 3.5. Principle of assay used for the determination of ME enzyme activity

3.6.6. Phenylalanine ammonia lyase (PAL)

One gram of each sample was weighed and homogenized by using liquid N_2 in a prechilled mortar and pestle. For extraction of PAL from each sample, 5 mL of 0.1 M sodium borate buffer (pH 8.8) containing 5 mM β-mercaptoethanol was added. The homogenized samples were then centrifuged for 20 min at 10,000xg and 4°C. The supernatant of each sample was collected and labelled as crude extract for the determination of PAL activity. The extraction of PAL from each sample was performed in triplicates.

For estimation of PAL enzyme activity, a total volume of 3.0 mL reaction mixture was prepared. It contained sodium borate buffer (0.1 M, pH 8.8), L-phenylalanine (15 mM) and 50 µL of crude extract. The reaction mixture was first preincubated for 20 min at 30°C in a water bath without L-phenylalanine to allow for an initial non-enzymatic decrease in absorbance. The reaction was then initiated with the addition of L-phenylalanine and observed for the increase in absorbance over a period of 60 min at a wavelength of 290 nm by using a UV-VIS spectrophotometer (SPECTRASCAN UV 2700, Thermo Scientific). To determine the activity of PAL enzyme, a standard curve of CA was prepared by taking different concentrations in the range of 0-200 µg/mL. The activity of PAL enzyme was then calculated from the standard curve of CA and expressed as µmol of CA produced min^{-1} mL^{-1} under the specified conditions. The PAL activity assay was carried out in triplicates and results were documented as milliunits (mU) of enzyme.

3.7. Estimation of total protein content

Total protein content in each crude extract was determined by using protein assay kit (Bio-Rad) as per instructions given by the manufacturer. The concentrated dye reagent (Bio-Rad) was diluted 5-fold with double distilled water and filtered through Whatman filter paper (Millipore). A total of seven different dilutions were prepared (0-150 µg/mL)

from aqueous stock solution of BSA (1mg/mL) and pipetted along with samples (10 µL) in separate wells of microtiter plate. To each well, 200 µL of filtered dye reagent was added; mixed and kept at room temperature for 5 min. The absorbance was recorded at 595 nm. The total protein content in each extract was calculated from the standard curve of BSA and expressed as µg mL^{-1}. The protein estimation was performed in triplicates

3.8. Mining NGS (Next Generation Sequencing) transcriptomes for key genes involved in picrosides biosynthesis and differential gene expression (DGE) analysis

The transcriptome datasets of *P. kurroa* accessions (genotypes) varying for P-I (PKS-1, PKS-5, PKS-4 and PKS-21) and P-II contents (PKST-3, PKST-5, PKST-16 and PKST-18) were generated and assembled (Table 3.2). The normalization and expression profiling was carried out through RSEM software with default parameters/commands used for the normalization of each library and consequently provided an output with Fragments Per Kilobase Per Million (FPKM) and Tags Per Million (TPM), the expected normalized read counts. FPKM values calculated as Log to the base 2 were recognized as delta Ct equivalent value or absolute expression.

Table 3.2. Transcripts in NGS transcriptomes generated from shoots and stolons of *P. kurroa* accessions varying for P-I and P-II contents

S. No.	*P. kurroa* accession	Shoots P-I %	Stolons P-I %	P-II %	Total %	Transcripts (number)
1.	PKS-1	2.38				1,43,637
2.	PKS-5	1.18				1,55,576
3.	PKS-4	0.49				1,57,372
4.	PKS-21	0.13				1,58,030
5.	PKST-3		0.17	2.65	2.82	1,29,599
6.	PKST-5		0.08	2.19	2.28	1,22,753
7.	PKST-16		1.05	1.52	2.57	1,31,236
8.	PKST-18		1.32	1.36	2.67	1,30,487

In these transcriptomes, a large numbers of transcripts have been generated and those encoding enzymes catalyzing regulatory reactions in different metabolic pathways were selected based on their connection with picrosides biosynthesis. The details of selected transcripts with their role in picrosides production are provided in Table 3.3. The shortlisted transcripts were used for DGE analysis using sequence similarity threshold of

>98%. Only those transcripts were selected and used for the analyses which were present in all the 8 different samples i.e. 4 accessions each of shoots and stolons. Hierarchical clustering of selected DGEs were performed using heatmaply, gplot2, plotly packages in R package.

Table 3.3. Details of transcripts encoding enzymes involved in different pathways and their plausible involvement in picrosides biosynthesis

Transcript encoding enzymes	Abbreviations	Function/Pathway	Flux to picrosides [Convergent (C)/ Divergent (D)]	
			P-I	P-II
1-deoxy-D-xylulose-5-phosphate synthase	DXPS	IPP & DMAPP production	C	C
3-Deoxy-D-arabinoheptulosonate 7-phosphate synthase	DAHPS	Entry step of Shikimate pathway	C	C
Hydroxymethylglutaryl-CoA reductase	HMGR	IPP production	C	C
3-hydroxyacyl CoA dehydrogenase	HADH	Benzoic acid biosynthesis	D	D
Anthranilate synthase	AS	Tryptophan biosynthesis	D	D
Tyrosine decarboxylase	TDC	Tyrosine degradation	D	D
Caffeic acid-3-O-methyltransferase	CMT	Ferulic acid production	D	C
Chalcone synthase	CHS	Flavonoids biosynthesis	D	D
Chorismate mutase	CM	Phenylalanine biosynthesis	C	C
Cinnamic acid-4-hydroxylase	C4H	p-coumaric acid production	D	C
Cinnamoyl CoA reductase	CCR	Guaiacyl lignin biosynthesis	D	D
Ferulic acid-5-hydroxylase	F5H	Syringyl lignin biosynthesis	D	D
Farnesyl pyrophosphate synthase	FPPS	Sesquiterpene biosynthesis	D	D
Geraniol synthase	GS	Monoterpene biosynthesis	C	C
Geranyl pyrophosphate synthase	GPPS	Terpene biosynthesis	C	C
Geranylgeranyl pyrophosphate synthase	GGPPS	Diterpene biosynthesis	D	D
Glucose-6-phosphate dehydrogenase	G6PDH	Pentose phosphate pathway	C	C
Hexokinase	HK	Glycolysis	C	C
Isocitrate dehydrogenase	ICDH	TCA cycle	D	D
Phytoene synthase	PYS	Carotenoid biosynthesis	D	D
Pyruvate kinase	PK	Glycolysis	C	C
Squalene synthase	SQS	Triterpene biosynthesis	D	D
4-coumarate CoA ligase	4CL	Flavonoids biosynthesis	D	D
Phenylalanine ammonia lyase	PAL	Cinnamic acid production	C	C
Phosphoenolpyruvate carboxykinase	PEPCK	Phosphoenolpyruvate production	C	C
Malate dehydrogenase	MDH	TCA cycle	D	D
Phosphomevalonate kinase	PMK	IPP production	C	C
4-diphosphocytidyl-2C-methyl-D-erythritol synthase	ISPD	IPP & DMAPP production	C	C
Geraniol-10-hydroxylase	G10H	Iridoid biosynthesis	C	C

3.9. RNA isolation and complementary DNA (cDNA) preparation

The isolation of total RNA was performed in triplicates by using TRIzol reagent (Ambion) as per instructions given by the manufacturer. Each sample was weighed to 0.1 g and kept in a prechilled mortar and pestle. The samples were then homogenized by using liquid N_2 in the presence of 1 mL TRIzol reagent (Ambion) and transferred to eppendorf centrifugation tubes (1.5 mL) followed by incubation at room temperature for 5 min. To each sample, 0.2 mL chloroform was added; vigorously mixed and kept at room temperature for 2-3 min. The samples were then centrifuged for 15 min at 12,000xg and 4°C. The upper aqueous layer from each sample was then transferred to a fresh centrifuge tube and added 0.5 mL of isopropanol followed by incubation at -20°C for 10 min. The samples were centrifuged for 10 min at 12,000xg and 4°C. The pellet of each sample thus obtained was washed twice with 70% ethanol, air dried and dissolved in nuclease free water (~50 µL). The isolated RNA was stored at -80°C and quantified at 260/280 nm by using a ND-2000 UV spectrophotometer (Nanodrop Technologies, Wilmington, DE, USA). The quality of isolated RNA was tested on 1% (*w/v*) agarose gel stained with ethidium bromide and visualized by observing UV fluorescence through gel documentation system (Alpha Innotech, USA). The synthesis of cDNA was performed in triplicates with 5 µg of total RNA by using Verso cDNA synthesis kit (Thermo scientific, US) as per instructions given by the manufacturer. The cDNA thus obtained was quantified by using ND-2000 UV spectrophotometer (Nanodrop Technologies, Wilmington, DE, USA); diluted with nuclease free water to make 100 ng concentration of each sample and subjected to gene expression analysis.

3.10. Gene expression analysis by using quantitative real time polymerase chain reaction (qRT-PCR)

The expression analysis of genes was performed in triplicates on CFX96 system (Bio-Rad Laboratories; Hercules CA) with the standard 96 well block. The primers corresponding to genes were designed from their sequences in *P. kurroa* transcriptomes by using Primer3 software (http://bioinfo.ut.ee/primer3-0.4.0/primer3/) (Table 3.4).

The expression analysis of each gene was performed in a reaction mixture of 12.5 µL which contained: 0.5 µL forward primer (10 pmol), 0.5 µL reverse primer (10 pmol), 6.25 µL iQ™ SYBR Green Supermix (Bio-Rad), 1 µL cDNA (100 ng) and 4.25 µL nuclease

free H$_2$O. The programme used in qRT-PCR was: initial denaturation for 3 min at 95°C; 39 cycles each of denaturation at 95°C for 10 s, annealing at 49-60°C for 20 s and extension at 72°C for 20 s followed by a final melt curve analysis. The housekeeping gene (26S rRNA) was used as an internal control for normalization of gene expression.

Table 3.4. Primers used for qRT-PCR analysis

Gene	Primer sequence	Fragment size (bp)	Annealing temperature ($^{\circ}$C)
26S	FP 5'-CACAATGATAGGAAGAGCCGAC-3' RP 5'-CAAGGGAACGGGCTTGGCAGAATC-3'	500	58
HK	FP 5'-ATGCTCCTTACCTACGTTCA-3' RP 5'-TCCTAACTGAACCCTCAAGA-3'	108	52
PK	FP 5'-AGCTTGTGGCTAAGTACAGG-3' RP 5'-TCCCCTGAATATGAGACTGT-3'	128	53
ICDH	FP 5'-TCGACATGATAACGTGGATA-3' RP 5'-TGTTATGACCTTGAGGCTCT-3'	112	52
MDH	FP 5'-CTGATTCTCAAGGAATTTGC-3' RP 5'-TACCTGCACTTTCAACCTCT-3'	114	51
ME	FP 5'-CAGCAGATCCTCACTTCTTC-3' RP 5'-CACATCCTTCAATCTCACCT-3'	117	52
G-6-PDH	FP 5'-GAAACCTGAGCATATTCGAG -3' RP 5'-GTTGTCTGGAACTGTTGGAT -3'	124	52
DAHPS	FP 5'- ACACCATTAAAGCTCCTTGT -3' RP 5'- TAACAGTCTGAGATCCACCA -3'	171	59
PAL	FP 5'- GCAAGATAGATACGCTCTAA -3' RP 5'- GTTCCTTGAGACGTCAAT -3'	136	49
DXPS	FP 5'-ACATTTAAGTTCAAGTCTGGGAGTG-3' RP 5'-ATGTGCACTCTCTTCTCTTTTAGGA-3'	110	56
ISPD	FP 5'-GAGAAAAGTGTATCTGTGCTTCTTAG-3' RP 5'-AATAACCTGCGGTGTATGCATTTCC-3'	150	56
HMGR	FP 5'-CGTTCATCTACCTTCTAGGGTTCTT-3' RP 5'-GACATAACAACTTCTTCATCGTCCT-3'	100	60
PMK	FP 5'-TGGATGTTGTCGCATCAGCACCTGG-3' RP 5'-GTAATAGGCAGTCCACTCGCTTCAA-3'	100	58
GS	FP 5'- TGGGTAGATTAGAAGCCAGA -3' RP 5'- CTGGTGATTTCTACCAGCTC -3'	139	52
G10H	FP 5'- TATCGAGCTTTTCAGTGGAT -3' RP 5'- GATGTGAGTCCTGTCGATTT -3'	136	52
CMT	FP 5'-GAAGATGCTCCTTCTTATCC-3' RP 5'-AACACTCGACCAGAATCAC-3'	187	53
C4H	FP 5'-GCAACATTGATGTTCTCAAC-3' RP 5'-TCCAGCTCTTCAAGGACTAT-3'	169	53

3.11. Statistical analyses

The one and two-way analysis of variance (ANOVA) followed by a Bonferroni test were performed on data in triplicates (mean ± SD) using GraphPad prism software version 6.0. The principle component analysis (PCA) was carried out by using XLSTAT- Pro 7.5 software (Addinsoft, New York, USA). The correlation analysis was carried out by determination of Pearson's correlation coefficients (PCC) which were represented as "correlogram" generated by using "Corrgram" function in R package [82]. To examine the correlations between gene expression profiles obtained from RNA-seq and qRT-PCR, log2 fold change values were estimated among different shoots and stolons accessions. The scatterplots were then created by comparing log2 fold change values determined by RNA-seq and qRT-PCR using GraphPad prism software version 6.0. The correlations were represented in terms of coefficient of determination i.e. R^2.

RESULTS

The results obtained while answering questions raised with the objectives outlined in the current study have been described in following sections.

4.1. Differential content phenotypes for P-I content in *P. kurroa*

The shoots obtained from field grown plants of *P. kurroa* exhibited 2.8-fold enhancement in P-I content (1.4%) as compared to *P. kurroa* shoots established in tissue culture conditions at 15°C which showed 0.5% P-I content (Figure 4.1). On the contrary, *P. kurroa* shoots established in tissue culture conditions at 25°C did not show detection of P-I. The HPLC chromatograms obtained from HPLC, which showed peaks of P-I in samples compared to authentic standard are depicted in Figure 4.2.
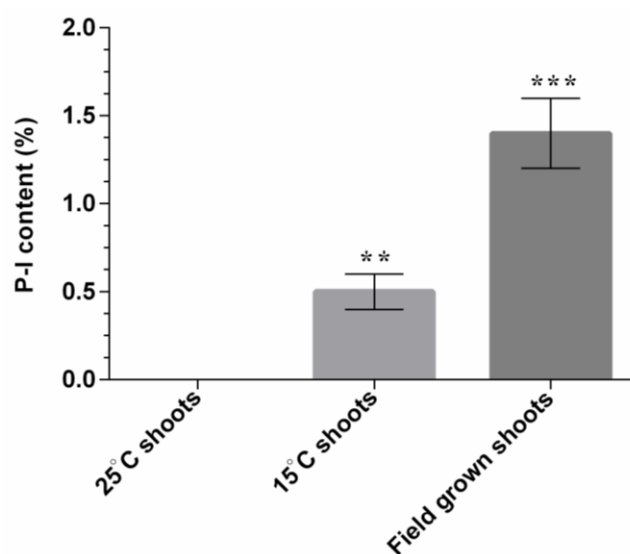
Figure 4.1. P-I content determined by HPLC in different conditions of *P. kurroa* growth. The data shown means ± SD (n = 3). Significance was evaluated between different samples and 25°C condition as sample control (**p<0.01, ***p<0.001).
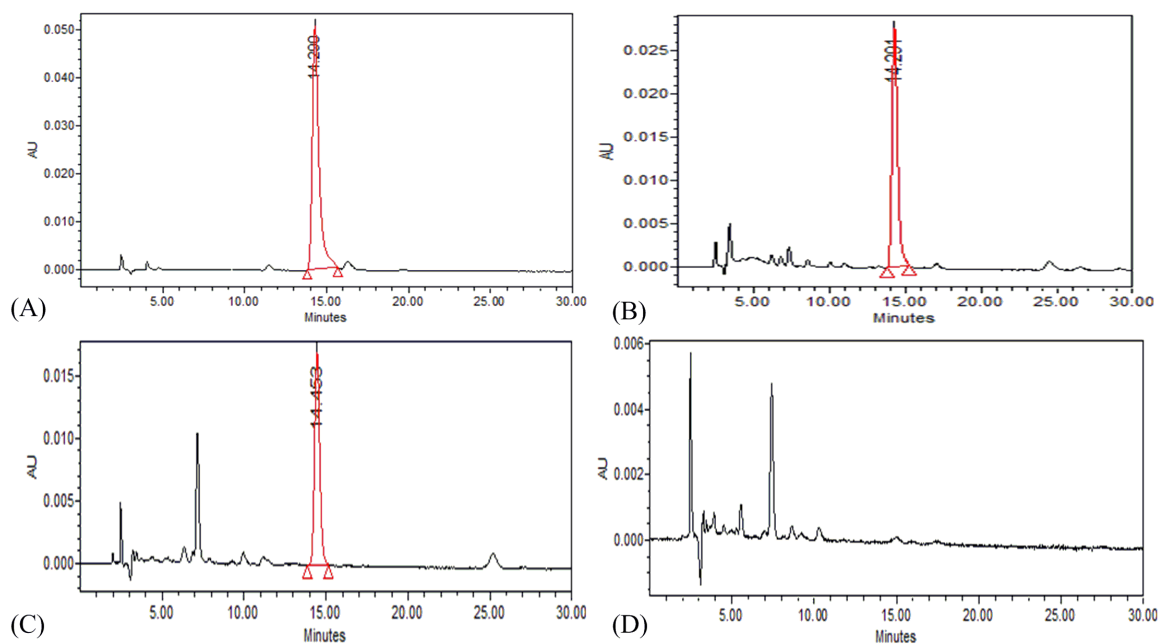
Figure 4.2. HPLC chromatograms of the P-I standard (A), field grown shoot (B), 15°C shoot (C), and 25°C shoot (D). AU denotes Absorbance Units.

4.2. Gene expression and activity profiles of primary metabolic enzymes vis-à-vis P-I biosynthesis in differential content conditions

The primary metabolic enzymes *viz.* HK, PK, ICDH, MDH and NADP$^+$-ME, which catalyze reactions considered as rate limiting in glycolysis and TCA cycle were examined for their patterns of gene expression and enzymes activities in differential conditions of P-I biosynthesis. The expression level of *HK* transcript was maximum in field grown shoots of *P. kurroa* with a normalized expression value of 2.0 and showed 8- and 87-fold increase as compared to its levels among *P. kurroa* shoots established in tissue culture conditions at 15°C and 25°C, respectively (Figure 4.3). The specific activity of HK enzyme was also consistent with its transcript levels and showed progressive increase with 0.004, 0.0176 and 0.032, U mg^{-1} protein in 25°C, 15°C and field grown shoots, respectively (Figure 4.3). The gene encoding PK enzyme also showed similar patterns of gene expression and enzyme activity as that of HK i.e. exhibiting the maximum value in field grown shoots followed by shoot cultures grown *in vitro* at 15°C and 25°C. The expression level of *PK* transcript showed 12.6- and 81.2-fold enhancement, whereas its specific activity revealed 4.8- and 6.2-fold increase in field grown shoots as compared to shoot cultures established at 15°C and 25°C, respectively (Figure 4.3). These results indicate the possible association of glycolysis with P-I biosynthesis in *P. kurroa*.

39
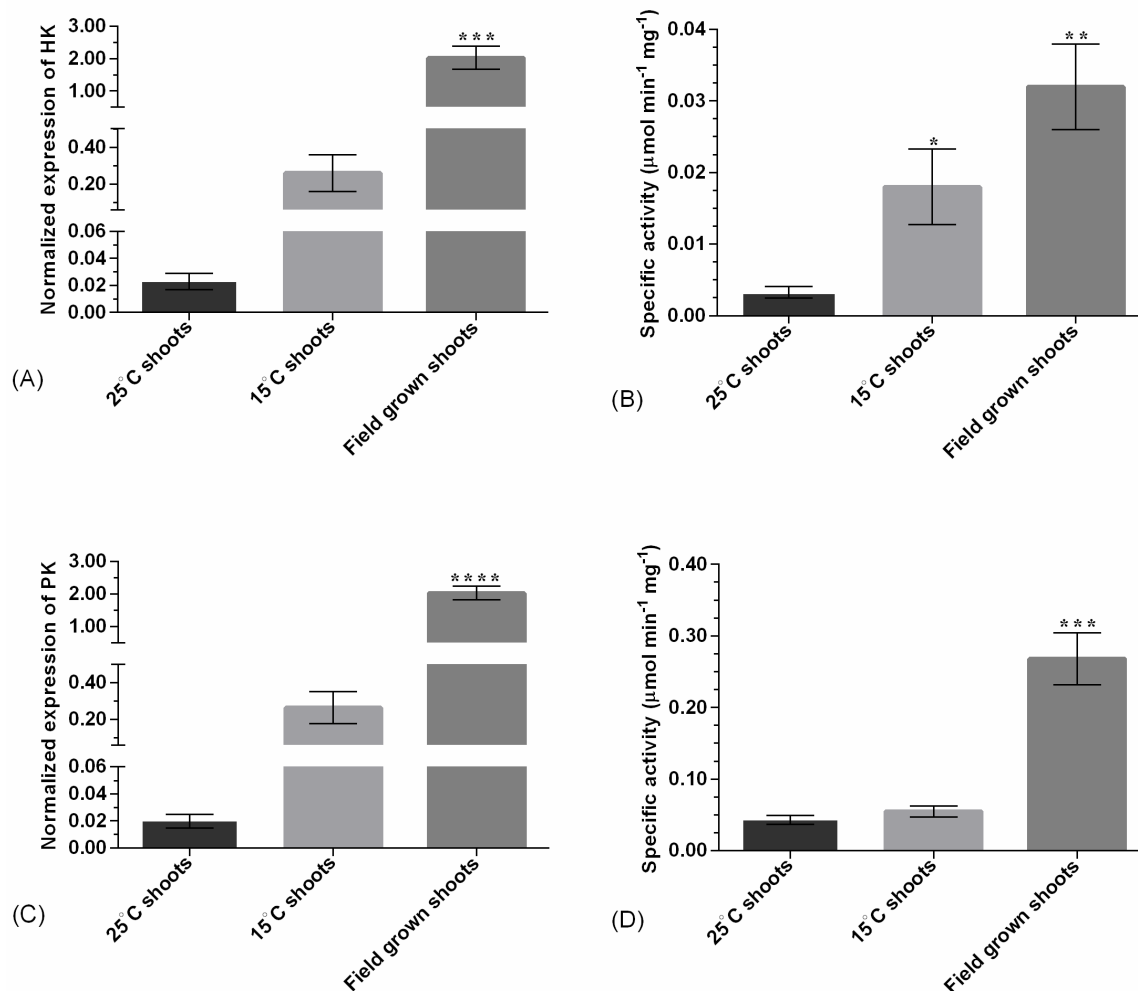
Figure 4.3. Catalytic activities and quantitative gene expression profiles of glycolytic enzymes in *P. kurroa* shoots grown in field and in tissue culture conditions (15°C and 25°C); (A, B) HK and (C, D) PK. The data has been presented as means ± SD (n = 3). Significance was assessed between different samples and 25°C condition as sample control (*p<0.05, **p<0.01, ***p<0.001, ****p<0.0001). Expression values were normalized with levels of 26S reference gene.

The analysis of TCA cycle enzymes, on the other hand, revealed that *ICDH* transcript exhibited 18.1- and 54.8-fold higher gene expression, while 11.7- and 35.7-fold enhanced specific activity, in field grown shoots as compared to shoot cultures established at 15°C and 25°C, respectively (Figure 4.4). In contrast, the expression levels of *MDH* and *NADP+-ME* transcripts were maximum in shoot cultures of *P. kurroa* established at 15°C with a normalized expression value of 1.0 and showed 1.7-, 13.9-, and 1.7-, 23.6-fold elevation as compared to shoots grown in field and at 25°C *in vitro*, respectively (Figure 4.4). Conversely, the specific activity of MDH enzyme was highest in field grown shoots

with 2.6 U mg^{-1} protein and exhibited 1.2- and 4.0-fold higher specific activity than in shoot cultures established at 15°C and at 25°C, respectively (Figure 4.4). Further, the pattern of specific activity for NADP$^+$-ME was distinct as it showed non-significant variation among shoots grown in field and at 15°C *in vitro*, followed by 3.1-fold higher specific activity as compared to *in vitro* shoot cultures at 25°C (Figure 4.4).
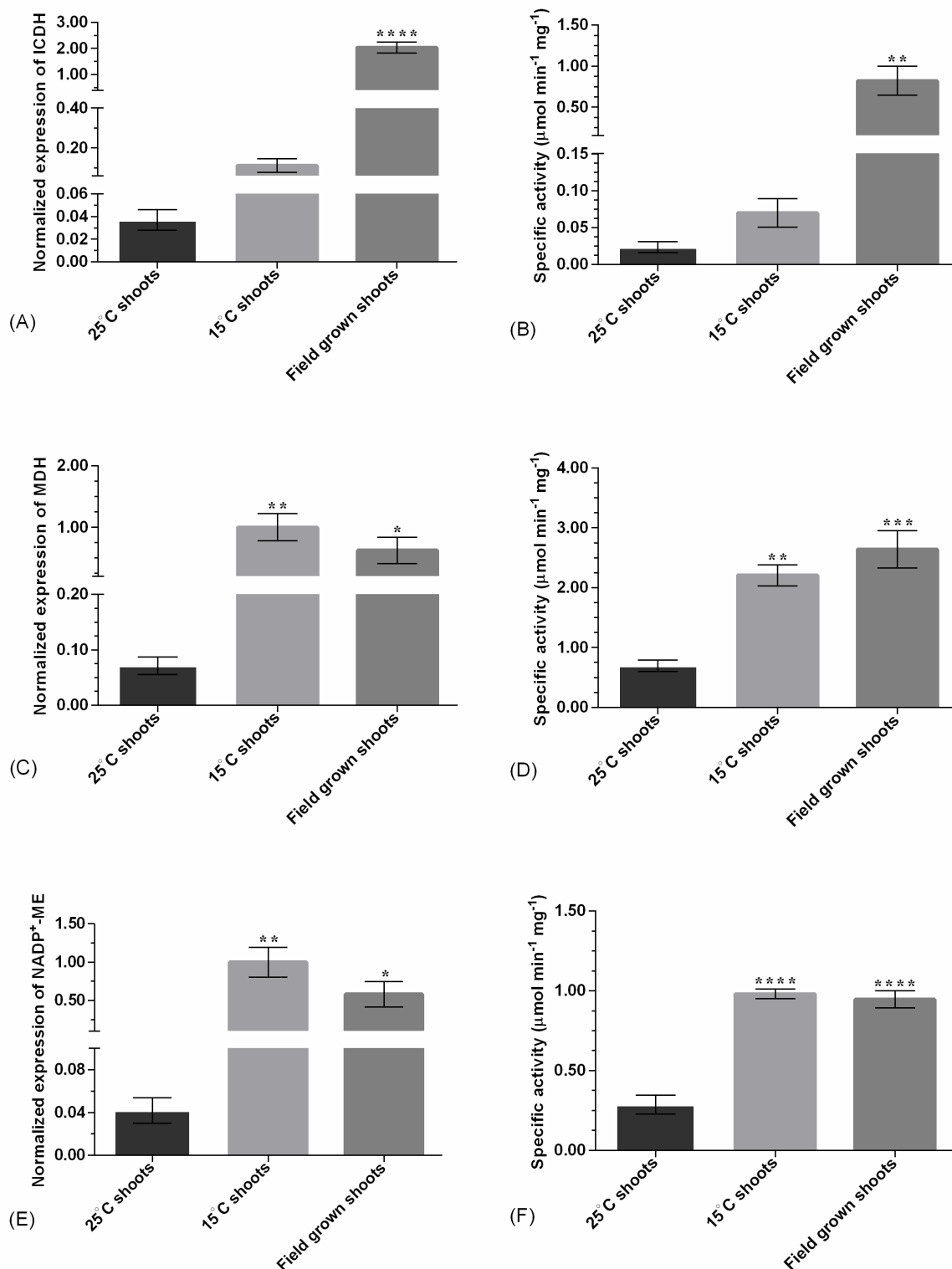
Figure 4.4. Catalytic activities and quantitative gene expression profiles of TCA cycle enzymes in *P. kurroa* shoots grown in field and in tissue culture conditions (15°C and 25°C); (A, B) ICDH, (C, D) MDH and, (E, F) NADP$^+$-ME. The data has been presented as means ± SD (n = 3). Significance was assessed between different samples and 25°C condition as sample control (*p<0.05, **p<0.01, ***p<0.001, ****p<0.0001). Expression values were normalized with levels of 26S reference gene.

4.3. Correlations between gene expression and catalytic activities of primary metabolic enzymes

The correlations between transcripts expression levels and catalytic activities of HK, PK, MDH, ICDH and NADP$^+$-ME were observed in different conditions of P-I biosynthesis i.e. *P. kurroa* shoots grown in field and those established *in vitro* at 15°C and 25°C. Interestingly, the correlations determined through PCC (r) revealed significant relationship between transcripts expression levels and catalytic activities of all the investigated enzymes (Table 4.1). The highest correlation was observed for ICDH, while MDH possessed lowest correlation. The positive correlations observed for the selected enzymes among different conditions of P-I biosynthesis indicate their association with the production of P-I in *P. kurroa*.

Table 4.1. The Pearson's correlation determined between activities and expression levels of selected enzymes

Gene	Correlation Coefficient (PCC, r)
HK	0.8837**
PK	0.9977**
MDH	0.7925*
ICDH	0.9994**
ME	0.9161**

*significant at ($p< 0.05$) **significant at ($p< 0.01$)

4.4. Levels of P-I at different growth stages of *P. kurroa*

The analysis of different growth stages (0, 10, 20, 30 and 40 days) of *P. kurroa* under *in vitro* conditions at 15°C revealed significant modulations in P-I content (Figure 4.5). When the plant growth reached from 0 to 10 days, the biosynthesis of P-I was initiated

and 0.02% P-I content was observed. Further, P-I content showed 2.16-fold elevation in 20 days old shoots of *P. kurroa* as compared to 10 days stage (Figure 4.5). The maximum enhancement in P-I content was observed in 30 days old *P. kurroa* shoot cultures with a significant fold change of 4.07 (p<0.001) as compared to 20 days stage of plant growth. After 30 days, the levels of P-I did not show significant increase as demonstrated by the analysis of P-I in 40 days old shoots cultures of *P. kurroa*.

4.5. Identification of differentially expressed primary and secondary metabolic pathway genes vis-à-vis P-I content in different growth stages of *P. kurroa* through qRT-PCR

To identify differentially expressed genes, total RNA was extracted from *P. kurroa* shoots grown under tissue culture conditions at $15°C$ for 0, 10, 20, 30 and 40 days. The cDNA was synthesized and subjected to qRT-PCR analysis which was performed for 13 genes belonging to glycolysis (*HK* and *PK*), TCA cycle (*ICDH* and *MDH*), pentose phosphate pathway (*G-6-PDH*), mevalonate pathway (*HMGR* and *PMK*), non-mevalonate pathway (*DXPS* and *ISPD*), shikimate/phenylpropanoid pathway (*DAHPS* and *PAL*) and iridoid pathway (*GS* and *G-10-H*) in all the samples. These genes were selected due to their rate limiting role in different pathways associated with P-I biosynthesis as shown in Figure 4.6.
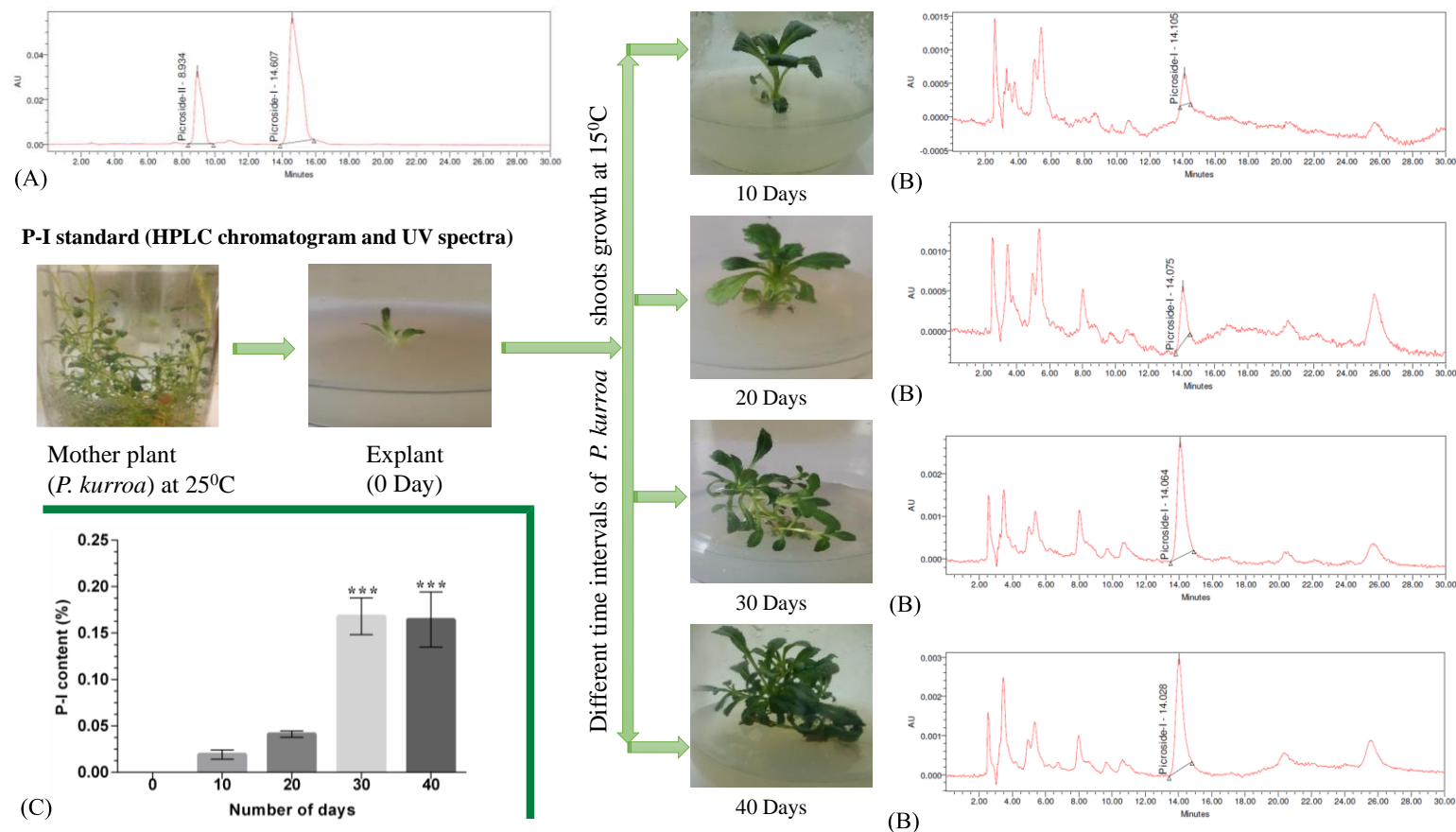
Figure 4.5. Time course changes in *P. kurroa* growth and P-I content at 15°C under tissue culture conditions; (A) HPLC chromatogram of P-I and P-II standards, (B) HPLC chromatogram of samples represented respective stages of growth and, (C) Bar graph showing variations in P-I content. The data has been presented as means ± SD (n = 3). Significance was assessed between samples collected at different time intervals and 0 day control (***$p<0.001$). AU, Absorbance Units
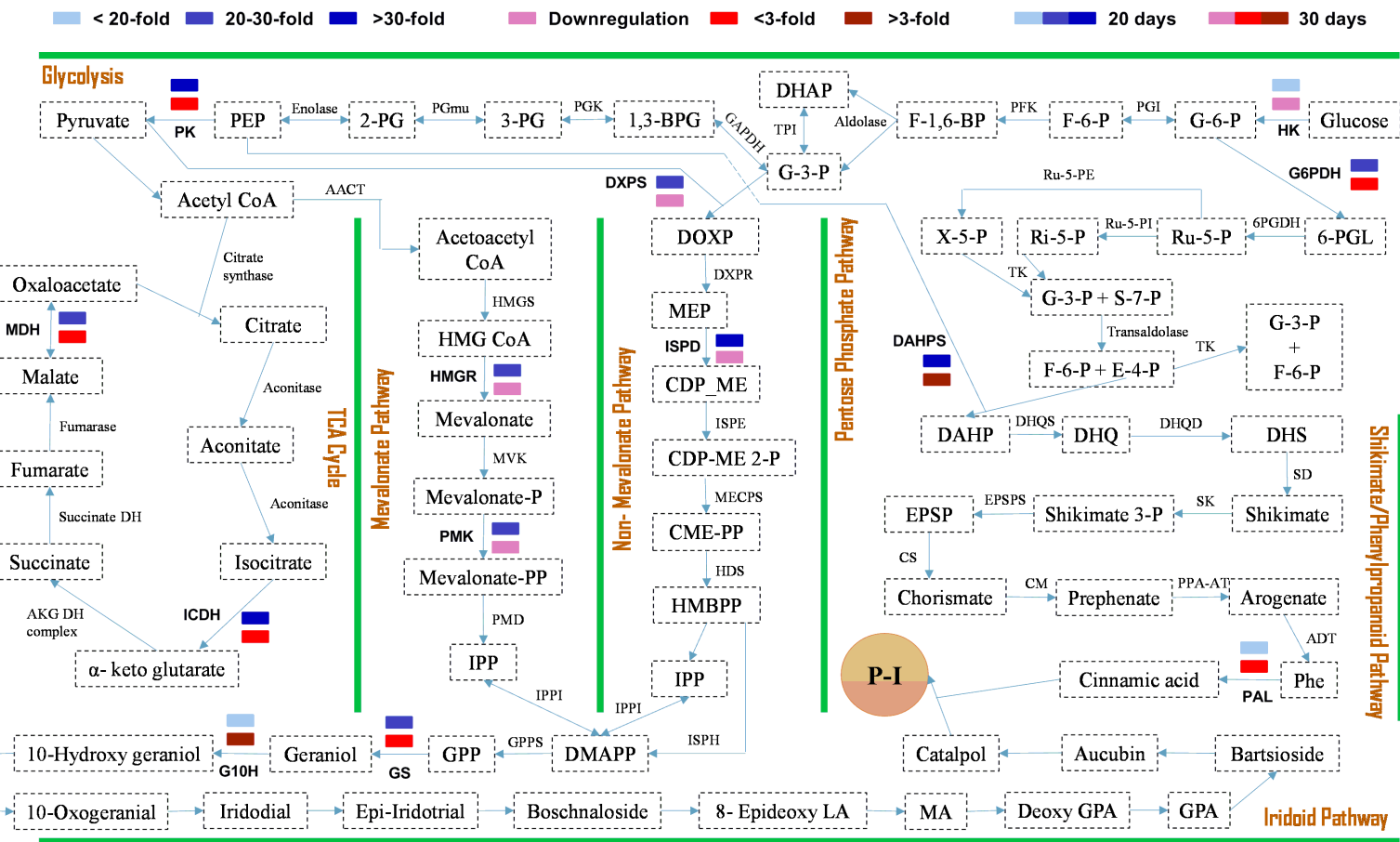
Figure 4.6. An overview of the primary (glycolysis, TCA cycle, pentose phosphate pathway) and secondary (MVA/MEP, shikimate/phenylpropanoid and iridoid, pathways) metabolic pathways which integrates into P-I biosynthesis. Rectangular squares coded with blue and red colors highlighted the expression levels of genes selected in all the integrated pathways at different time intervals of *P. kurroa* growth; after 20 days and, after 30 days, respectively.

The analysis of genes expression levels in *P. kurroa* shoot cultures reached to 10 days stage at 15°C revealed non-significant modulations as compared to initial stage of plant growth i.e. zero day explant. However, the shoot cultures reached to 20 days stage exhibited significant increase in the expression of transcripts *viz. HK*, *G6PDH*, *ICDH*, *DXPS*, *ISPD*, *HMGR* and *PMK* with 17.9-, 16.6-, 86.6-, 91.1-, 192.5-, 22.1- and 25.9-fold, respectively as compared to zero day explant (Figure 4.7). The highest increase in expression levels observed for DXPS and ISPD genes imply that non-mevalonate pathway provides major contribution towards P-I biosynthesis upto 20 days in *P. kurroa* shoot cultures at 15°C.

The investigation of transcripts expression levels in shoot cultures reached to 30 days stage, on the other hand, revealed 65.7-, 30.1-, 121.1-, 31.8-, 122.2-, 54.6-, 201- and 91.4-fold significant up-regulation of *PK*, *G6PDH*, *ICDH*, *MDH*, *GS*, *G10H*, *DAHPS* and *PAL* genes, respectively as compared to zero day explant (Figure 4.7). The maximum significant elevation in expression levels of the transcripts *viz. DAHPS*, *PAL*, *GS* and *G10H*, catalyzing rate limiting steps in the two core pathway modules of P-I biosynthesis i.e. shikimate/phenylpropanoid and iridoid pathways at 30 days stage, indicate their combined role in stimulation of P-I production. Further, the gene expression levels in shoot cultures reached to 40 days stage, did not show significant up-regulation as compared to zero day explant (Figure 4.7). It was thus evident from these results that the selected genes involved in primary and secondary metabolic pathways are likely to be associated with regulation of P-I biosynthesis in *P. kurroa*.
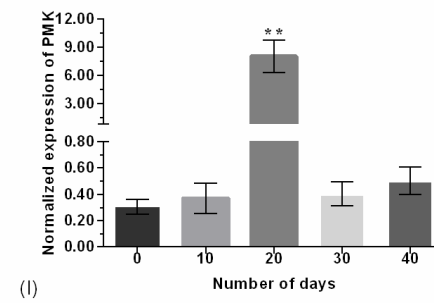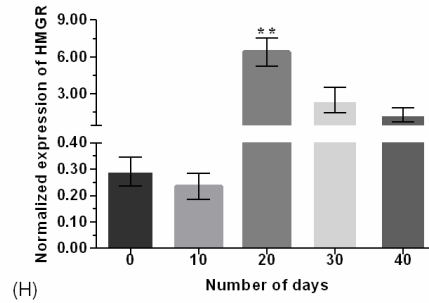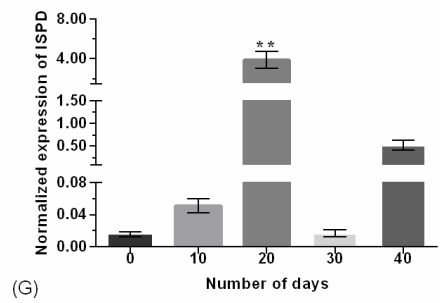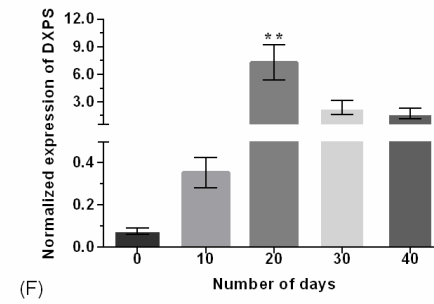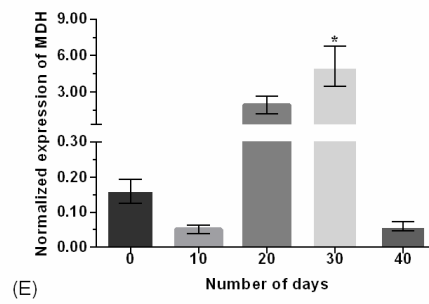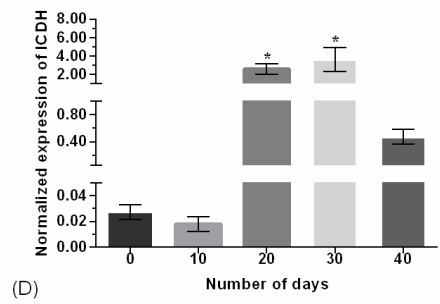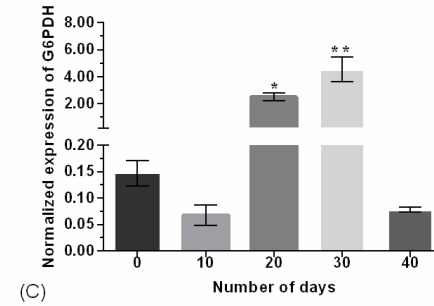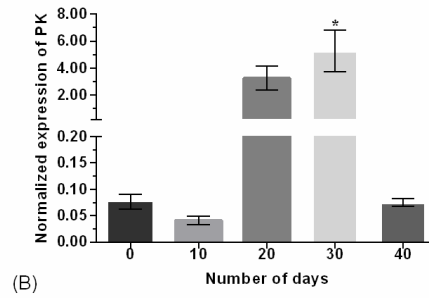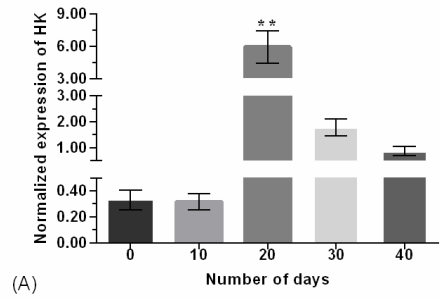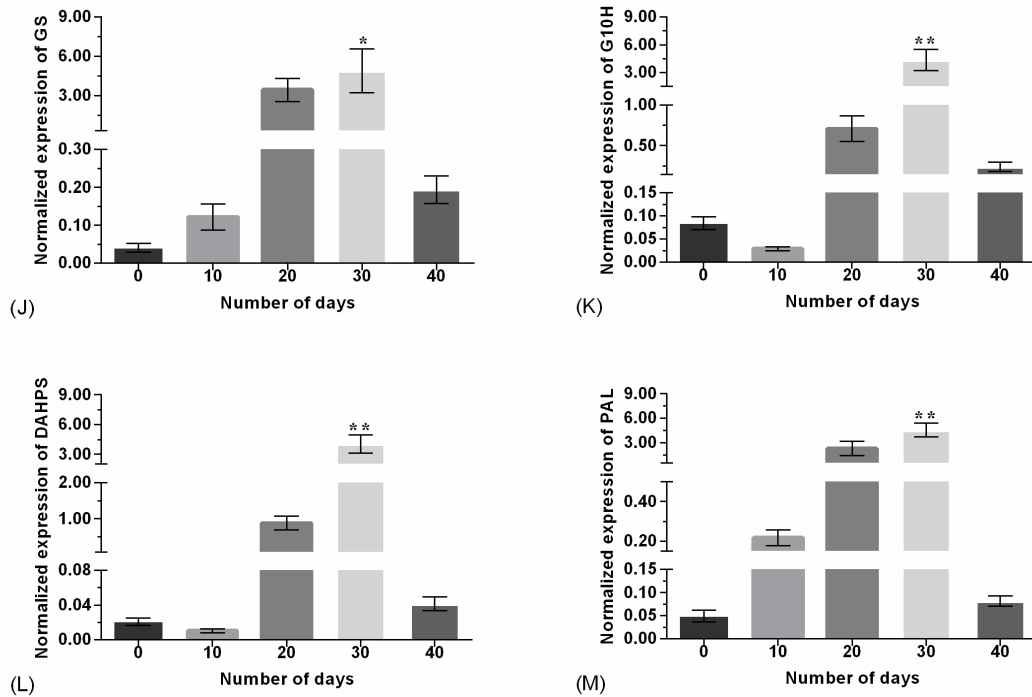
Figure 4.7. Time course changes in the expression levels of selected genes at 15°C *in vitro*; (A) *HK*, (B) *PK*, (C) *G6PDH*, (D) *ICDH*, (E) *MDH*, (F) *DXPS*, (G) *ISPD*, (H) *HMGR*, (I) *PMK*, (J) *GS*, (K) *G10H*, (L) *DAHPS* and, (M) *PAL*. The data has been presented as means $\pm$ SD (n = 3). Significance was assessed between samples collected at different time intervals and 0 day control (*p<0.05, **p<0.01). Expression values were normalized with levels of 26S reference gene.

4.6. Principal component analysis (PCA)

PCA was used to explore the sources of variations within the gene expression patterns, in which observations were *P. kurroa* shoots grown at 15°C for 0, 10, 20, 30, and 40 days and variables were normalized gene expression estimates for each of the selected 13 genes along with the P-I content. The scree plot between variability, eigen-values and principal components generated after PCA analysis showed that the largest variation was explained by the principal component 1 i.e. F1 contributing 75.85% followed by F2 (12.97%), F3 (8.92%) and F4 (2.26%) components (Figure 4.8). Thus, our PCA analysis indicated that the first two components (F1 and F2) best described the sources of variation between the different stages of *P. kurroa* growth. Moreover, F1 versus F2 biplots were redrawn with genes highlighted using blue dot symbols and different conditions of *P. kurroa* growth using red dots (Figure 4.9). It was inferred from the biplot

48

that different genes are grouped in two separate zones (group 1 and 2) around the origin. This organization is best exemplified by the categorization that the up-regulated genes at 20 days of *P. kurroa* growth were found loaded in group 2 (purple color) while those up-regulated at 30 days of *P. kurroa* growth were found loaded in group 1 (red color). Further, inspection of group 1 and 2 genes revealed that group 1 genes with high expression levels at 30 days of *P. kurroa* growth are related to pentose phosphate, shikimate/phenylpropanoid, TCA cycle, glycolysis and iridoid pathways, while group 2 genes with high expression levels at 20 days of *P. kurroa* growth are related to glycolysis, MVA and MEP pathway. Moreover, ISPD related to MEP pathway was also included in group 2 cluster on the basis of its distance from the origin (Figure 4.9).
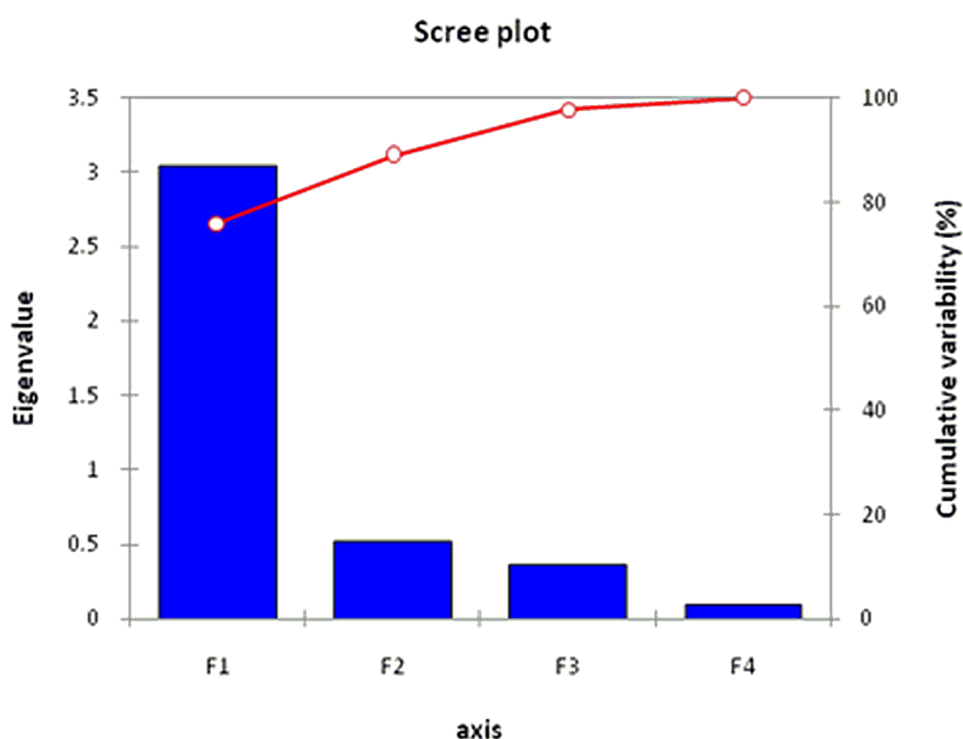
Figure 4.8. Scree plot for principal components (F1 - F4), their respective Eigen values, and cumulative variability. Major variance was contributed by components 1 and 2 while partial contribution came from components 3 and 4.
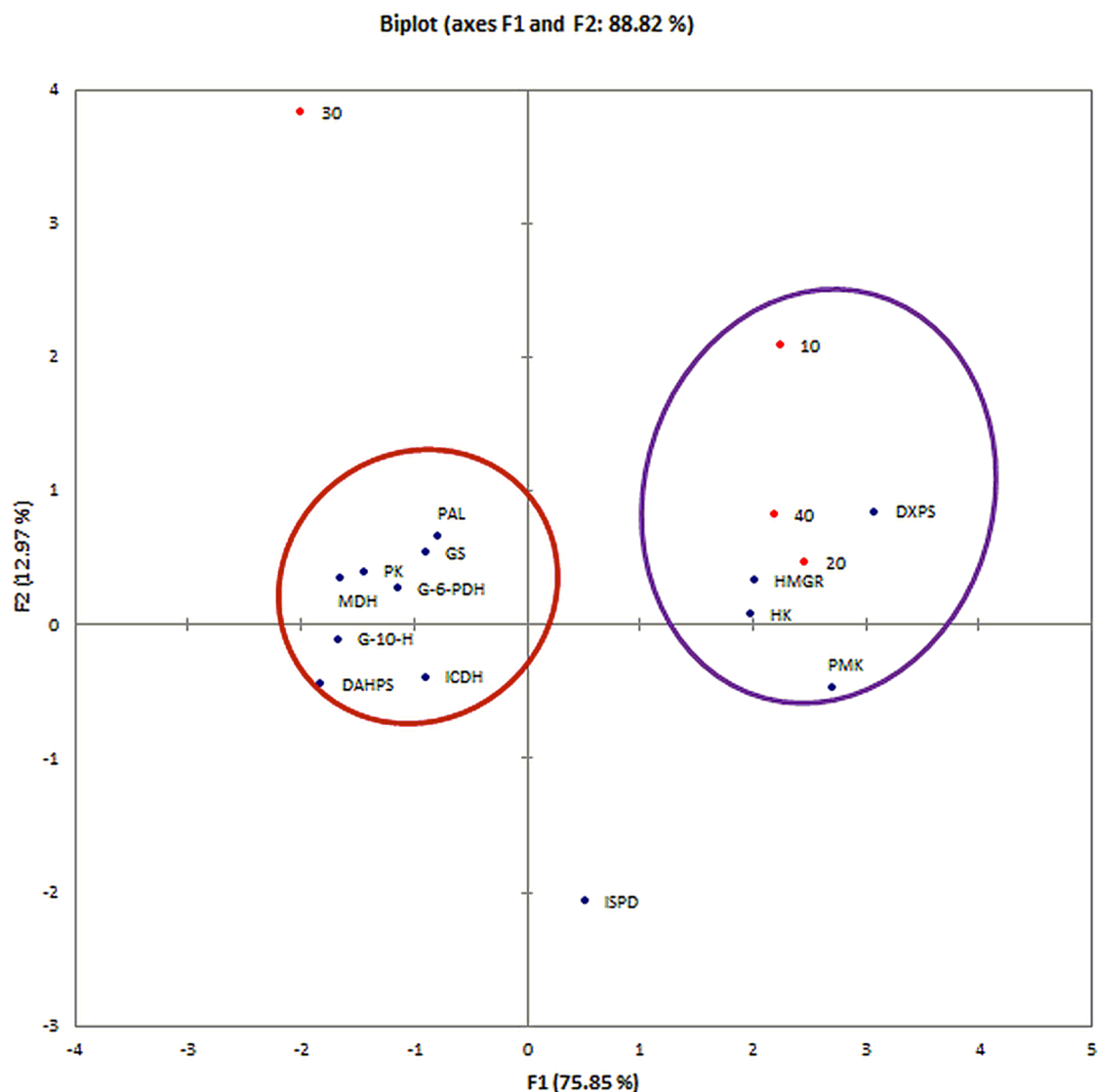
Figure 4.9. Biplot (F1 and F2) showing different conditions *i.e.* 10, 20, 30, and 40 days in red dots as observations and thirteen genes as loadings in blue dots. Genes grouped in red circle are highly correlated with 30 days observation, whereas genes that are grouped in purple circle are highly correlated with 20 days observation.

4.7. Optimization of precursors concentrations for maximum P-I production

Different concentrations of CA (70, 150 and 230 μM), CAT (30, 70 and 150 μM) and mixture of CA and CAT (70 μM CA+30 μM CAT, 150 μM CA+70 μM CAT and 230 μM CA+150 μM CAT), were investigated for their influence on P-I production in shoot cultures of *P. kurroa* established at 15°C. The maximum up-regulation in P-I content was observed at 150 μM CA and the mixture of 150 μM CA+70 μM CAT with 1.6- and 4.2-fold, respectively as compared to control i.e. shoot cultures without precursor treatment

(Figure 4.10). In contrast, different concentrations of CAT did not increase P-I content upon comparison with control. These observations infer 150 µM CA and 150 µM CA+70 µM CAT as optimum concentrations for P-I production *in vitro*. The chromatograms obtained from HPLC showing peaks of P-I in samples treated with optimum concentrations of the above precursors as compared to authentic standard are provided in Figure 4.11.
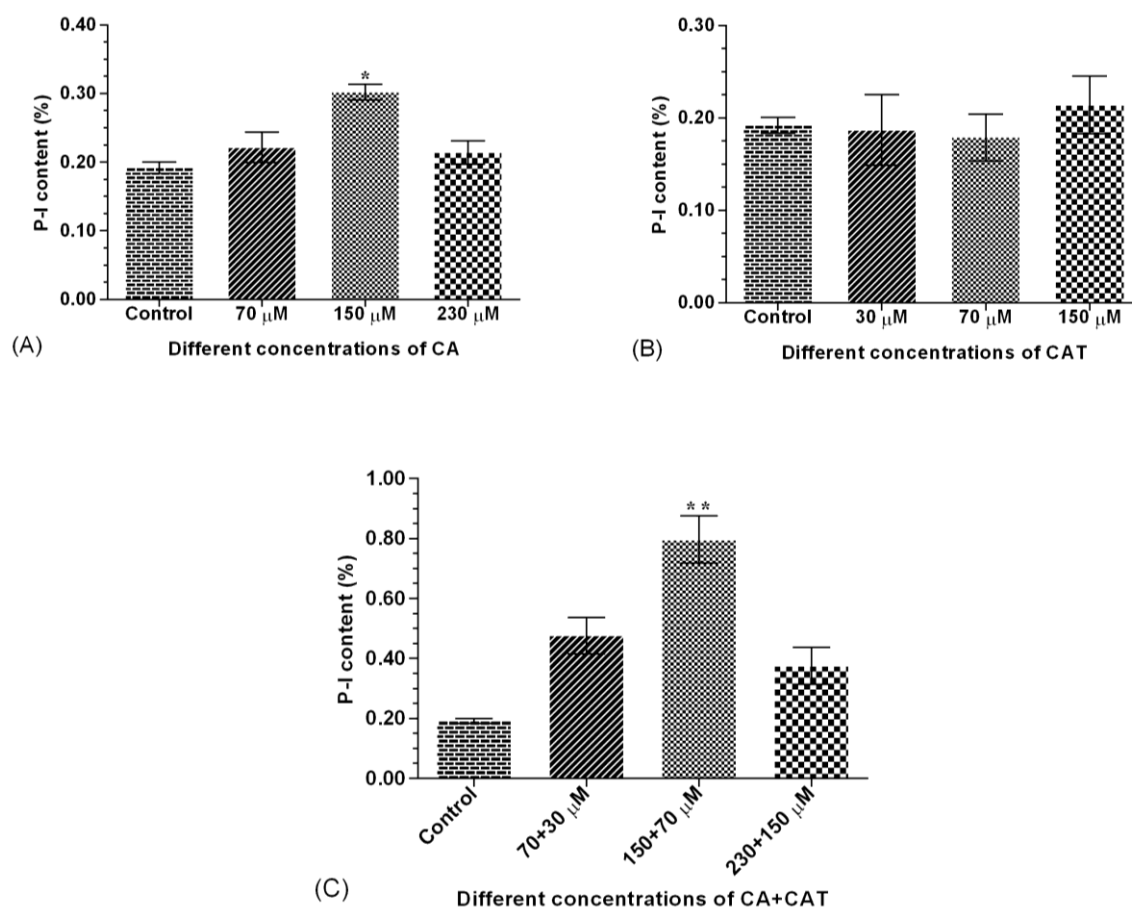
Figure 4.10. Determination of the optimum concentration for different precursor treatments: (A) CA, (B) CAT and, (C) CA+CAT. The optimum concentrations were determined by observing their effects on increase in the P-I content. The data has been presented as means ± SD (n = 3). Significance was assessed within each fed samples between different concentrations of treatments and untreated control (*p<0.05, **p<0.01).
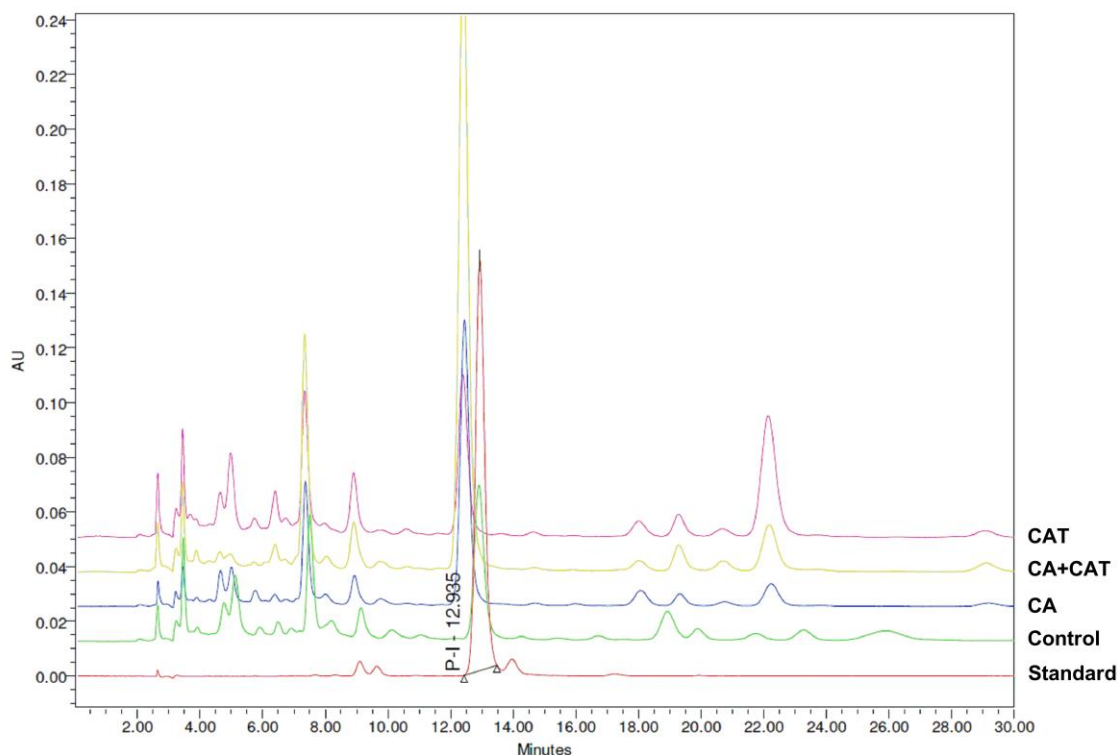
Figure 4.11. HPLC chromatograms of P-I standard and samples i.e. control, CA, CAT and CA+CAT. AU denotes Absorbance Units.

4.8. Influence of CA, CAT and CA+CAT treatments on CA and p-CA contents

The *P. kurroa* shoot cultures fed with optimum concentrations of CA (150 µM), CAT (150 µM) and CA+CAT (150 µM CA+70 µM CAT) along with control (untreated shoots) were analysed for CA and p-CA contents through HPLC. The analysis of CA content revealed 3.8-fold increase in shoot cultures fed with CA+CAT; while it showed non-significant modulation in CA and CAT fed shoot cultures as compared to control (Figure 4.12). Conversely, p-CA content showed 1.5-fold significant elevation in CA treated shoot cultures while non-significant increase was observed in CA+CAT and CAT fed shoot cultures as compared to control (Figure 4.12). The chromatograms obtained from HPLC showing peaks of CA and p-CA in samples treated with optimum concentrations of precursors as compared to their authentic standards are given in Figure 4.13.
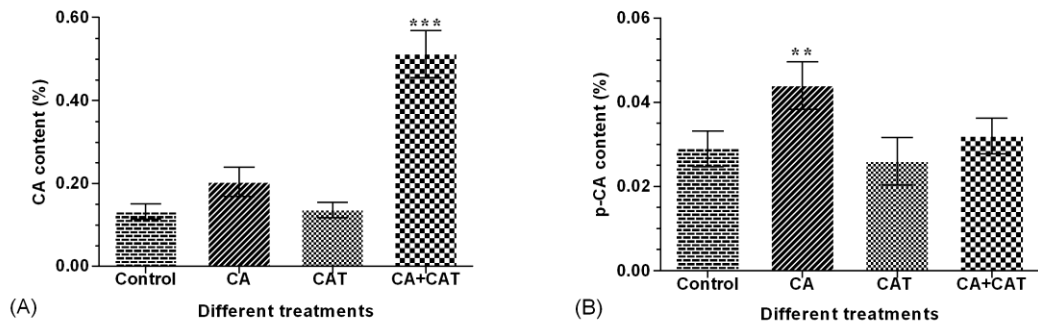
Figure 4.12. Effect of different precursor treatments on the production of tested metabolites: (A) CA and (B) p-CA. The data has been presented as means ± SD (n = 3). Significance was assessed between different treatments and control (**$p<0.01$, ***$p<0.001$).
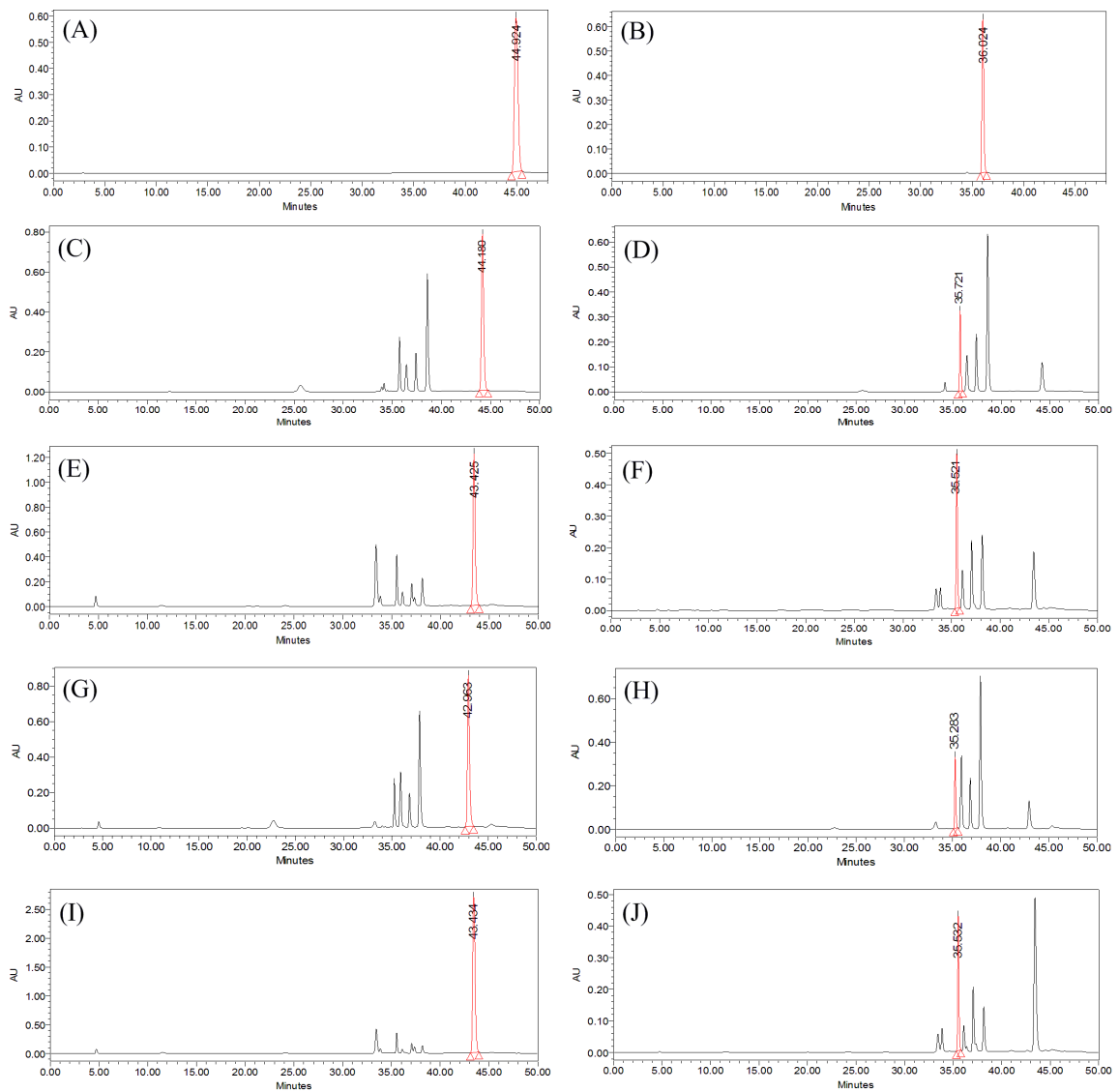
Figure 4.13. HPLC chromatograms of CA standard (A), p-CA standard (B), control (C, D), CA fed shoots (E, F), CAT fed shoots (G, H), and CA+CAT fed shoots (I, J). AU denotes Absorbance Units.

4.9. Expression profiling of shikimate/phenylpropanoid and iridoid pathways genes in shoot cultures fed with optimum concentrations of CA, CAT and CA+CAT

The expression levels of genes catalyzing rate limiting steps in iridoid and shikimate/phenylpropanoid pathways were determined through qRT-PCR in shoot cultures of *P kurroa* fed with optimum concentrations of CA (150 μM), CAT (150 μM) and CA+CAT (150 μM CA+70 μM CAT). The analysis of shoot cultures fed with CA revealed non-significant alterations in expression levels of genes encoding GS, G10H, DAHPS and C4H enzymes, while reduced levels of *PAL* and *CM* transcripts with 8.2- and 3-fold were observed as compared to control shoot cultures (Figure 4.14). In contrast, the shoot cultures fed with CA+CAT showed up-regulation of *DAHPS* and *CM* transcripts with 2.4- and 1.8-fold, respectively, whereas genes encoding GS, PAL and C4H enzymes were down-regulated by 2.4-, 6.2-, and 1.4-fold, respectively as compared to control shoot cultures. The transcript level of *G10H* showed non-significant alteration in CA+CAT fed shoot cultures as compared to control (Figure 4.14). Moreover, the investigation of *P. kurroa* shoot cultures fed with CAT at its optimum concentration revealed down-regulated transcript levels of GS, G10H and C4H enzymes by 12.9-, 2.7-, and 1.5-fold, respectively as compared to control shoot cultures. However, non-significant alterations in expression levels of transcripts encoding PAL, CM and DAHPS enzymes were observed among CAT fed shoot cultures as compared to control (Figure 4.14).

It was thus evident from these results that significant alterations in the expression levels of selected genes to the tune of P-I content in *P. kurroa* shoot cultures fed with CA, CAT and CA+CAT might be due to their regulatory role in P-I biosynthesis.
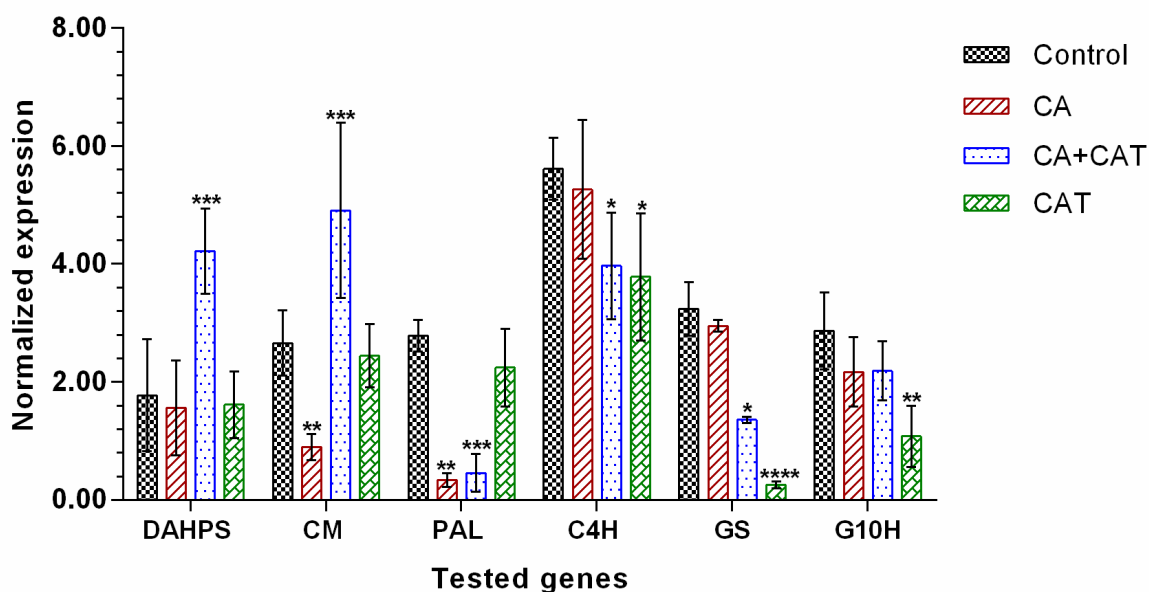
Figure 4.14. Expression profiles of selected shikimate/phenylpropanoid and iridoid pathways genes in CA, CAT and CA+CAT fed shoot cultures of *P. kurroa*. The data has been presented as means ± SD (n = 3). Significance was assessed for each gene between different treatments and untreated control (*$p<0.05$, **$p<0.01$, ***$p<0.001$, ****$p<0.0001$). Expression values were normalized with levels of 26S reference gene.

4.10. Effect of CA, CAT and CA+CAT treatments on PAL activity

The determination of activity for PAL enzyme in *P kurroa* shoot cultures fed with optimum concentrations of CA (150 μM), CAT (150 μM) and CA+CAT (150 μM CA+70 μM CAT) revealed significant differences as compared to control shoot cultures. The activity of PAL enzyme showed significant up-regulation in shoot cultures fed with CA+CAT by 1.2-fold as compared to control shoot cultures (Figure 4.15). In contrast, PAL activity was significantly down-regulated in *P. kurroa* shoot cultures fed with CA by a fold change of 1.2, whereas it showed non-significant modulation in CAT fed shoot cultures of *P. kurroa* upon comparison with control shoot cultures (Figure 4.15).
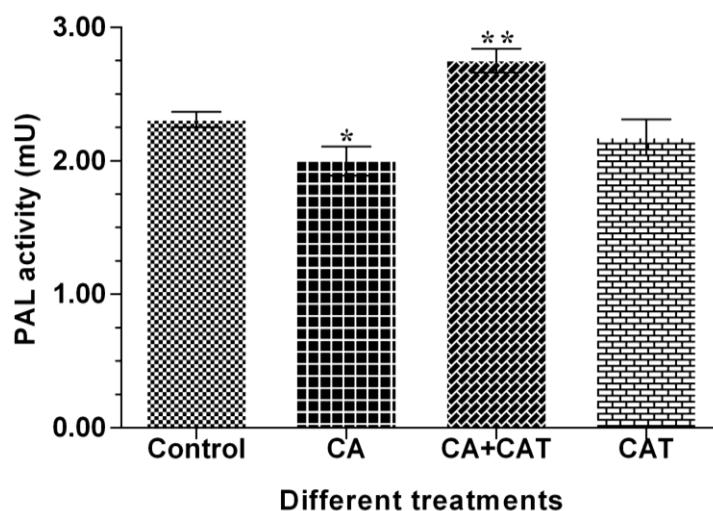
Figure 4.15. Activity profiles of PAL in CA, CAT and CA+CAT fed shoot cultures of *P. kurroa*. The data has been presented as means ± SD (n = 3). Significance was assessed between different treatments and untreated control (*$p<0.05$, **$p<0.01$).

4.11. Correlations between selected genes and metabolite levels from control, CA, CAT and CA+CAT fed shoot cultures of *P. kurroa*

The correlations in the form of Pearson's correlation coefficient i.e. PCC were observed among selected genes of shikimate/phenylpropanoid pathway (*DAHPS*, *CM*, *PAL* and *C4H*), iridoid/monoterpene pathway (*GS* and *G10H*) and contents of tested metabolites (P-I, CA and p-CA) between different precursor's treatments *viz.* control, CA, CAT and CA+CAT. The correlations are displayed as correlogram and are given in Figure 4.16. The correlation analysis revealed that P-I content was significantly associated with CA content (PCC, 0.99) and transcripts levels of DAHPS (PCC, 0.97) and CM (PCC, 0.78) enzymes with high positive correlation coefficient (Figure 4.16). Moreover, a low positive correlation of P-I content was also observed with p-CA content (PCC, 0.31) and gene encoding G10H enzyme (PCC, 0.14). In contrast to this, P-I content was negatively correlated with transcripts levels of GS (PCC, -0.19), PAL (PCC, -0.68) and C4H (PCC, -0.42) enzymes (Figure 4.16). It was thus evident form these correlations that DAHPS, CM, CA and G10H enzymes might play an important role in the P-I biosynthesis whereas PAL and GS enzymes could be the potential regulatory sites of its biosynthesis in shoot cultures of *P. kurroa*.
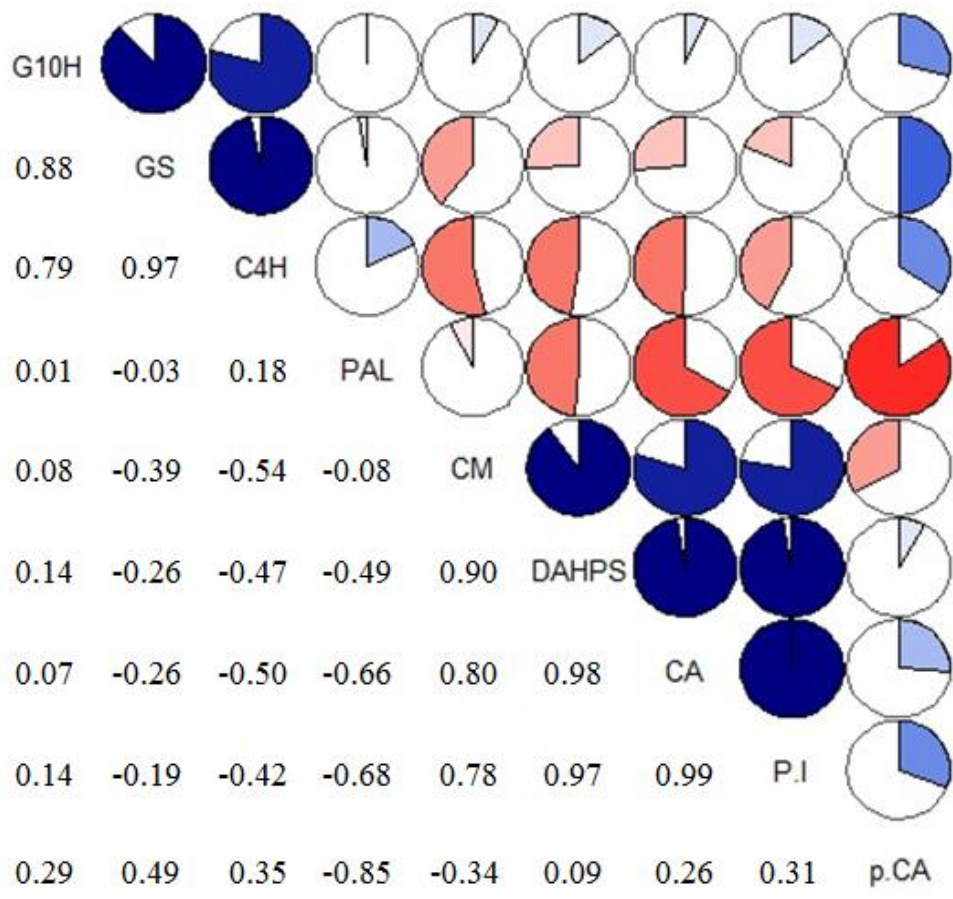
Figure 4.16. Correlations of tested genes and metabolites data depicted as correlogram. PCC in genes and metabolites from the control, CA, CAT and CA+CAT treatment groups. The data has been presented in the form of pie graphs filled in proportion to the PCC values. Positive correlations are represented by blue colored pie graphs filled clockwise while red colored pie graphs filled anti-clockwise indicate negative correlations.

4.12. Picrosides (P-I and P-II) contents in different accessions of *P. kurroa*

A total of 10 different accessions were analyzed for P-I and P-II contents separately in shoots and stolons tissues (on fresh weight basis) of *P. kurroa*. The analysis of shoot tissues of different *P. kurroa* accessions revealed significant variations in P-I content (Figure 4.17a). The maximum level of P-I was observed in PKS-1 which showed 1.9-, 2.1-, 2.3-, 2.5-, 3.4-, 3.6-, 3.6-, 4.7- and 17.7-fold increment over PKS-5, PKS-2, PKS-3, PKS-26, PKS-16, PKS-18, PKS-14, PKS-4 and PKS-21, respectively (Figure 4.17a). In contrast, P-II was not detected in shoots of *P. kurroa* plants. It was evident from the results that PKS-1 and PKS-5 showed maximum P-I content and thus, referred to as high

P-I content accessions of *P. kurroa*. Conversely, PKS-4 and PKS-21 showed minimum P-I content and thus, referred to as low P-I content accessions of *P. kurroa*.

Upon analysis of stolons portions of different *P. kurroa* accessions, significant modulations in both P-I and P-II contents were observed (Figure 4.17b). The maximum P-II content i.e. 2.65% was observed in PKST-3 which showed significant progressive decrease leading to PKST-18 with 1.9-fold lower P-II content (Figure 4.17b). In contrast, the minimum P-I content of 0.01% was detected in PKST-4 followed by non-significant increase in PKST-5 (0.08%) and PKST-3 (0.17%) stolons. Further, the stolons of PKST-1, PKST-2, PKST-14, PKST-26, PKST-16 and PKST-18 showed significant progressive increase in P-I content with 5.3-, 8.6-, 8.8-, 10.2-, 13.1- and 16.5-fold, respectively as compared to PKST-5 (Figure 4.17b). These observations imply that PKST-3 and PKST-5 stolons contained maximum P-II content but minimum P-I content and thus, referred to as high P-II content accessions of *P. kurroa*. Conversely, PKST-16 and PKST-18 stolons contained minimum P-II but maximum P-I content and thus, referred to as low P-II content accessions of *P. kurroa*.

(a)

(b)
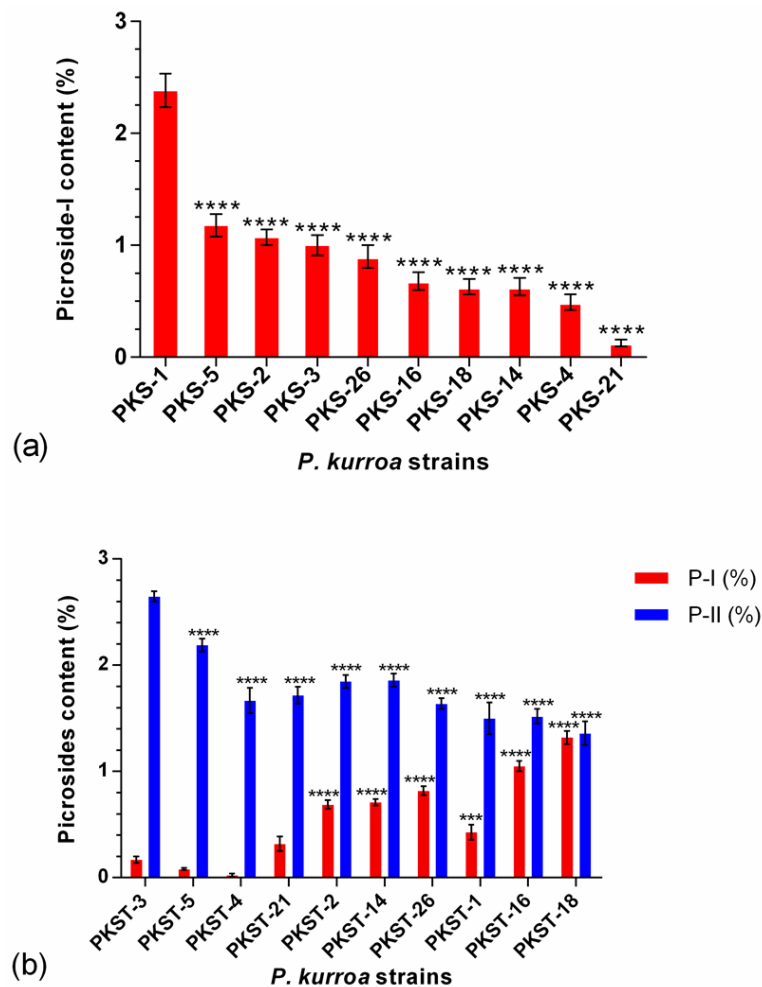
Figure 4.17. Determination of picrosides contents in different tissues of *P. kurroa* accessions; (a) shoots and, (b) stolons. The data presented as means ± SD (n = 3). Significance was assessed within picrosides contents between different accessions (***$p<0.001$, ****$p<0.0001$).

4.13. Alterations in the levels of intermediate metabolites of shikimate/ phenylpropanoid pathway among *P. kurroa* accessions

The shoots and stolons of *P. kurroa* accessions selected for high and low P-I/P-II contents were examined for the levels of intermediate metabolites in shikimate/phenylpropanoid pathway *viz.* CA, p-CA, FA, PA and VA.

4.13.1. Intermediate metabolites contents among shoot tissues of *P. kurroa* accessions

The investigation of shoot tissues revealed that PKS-1 contained maximum CA content of 0.5% which showed significant progressive decrease in PKS-5, PKS-4 and PKS-21 with 1.5-, 2.5- and 5.3-fold, respectively (Figure 4.18b). These results are similar to P-I accumulation patterns in selected shoot tissues of *P. kurroa*. In contrast, the lowest p-CA content (0.04%) was observed in PKS-1 and showed significant increase in PKS-5 and PKS-21 with 2.1- and 5.9-fold, respectively. The p-CA content of PKS-4 showed non-significant alteration as compared to PKS-1 shoots (Figure 4.18b). Further, the examination of FA content in shoot tissues revealed 2-fold significant elevation in PKS-21 as compared to PKS-1, PKS-5 and PKS-4 accessions (Figure 4.18b). Moreover, the VA content showed non-significant modulation among all the four selected shoots of *P. kurroa*. The PA content was not detected in the selected shoots of *P. kurroa*. It was thus evident from these results that CA is positively correlated with P-I content in shoots with Pearson correlation coefficient (PCC) of 0.99 (Figure 4.18c). The chromatograms obtained from HPLC showing the peaks of CA, p-CA, PA, FA and VA in shoot tissues of different *P. kurroa* accessions as compared to their authentic standards are provided in Figure 4.19.
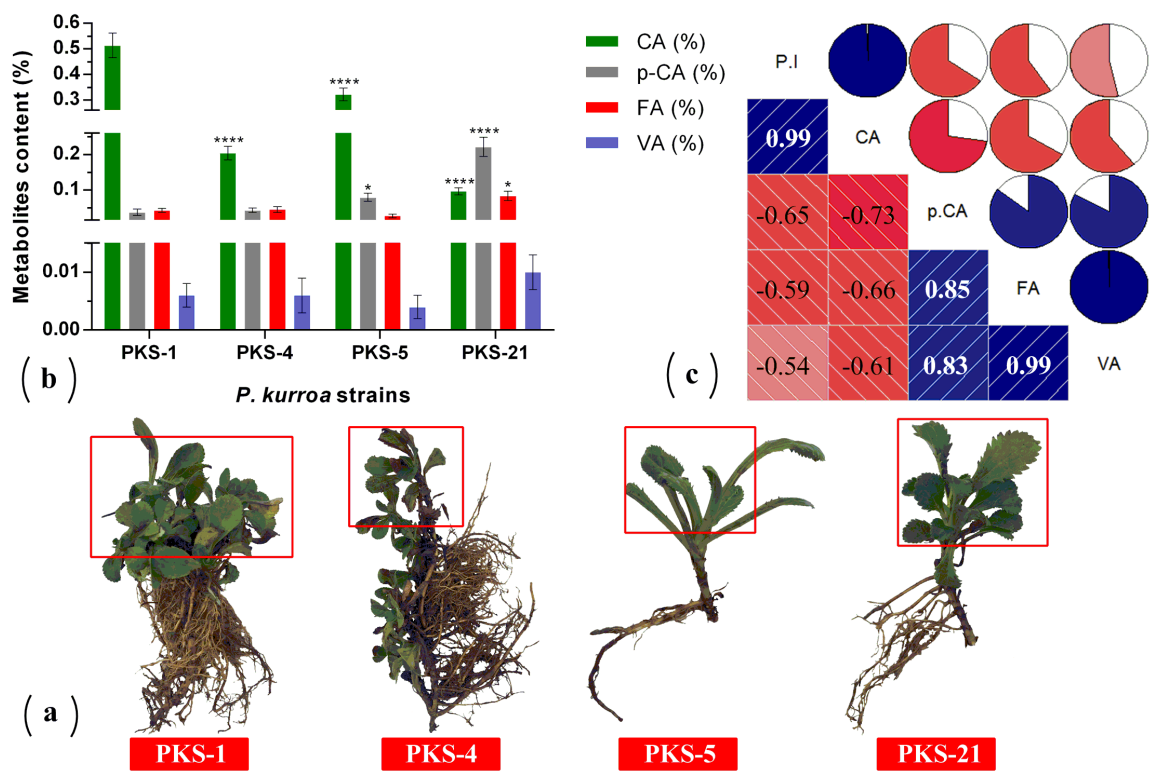
Figure 4.18. Comparative analysis of intermediate metabolites contents among shoot tissues of *P. kurroa* accessions; (a) different *P. kurroa* accessions selected for shoots; (b) variations in metabolites contents among shoots and; (c) correlogram showing correlations between tested metabolites and picrosides contents among shoots. Correlations are presented in the form of pie graphs filled in proportion to the Pearson's correlation coefficient values. Clock-wise occupied with blue color depict positive correlations while anti-clockwise pie graphs filled with red color indicate negative correlations. The data has been presented as means ± SD (n = 3). Significance was assessed within metabolites contents between different accessions (*$p<0.05$, ****$p<0.0001$).
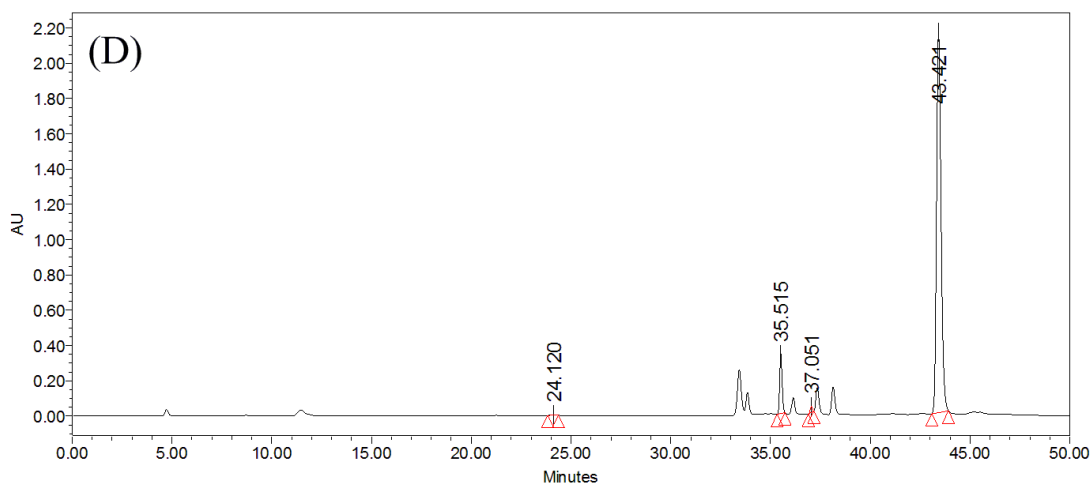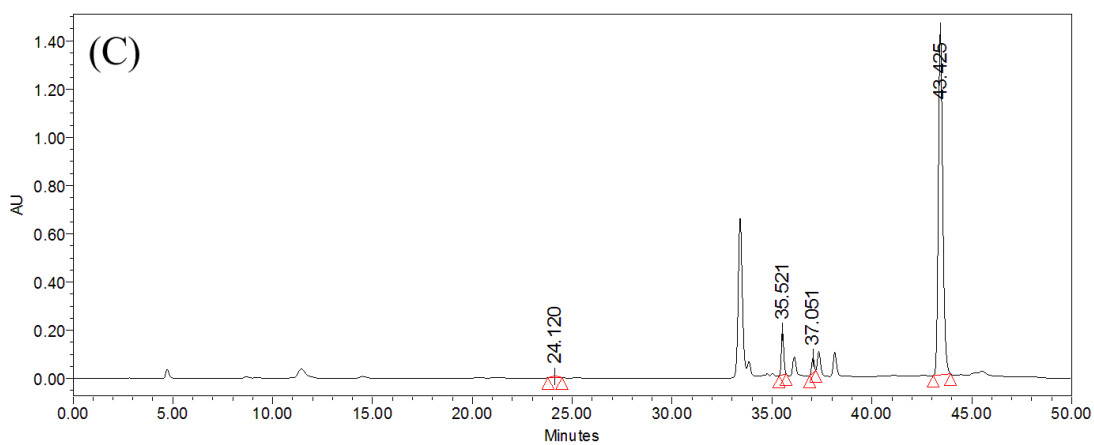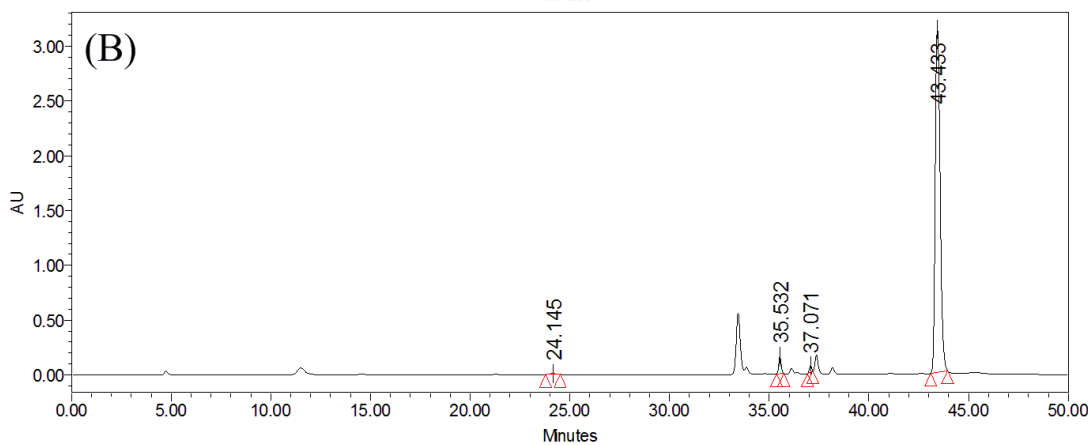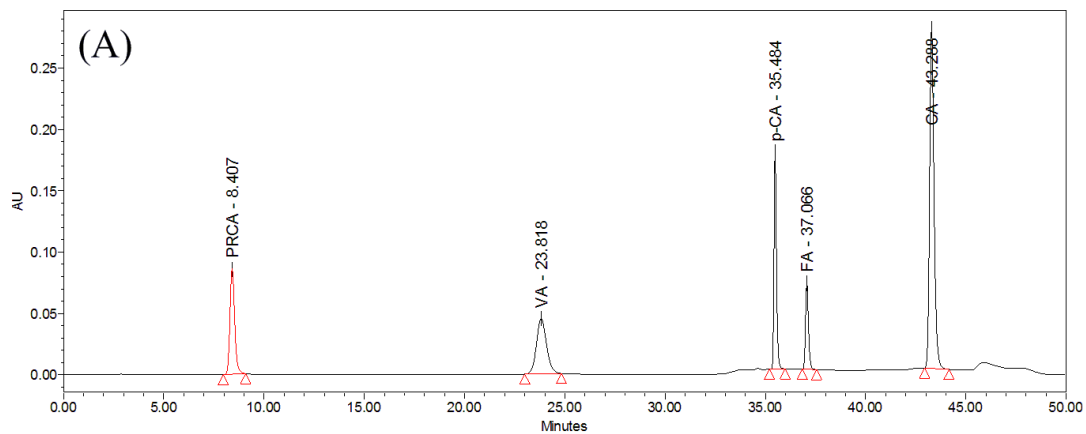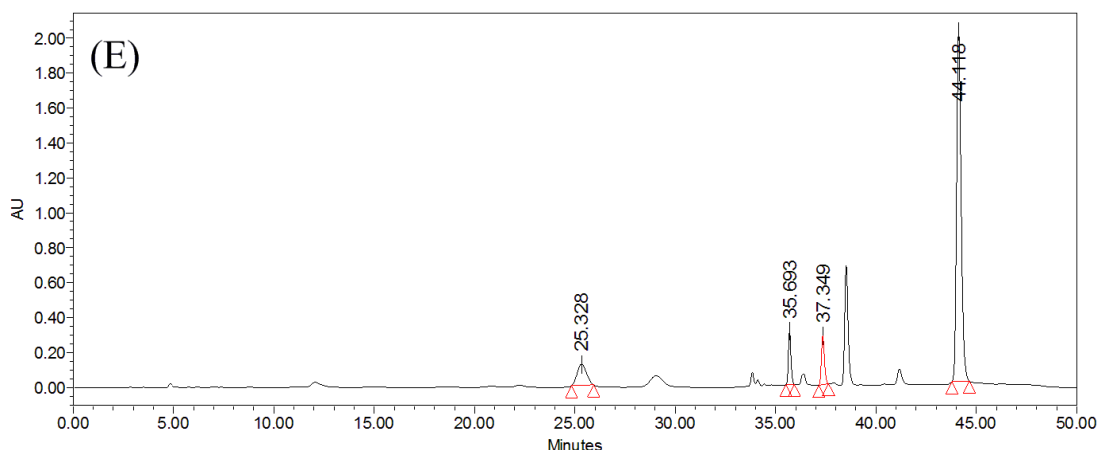
Figure 4.19. HPLC chromatograms of the CA, p-CA, FA, PA/PRCA and VA standards (A); PKS-1 shoots (B); PKS-4 shoots (C); PKS-5 shoots (D); and PKS-21 shoots (E). AU denotes Absorbance Units.

4.13.2. Intermediate metabolites contents among stolon tissues of *P. kurroa* accessions

The investigation of four different stolons revealed that PKST-18 contained maximum CA content of 0.2% which showed significant increase of 4.7-fold as compared to PKST-3 (Figure 4.20b). The CA content of PKST-3 showed non-significant modulation with PKST-5 and PKST-16 stolons. The analysis of p-CA content showed non-significant alterations in all the four selected stolons of *P. kurroa*. Upon examination of FA content, we observed highest level in PKST-5 (0.2%) which exhibited 1.7-fold significant increase as compared to PKST-3, PKST-16 and PKST-18 (Figure 4.20b). In contrast, highest VA content was observed in PKST-3 and PKST-5 followed by significant decrease in PKST-16 and PKST-18 with 2.2- and 1.3-fold, respectively (Figure 4.20b). Moreover, PA content was not observed in the stolons of *P. kurroa*. These observations infer positive correlations of p-CA and VA with P-II through PCC of 0.45 and 0.79, respectively (Figure 4.20c). The chromatograms obtained from HPLC, which showed peaks of CA, p-CA, PA, FA and VA in stolon tissues of different *P. kurroa* accessions compared to their authentic standards are provided in Figure 4.21.
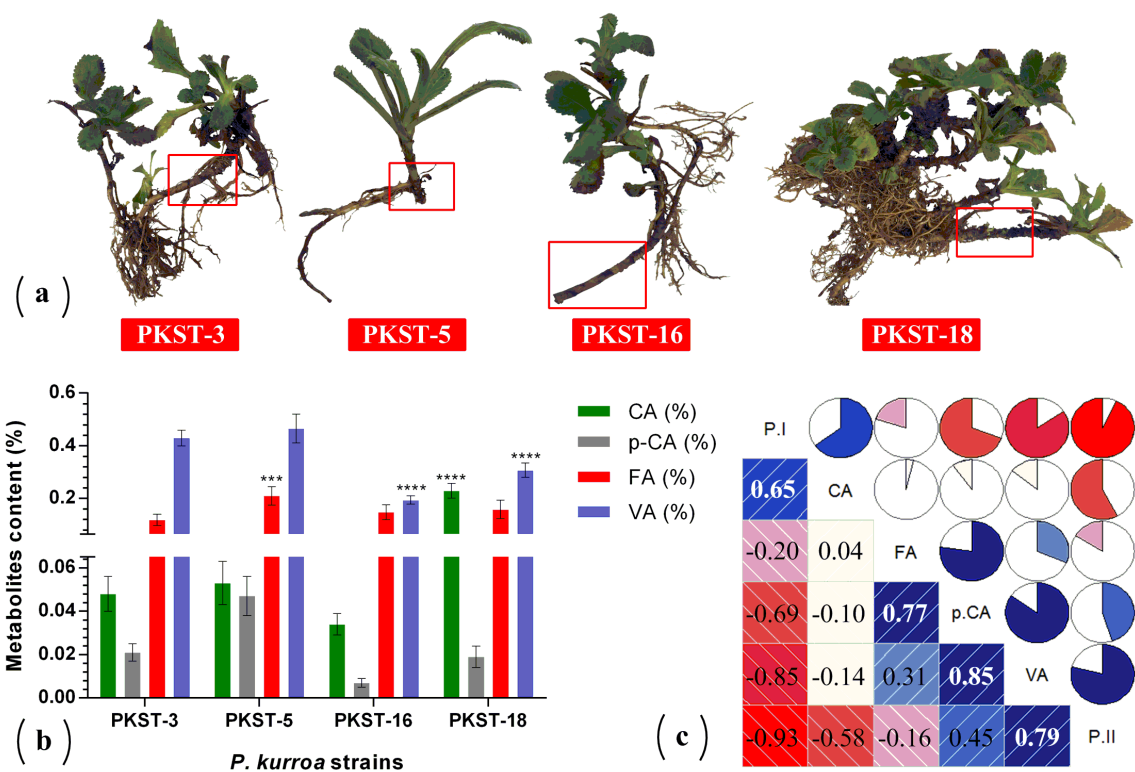
Figure 4.20. Comparative analysis of intermediate metabolites contents among stolon tissues of *P. kurroa* accessions; (a) different *P. kurroa* accessions selected for stolons; (b) variations in metabolites contents among stolons and; (c) correlogram showing correlations between tested metabolites and picrosides contents among stolons. Correlations are presented in the form of pie graphs filled in proportion to the Pearson's correlation coefficient values. Clock-wise occupied with blue color depict positive correlations while anti-clockwise pie graphs filled with red color indicate negative correlations. The data presented as means ± SD (n = 3). Significance was assessed within metabolites contents between different accessions (***$p<0.001$, ****$p<0.0001$).
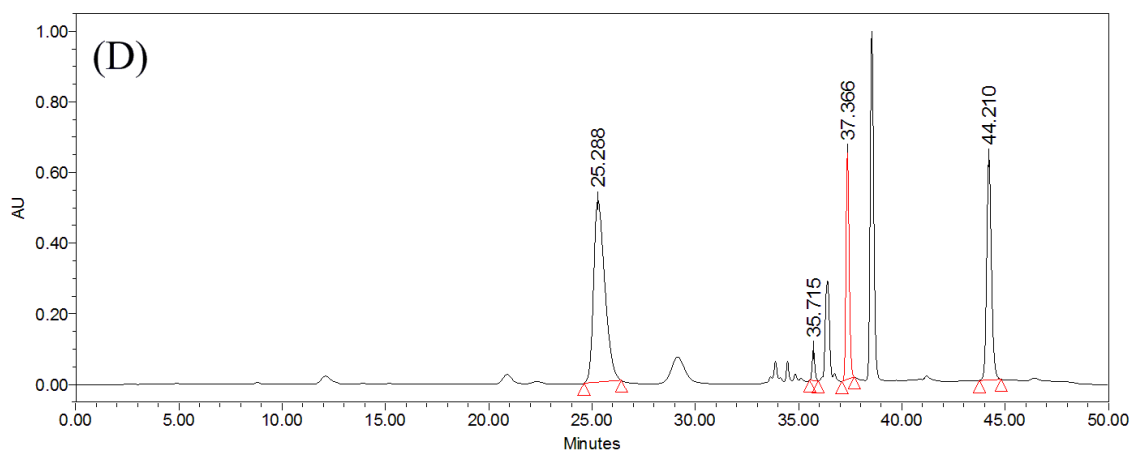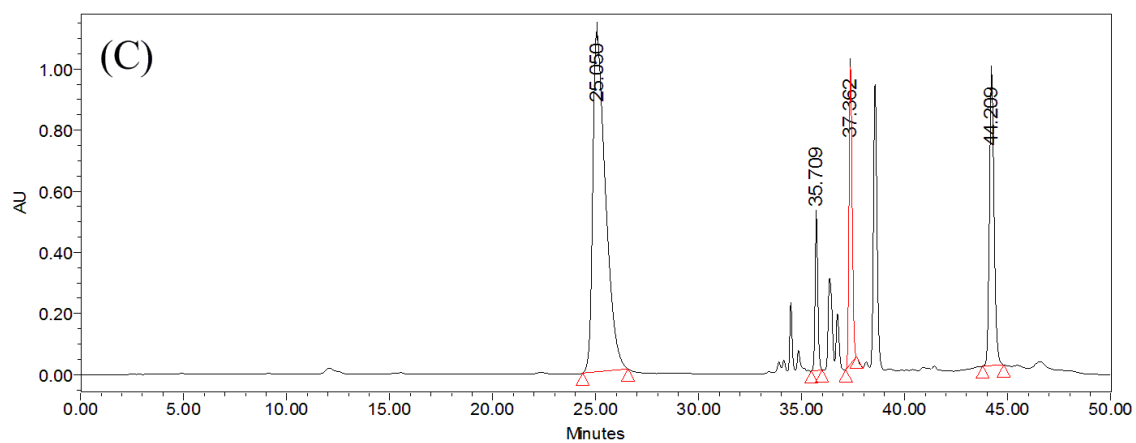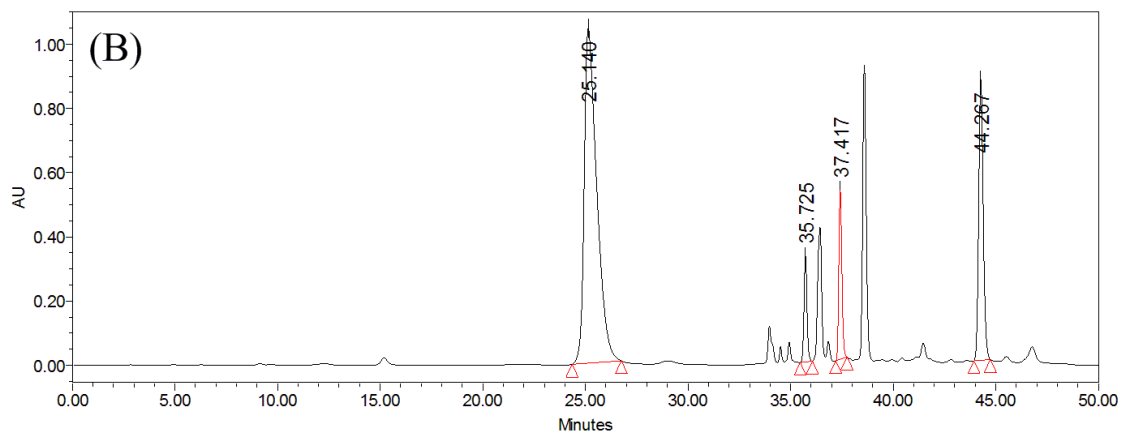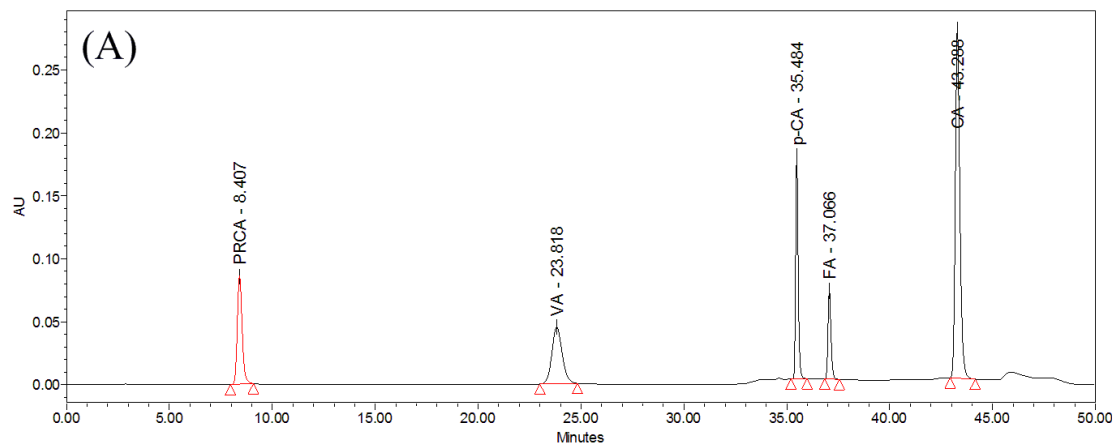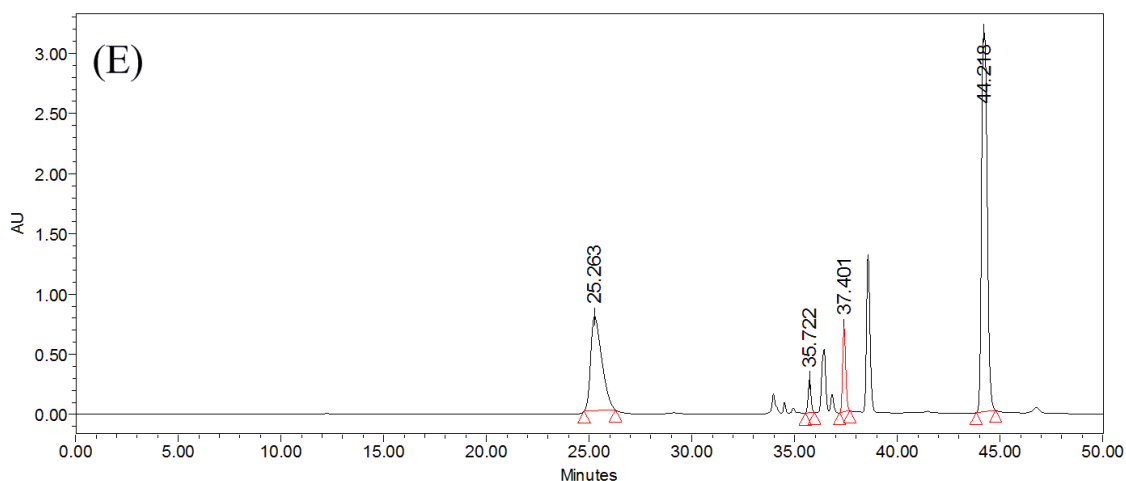
Figure 4.21. HPLC chromatograms of the CA, p-CA, FA, PA/PRCA and VA standards (A); PKST-3 stolons (B); PKST-5 stolons (C); PKST-16 stolons (D); and PKST-18 stolons (E). AU, Absorbance Units.

4.14. Alterations in picrosides and intermediate metabolites contents among shoot cultures fed with p-CA, FA, PA, P-II and VA+CAT

The *in vitro* grown shoot cultures of *P. kurroa* were treated with 150μM concentration of PA, FA and p-CA along with combination of 150μM VA and 70μM CAT to observe their effects on the CA, p-CA, FA, VA, P-I and P-II contents (Figure 4.22a-c). The analysis of CA content revealed 2.2- and 1.7-fold significant increase in shoot cultures treated with FA and p-CA, respectively, whereas 1.3-fold significant decrease was observed in VA+CAT fed shoot cultures as compared to *P. kurroa* shoots without treatment i.e. control shoots (Figure 4.22a). The p-CA content, on the other hand showed non-significant modulations in all the fed shoots as compared to control. The investigation of FA content revealed a significant increase of 2.9-fold in shoot cultures treated with FA as compared to untreated shoots. In contrast, 1.9- and 2-fold significant elevation in VA content was observed in shoot cultures fed with FA and VA+CAT, respectively as compared to control (Figure 4.22a). Moreover, the examination of P-I content revealed 1.8-fold significant enhancement in shoot cultures fed with p-CA as compared to control. Conversely, small level of P-II i.e. 0.04% was only detected in *P. kurroa* shoot cultures treated with VA + CAT (Figure 4.22a). Thus, it was evident from these results that VA and P-II shared high positive correlation with PCC of 0.64 and the former was also positively correlated with CA and FA with PCC of 0.19 and 0.22, respectively (Figure 4.22c).

Since, P-II was only detected in VA+CAT fed shoots, therefore, different concentrations of VA + CAT (25 µM VA + 25 µM CAT, 70 µM VA + 70 µM CAT, 70 µM VA + 150 µM CAT, 150 µM VA + 150 µM CAT and 230 µM VA + 230 µM CAT) were further tested to observe their influence on the P-II content. The data revealed non-significant alterations in P-II content among *P. kurroa* shoot cultures treated with different concentrations of VA+CAT (Figure 4.22b). Moreover, the P-II content also exhibited non-significant alteration in shoot cultures fed with P-II while 0.2% P-II was observed in the media remained after the sampling of shoot cultures treated with P-II (Figure 4.22b). It was thus evident from these results that exogenous P-II was not taken up by the plants in its pure form.
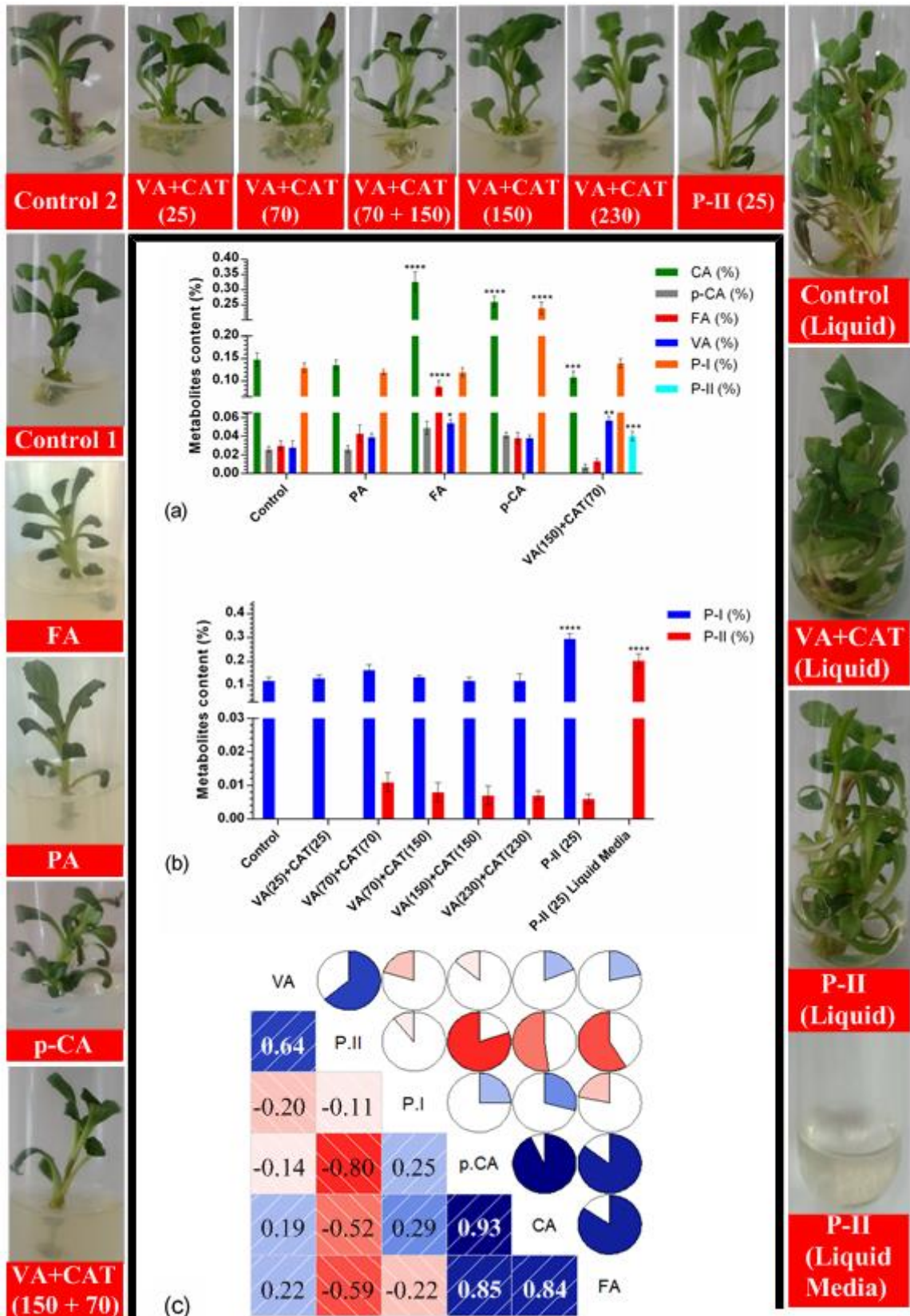
Figure 4.22. Effects of various precursors feeding on the contents of tested metabolites; (a) variations in metabolites contents between different precursor treatments i.e. PA, FA and p-CA at 150 µM concentration along with 150 µM VA + 70 µM CAT; (b) variations in picrosides contents among different concentrations of VA+CAT along with P-II and liquid media remained after the collection of samples and; (c) correlogram showing correlations between tested metabolites and picrosides contents among different precursors treated samples. Correlations are presented in the form of pie graphs filled in proportion to the Pearson's correlation coefficient values. Clock-wise occupied with blue color depict positive correlations while anti-clockwise pie graphs filled with red color indicate negative correlations. The data has been presented as means ± SD (n = 3). Significance was assessed within metabolites contents between different precursor's treatments (*$p<0.05$, **$p<0.01$, ***$p<0.001$, ****$p<0.0001$).

4.15. Correlation analysis between picrosides contents and transcripts abundance values (FPKM)

To get insight into flux dynamics of different metabolic modules connected to picrosides biosynthesis, correlation maps were constructed between the FPKM values of selected gene transcripts and picrosides content among different shoots and stolons accessions of *P. kurroa* (Figure 4.23). The transcripts encoding enzymes catalyzing regulatory reactions in different metabolic pathways were selected based on their connection with picrosides biosynthesis. The details of selected transcripts with their role in picrosides production are provided in Table 3.3.

The correlation analysis among selected accessions of shoots *viz.* PKS-1, PKS-5, PKS-4 and PKS-21 revealed positive correlations of *PAL* (0.66), *PEPCK* (0.60), *DAHPS* (0.92), *4CL* (0.57), *PK* (0.03), *AS* (0.45), *GS* (0.09) and *G6PDH* (0.24) with P-I content while rest of the selected gene transcripts showed negative correlations (Figure 4.23d). In contrast, the correlation analysis among selected accessions of stolons *viz.* PKST-3, PKST-5, PKST-16 and PKST-18 revealed positive correlations of *PYS* (0.19), *DXPS* (0.43), *PAL* (0.28), *HMGR* (0.94), *HADH* (0.13), *C4H* (0.60), *DAHPS* (0.79) and *GS* (0.51) with P-II content while remaining selected gene transcripts showed negative correlations (Figure 4.23c). These observations implied that *DAHPS*, *PAL*, *PEPCK* and *4CL* showing high positive correlations (>0.60) with P-I content might be considered as

the key candidate genes for P-I biosynthesis. Conversely, *HMGR*, *C4H*, *DAHPS* and *GS* might play an important role in the biosynthesis of P-II in *P. kurroa*.
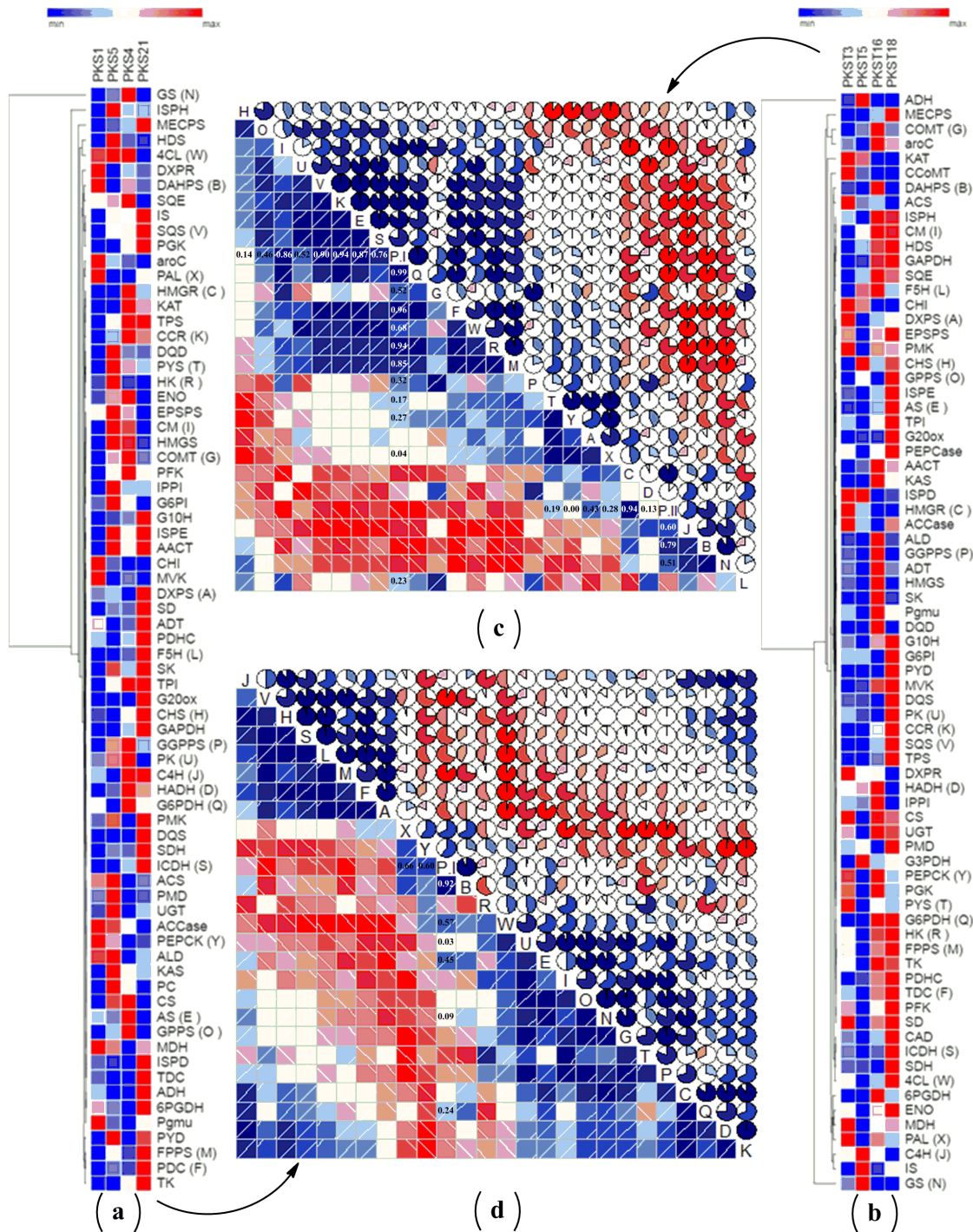
Figure 4.23. Differential expression analysis of genes involved in secondary metabolism among different tissues of *P. kurroa* accessions; (a, b) cluster analysis of differentially expressed genes patterns between different *P. kurroa* accessions selected for shoots and stolons, respectively; (c, d) Correlations in terms of Pearson's correlation coefficients depicted using correlogram between selected genes and metabolites contents among

different stolons and shoots, respectively. The data is represented in the form of pie graphs filled in proportion to the Pearson's correlation coefficient values. Clock-wise occupied with blue color depict positive correlations while anti-clockwise pie graphs filled with red color indicate negative correlations.

4.16. Gene expression profiling among selected accessions of *P. kurroa*

To confirm the differential gene expression patterns obtained through transcriptomes analysis, six genes were randomly selected (having both positive and negative correlations with P-I and P-II contents) and further tested using qRT-PCR. Among the selected different accessions of shoots, the transcripts levels of *DAHPS* showed non-significant modulations (Figure 4.24a). The expression level of *CMT* displayed 1.8-, 1.7- and 3.3-fold significant increase in PKS-4, PKS-5 and PKS-21, respectively as compared to PKS-1 (Figure 4.24b). In contrast, the expression level of *PAL* was maximum in PKS-1 which showed significant decrease in PKS-4, PKS-5 and PKS-21 with 10.7-, 18- and 1.3-fold, respectively (Figure 4.24c). The transcript levels of *C4H* exhibited significant elevation in PKS-4 and PKS-21 with 1.3- and 2.4-fold, respectively, while 2.8-fold significant decrease was observed in PKS-5 as compared to PKS-1 (Figure 4.24d). Moreover, the transcript level of *G10H* showed 3.3- and 2.5-fold significant increment in PKS-5 and PKS-21, respectively compared to PKS-1 (Figure 4.24e). The expression level of HK showed 3.4-fold significant decrease in PKS-4 compared to PKS-1 (Figure 4.24f).

The expression analysis of *DAHPS* gene among different accessions of stolons revealed 2.8-fold significant decrease in PKST-16 as compared to PKST-3 (Figure 4.25a). The expression level of *CMT* displayed 4.5- and 4.4-fold significant increase in PKST-16 and PKST-18, respectively as compared to PKST-3 (Figure 4.25b). In contrast, the expression level of *PAL* showed 10.4-fold significant decrease in PKST-5 as compared to PKST-3 (Figure 4.25c). The transcript level of *C4H* was maximum in PKST-3 which showed significant decrease in PKST-5, PKST-16 and PKST-18 with 2.1-, 2.4- and 5.9-fold, respectively (Figure 4.25d). The transcript level of *G10H* exhibited 1.8-fold significant increment in PKST-16 as compared to PKST-3 (Figure 4.25e). Moreover, the expression level of HK showed 3.2- and 2.8-fold significant elevation in PKST-16 and PKST-18, respectively as compared to PKST-3 (Figure 4.25f).

Finally, the correlations between differential gene expression patterns of six selected genes obtained from transcriptomes data and qRT-PCR were determined and we observed

a coefficient of determination (R^2) ≥ 0.75 which indicates a good positive correlation (Figure 4.26). It was thus evident from the results that gene expression patterns investigated by qRT-PCR were corroborated with those obtained by RNA-seq analysis, thereby supporting the reliability of our transcriptomes data.
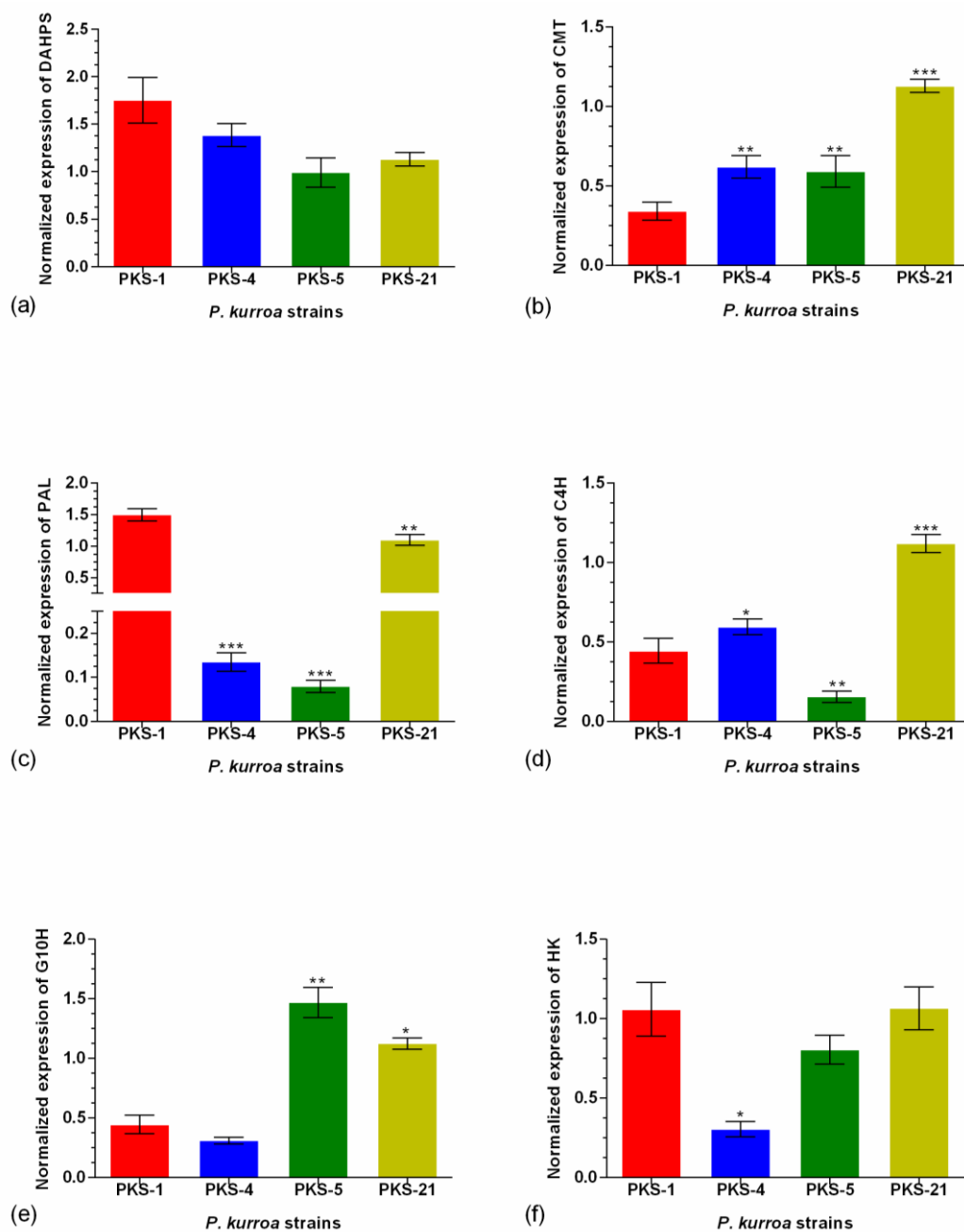
Figure 4.24. Expression profiling of different genes in selected shoot tissues of *P. kurroa* accessions; (a) *DAHPS*, (b) *CMT*, (c) *PAL*, (d) *C4H*, (e) *G10H* and, (f) *HK*. Expression values were normalized with levels of 26S reference gene. The data has been presented as means ± SD (n = 3). Significance was assessed for each gene between different shoots accessions (*$p<0.05$, **$p<0.01$, ***$p<0.001$).
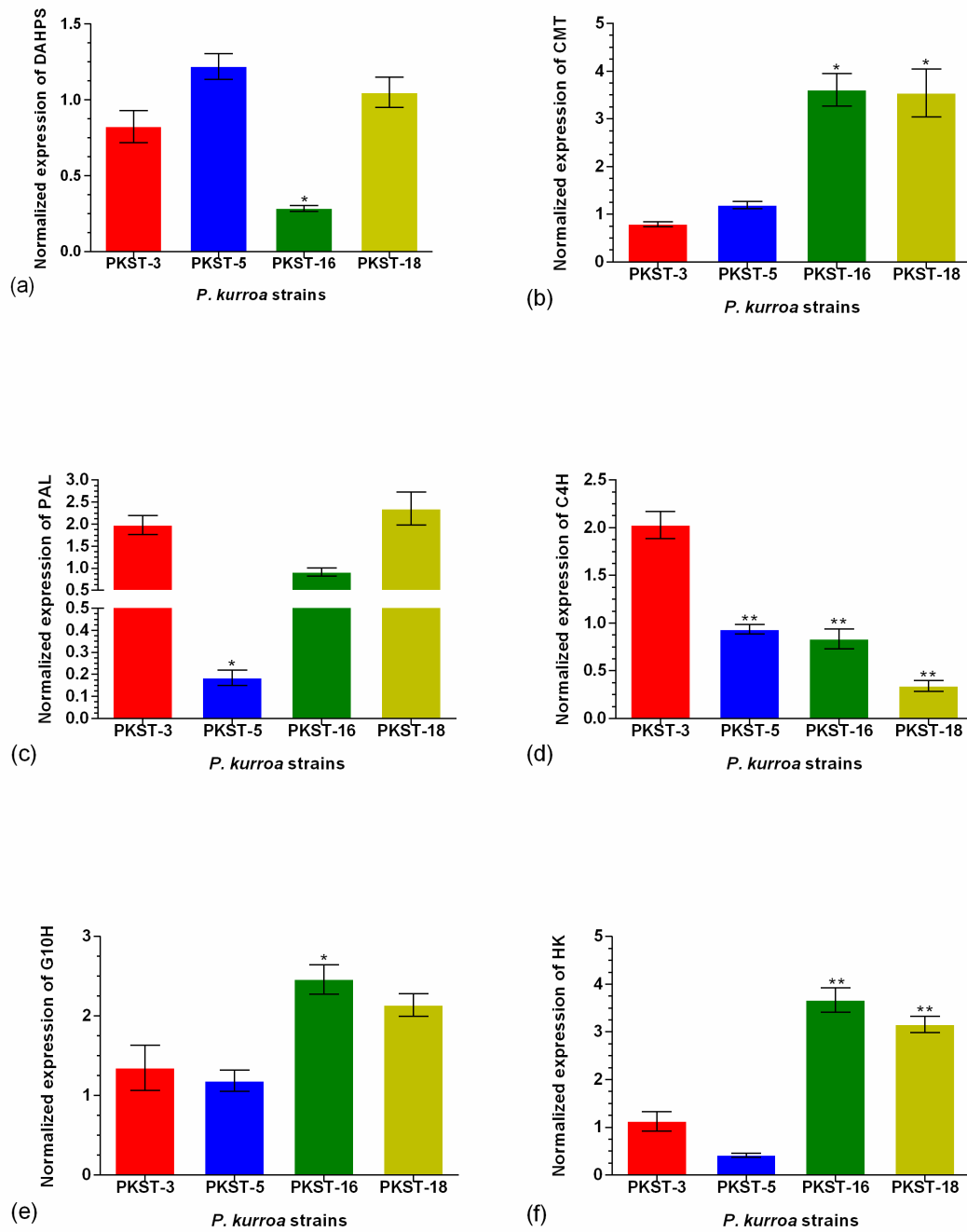
Figure 4.25. Expression profiling of different genes in selected stolon tissues of *P. kurroa* accessions; (a) *DAHPS*, (b) *CMT*, (c) *PAL*, (d) *C4H*, (e) *G10H* and, (f) *HK*. Expression values were normalized with levels of 26S reference gene. The data has been presented as means ± SD (n = 3). Significance was assessed for each gene between different stolons accessions. (*$p<0.05$, **$p<0.01$).
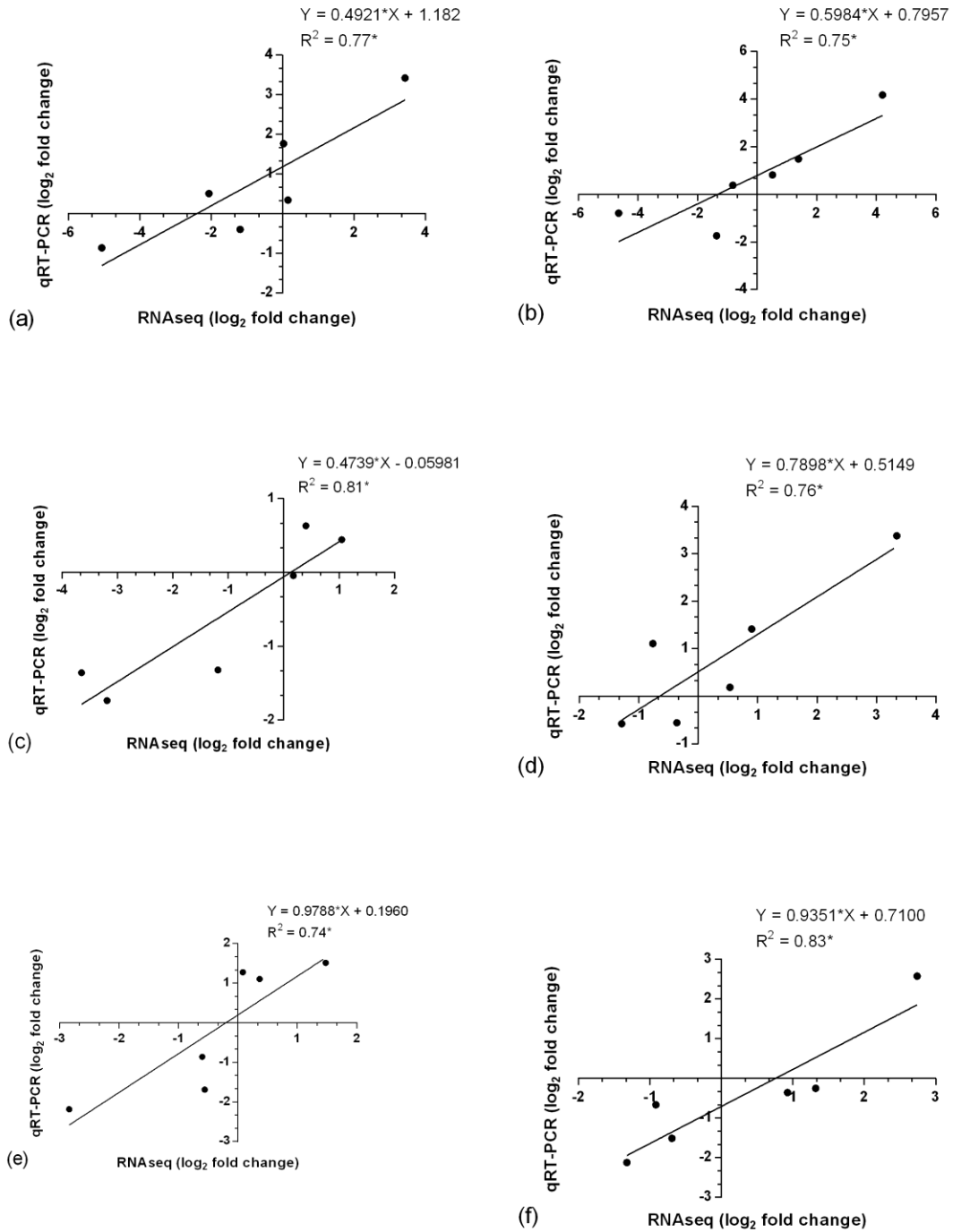
Figure 4.26. Correlations determined between differential gene expression patterns of selected genes among transcriptomes data and qRT-PCR in different tissues of *P. kurroa* accessions; (a) PKS-1 *vs* PKS-4, (b) PKS-1 *vs* PKS-5, (c) PKS-1 *vs* PKS-21, (d) PKST-3 *vs* PKST-5, (e) PKST-3 *vs* PKST-16 and, (f) PKST-3 *vs* PKST-18. R^2 = Coefficient of determination.

DISCUSSION

It is known that a large number of genes are involved in interlinking metabolic processes, including primary metabolism (glycolysis, TCA cycle and pentose phosphate pathway) and secondary metabolism (shikimate/phenylpropanoid, MVA/MEP and monoterpene biosynthetic pathways). This makes deciphering of biosynthetic pathways for plant secondary metabolites a highly cumbersome process considering the complexity of their genetic architecture and low levels of metabolic intermediates and corresponding enzymes catalyzing the steps *in planta* [72]. Further, the secondary metabolites are mostly synthesized in a tissue specific manner [73-74] which again add complications in elucidation of their biosynthetic routes and associated genes information.

The metabolic network of picrosides production is overwhelmingly complex as multiple pathways contribute to their biosynthesis in *P. kurroa* including MVA, MEP, shikimate/phenylpropanoid and monoterpene biosynthetic pathway i.e. iridoid pathway [14, 16]. However, it is not yet established how these pathways get stimulus from primary metabolism (known to provide precursors for secondary metabolism) to produce P-I and P-II in *P. kurroa*. Moreover, the scarcity of knowledge about the key genes corresponding to picrosides (P-I and P-II) biosynthesis in *P. kurroa* encouraged us to investigate the detailed role of genes related to different feeder pathways for picrosides biosynthesis. Therefore, to elucidate the complete metabolic basis for picrosides biosynthesis in *P. kurroa*, we have established the potential connecting links between primary metabolism (glycolysis, TCA cycle and pentose phosphate pathway) and secondary metabolic pathways (shikimate/phenylpropanoid pathway, MVA, MEP and iridoid/monoterpene pathway), followed by unravelling the exact routes of P-I and P-II biosynthesis.

The primary metabolic enzymes catalyzing rate limiting steps in glycolysis and TCA cycle were selected *viz.* HK, PK, MDH, ICDH and NADP$^+$-ME. These enzymes showed gene expression and enzyme activity profiles vis-à-vis P-I content in differential conditions of *P. kurroa* growth i.e. field grown (PKSS, 2.7% P-I) and tissue culture grown conditions [(PKS-25, P-I not detected) and (PKS-15, 0.6% P-I)]. This observation suggested that these enzymes are likely to trigger P-I production in *P. kurroa* shoots. This result is in agreement with a previous study which showed that altered activities of

glycolytic enzymes in rice plants infected with *Rhizoctonia solani* Kuhn consequently affected phenylpropanoid pathway [83]. However, the changes observed in the present study among gene expression patterns and activities of HK, PK, MDH, ICDH and NADP$^+$-ME might also be due to alterations in environmental conditions which are known to affect plants in terms of their physiology, biochemistry and gene regulation pathways [84].

Therefore, to eliminate the environmental variations and get a deep insight to how primary metabolic pathways integrate with secondary metabolism for P-I production, we investigated the metabolic basis of P-I biosynthesis in 0, 10, 20, 30 and 40 days grown shoots of *P. kurroa* at 15°C temperature condition *in vitro*. The rate limiting enzymes of glycolysis (HK and PK), pentose phosphate pathway (G6PDH), TCA cycle (ICDH and MDH), shikimate/phenylpropanoid pathway (DAHPS and PAL), MEP (DXPS and ISPD), MVA (HMGR and PMK) and iridoid/monoterpene pathway (GS and G10H) were selected and subjected to gene expression analysis in 0-40 days grown shoots of *P. kurroa*. The expression levels of all the selected genes encoding enzymes which catalyze rate limiting steps did not show any alteration in 10 days old shoots compared to the explant (zero day stage), which is in tune with the negligible change in P-I content. This might indicate that initially accumulated metabolites in *P. kurroa* shoots caused little increase in P-I content and plant cells acclimatized to culture conditions during early stages of plant growth. This was also supported by the biplot generated through PCA analysis which did not show the distribution of selected genes around 10 days of *P. kurroa* growth condition (Figure 4.9). Further, the growth of *P. kurroa* shoots from 10 to 20 days *in vitro* revealed 2.16-fold higher P-I content. During this period, the expression levels of *PAL*, *HK* and *G10H* genes showed minimum increase (< 20-fold), followed by *MDH*, *HMGR*, *DXPS*, *G6PDH*, *GS* and *PMK* genes (20 - 30-fold increase); while *PK*, *ICDH*, *ISPD* and *DAHPS* showed maximum enhancement in transcript levels with > 40-fold increase (Figure 5.1a).
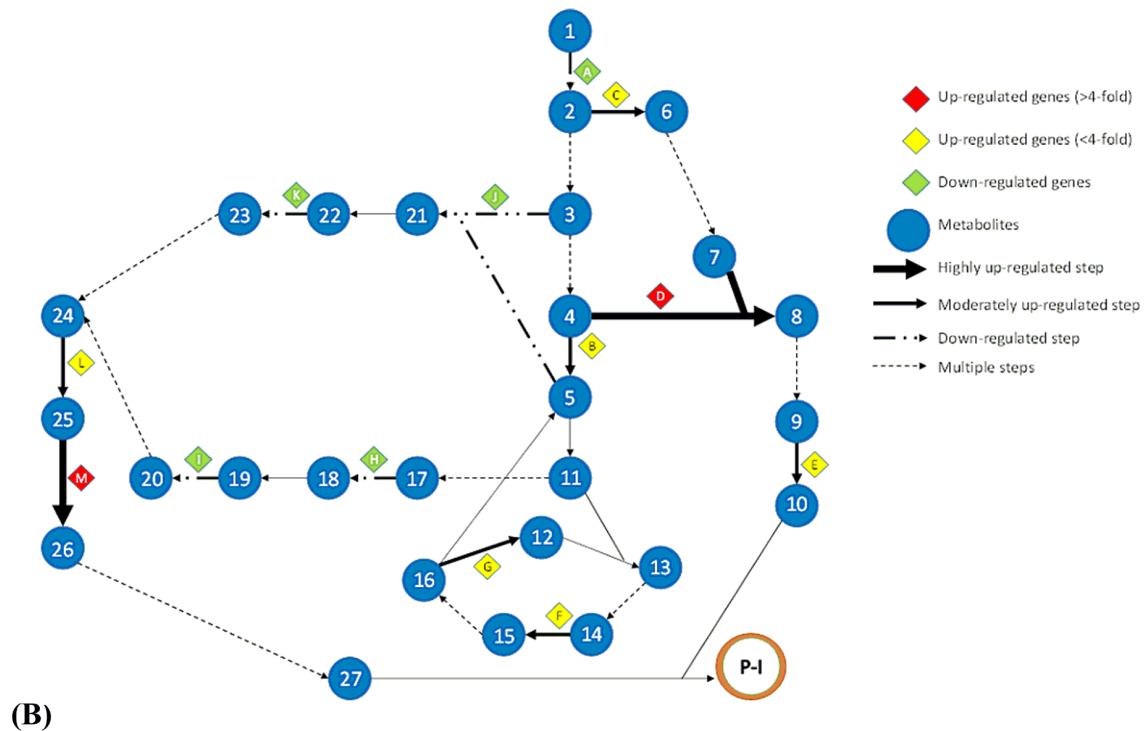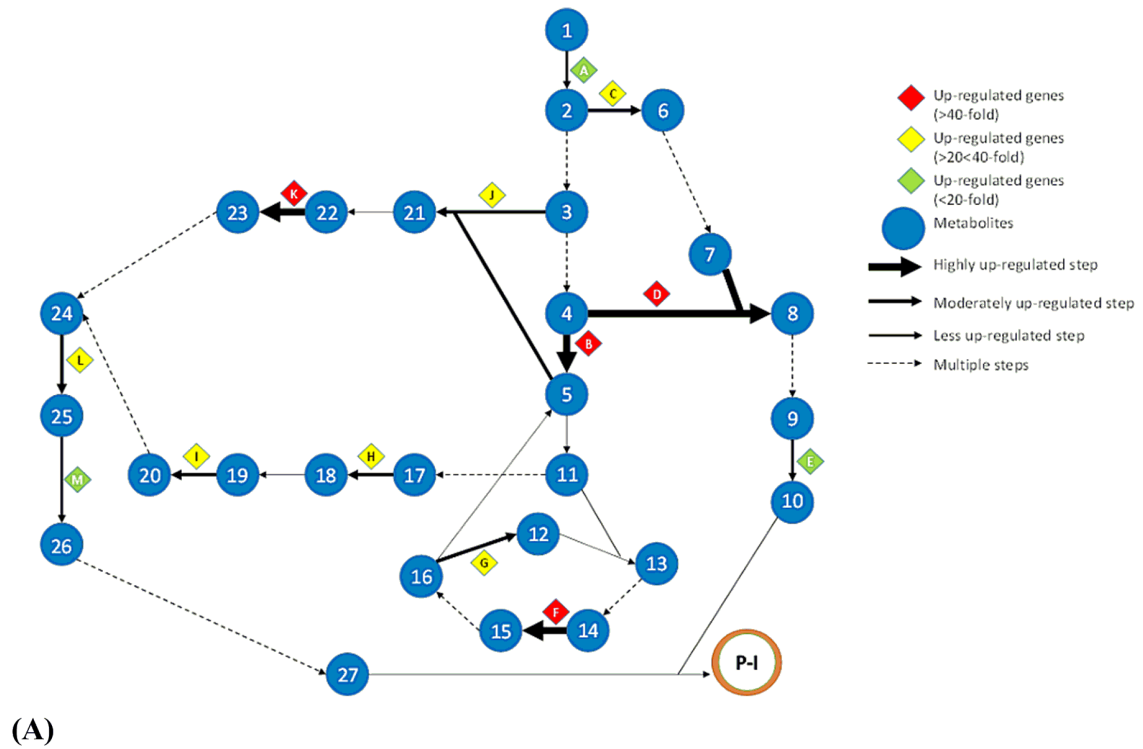
Figure 5.1. A conceptual network of the different pathways revealed from the gene expression data that expose P-I biosynthesis-relevant genes at different time intervals of *P. kurroa* growth; (A) 20 days and, (B) 30 days. The structures were coded with different colors to highlight the genes and steps with important roles in P-I biosynthesis. 1, Glucose; 2, Glucose-6-phosphate; 3, Glyceraldehyde-3-phosphate; 4,

Phosphoenolpyruvate; 5, Pyruvate; 6, 6-phosphogluconolactone; 7, Erythrose-4-phosphate; 8, 3-Deoxy-D-arabinoheptulosonate 7-phosphate; 9, Phenylalanine; 10, *trans*-cinnamic acid; 11, Acetyl CoA; 12, Oxaloacetate; 13, Citrate; 14, Isocitrate; 15, *α*-keto glutarate; 16, Malate; 17, 3-hydroxy-3-methylglutaryl coenzyme A; 18, Mevalonate; 19, Mevalonate phosphate; 20, Mevalonate pyrophosphate; 21, 1-deoxy-D-xylulose-5-phosphate; 22, 2-C-methyl-D-erythritol; 23, 4-(CDP)-2-methyl-D-erythritol; 24, Geranyl pyrophosphate; 25, Geraniol; 26, 10-hydroxy geraniol; 27, Catalpol; A, HK; B, PK; C, G6PDH; D, DAHPS; E, PAL; F, ICDH; G, MDH; H, HMGR; I, PMK; J, DXPS; K, ISPD; L, GS; M, G10H.

The gene encoding PK enzyme catalyzes the rate limiting step in glycolysis and its increased expression would produce higher content of pyruvate, which is the precursor allocating carbon units to TCA cycle, MVA and MEP pathways [49]. The activation of TCA cycle was observed by increased expression of the gene encoding ICDH enzyme, which could stimulate *P. kurroa* growth through enhanced ATP production and concurrently increased flux through TCA cycle. This would lead to enhanced oxaloacetate production which might increase P-I biosynthesis through re-allocating flux towards pyruvate formation by NADP$^+$-ME [85]. Moreover, the elevated pyruvate levels mediated activation of MEP pathway was revealed by higher transcript levels of *ISPD* as compared to *HMGR* and *PMK*; the enzymatic steps catalyzing rate limiting steps in MVA pathway [15]. This might indicate that MEP pathway has major contribution towards P-I biosynthesis rather than MVA pathway in *P. kurroa*. This statement is also supported by a previous study which reported that MEP pathway contributed to hemi-, mono-, and diterpenes, whereas MVA pathway provided precursors for sesquiterpene biosynthesis [86]. Therefore, it is likely that enhanced transcript levels of *ISPD* might result in higher accumulation of GPP, a starting moiety for monoterpene biosynthesis. However, the moderate increase in expression levels of *GS* and *G10H* genes might point out that these genes limit the conversion of accumulated GPP to produce catalpol, the immediate precursor of P-I biosynthesis, in 20 days old shoots of *P. kurroa*. On the other hand, the activation of shikimate/phenylpropanoid module of P-I biosynthesis as indicated by elevated transcript level of *DAHPS*, might enhance the production of phenylalanine which is the substrate for PAL enzyme [87]. The relatively small boost in expression level of *PAL* gene compared to *DAHPS* further limits P-I biosynthesis in 20 days old *P. kurroa* shoots as it catalyzes the production of immediate precursor to P-I i.e. CA [16].

The analysis of 30 days old shoots of *P. kurroa* showed maximum increase in P-I content i.e. 4.07-fold compared to 20 days old shoots. The gene expression analysis revealed down-regulation of *DXPS*, *PMK*, *HMGR*, *ISPD* and *HK*, which indicated that these genes might be involved in the accumulation of P-I precursors for 20 days of *P. kurroa* growth *in vitro*. Further, the maximum increase in expression levels were observed for *DAHPS* and *G10H* followed by genes encoding PAL and GS enzymes, which also showed significant increase in transcript levels at 30 days stage compared to 20 days old shoots of *P. kurroa* (Figure 5.1b). However, the expression levels of all the selected genes encoding enzymes which catalyze the rate limiting steps were restored in 40 days old *P. kurroa* shoots as observed in the 10 days stage of plant growth. Since P-I content also showed non-significant variation from 30 to 40 days stage, it was likely that the selected genes were associated with P-I content in *P. kurroa* shoots. Therefore, on the basis of temporal effects on genes expression patterns we can speculate that *G10H* and *DAHPS* act in conjunction for the enhanced P-I production in *P. kurroa* as evident from their highest expression levels in 30 days grown shoots where the P-I content was also maximum.

To validate the observation that shikimate/phenylpropanoid and iridoid/monoterpene pathways act in conjunction for the increased production of P-I in *P. kurroa*, we carried out metabolic flux analysis by *in vitro* feeding of CA and CAT, the immediate biosynthetic precursors of P-I. The results revealed that exogenous feeding of CAT alone did not increase the contents of CA, p-CA and P-I *in vitro* compared to control shoots (without treatment). This was possibly due to limited CA availability in CAT fed shoots, which was also supported by down-regulated expression level of *C4H* transcript encoding the enzyme catalyzing the conversion of CA to p-CA [88]. Moreover, the reduced levels of transcripts encoding GS and G10H enzymes were observed in CAT fed shoots, which might indicate the possible accumulation of exogenously supplied CAT and its involvement in flux limitation through the iridoid pathway leading to unaltered P-I content compared to control (Figure 5.2).
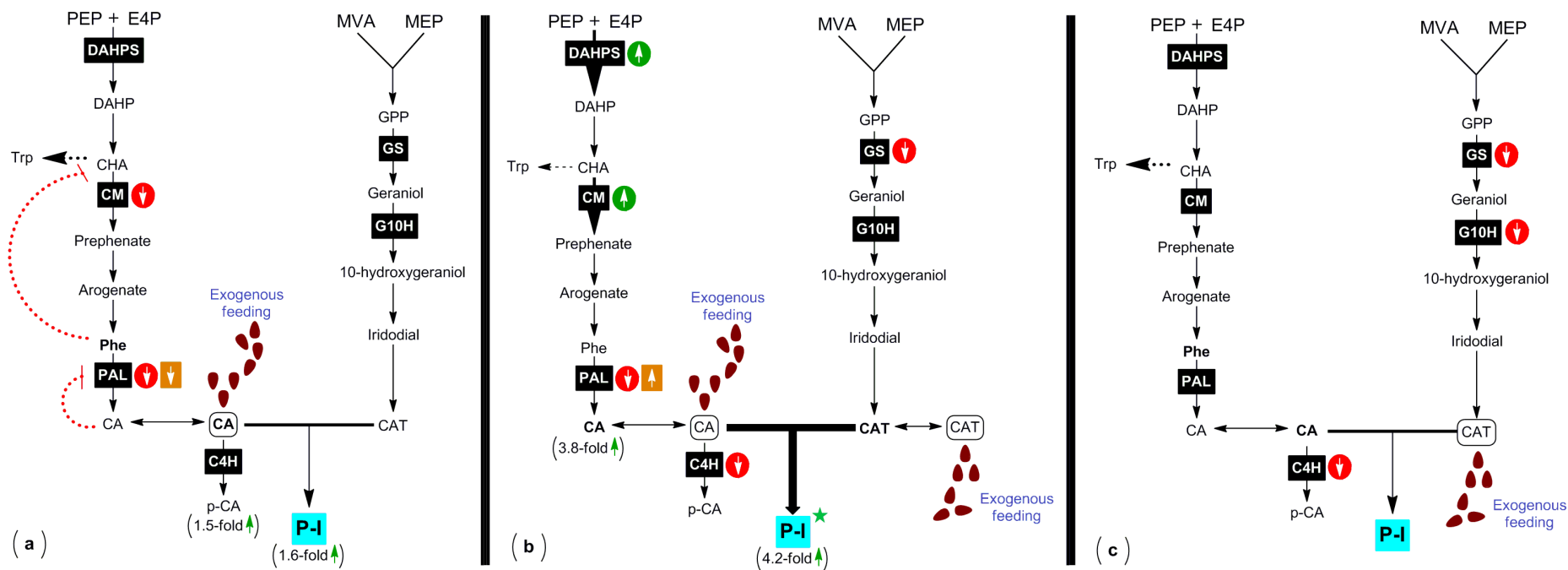
Figure 5.2. Influence of different precursors treatment on the fluxes through iridoid/monoterpene and shikimate/phenylpropanoid pathways; (a) CA, (b) CA+CAT, and (c) CAT. The symbols were added and structures were coded with different colors to highlight the effects occurring on the P-I biosynthesis in different treatments. Gene expressions were highlighted with a green circle with arrow pointing up showing up-regulation while a red circle with arrow pointing down showing down-regulation. Orange colored boxes with arrows pointing up and down indicate up-regulation and down-regulation of PAL enzyme, respectively. Red colored loops indicate feedback inhibition effect. Bold arrows indicate the up-regulation of respective steps. Green colored stars indicate high significant increase.

In contrast, the analyses of *in vitro* grown *P. kurroa* shoots fed only with CA revealed significant elevation in both P-I (1.6-fold) and p-CA (1.5-fold) contents but non-significant alteration was observed in CA content as compared to control. It might indicate that exogenous CA stimulated the flux of shikimate/phenylpropanoid pathway towards both p-CA and P-I production but simultaneously restricted the endogenous CA biosynthesis (Figure 5.2). This statement was also supported by feedback inhibition effect observed on the PAL enzyme, which showed significantly reduced transcript level and enzyme activity in CA fed shoots compared to control (Figure 5.2). Moreover, the down-regulated expression level of gene encoding CM enzyme observed in CA fed shoots indicated that accumulation of phenylalanine due to feedback inhibition effect on PAL enzyme might direct the shikimate/phenylpropanoid pathway flux towards tryptophan biosynthesis by regulating the formation of chorismate, the common substrate for anthranilate synthase and CM enzymes [89].

Interestingly, the P-I content showed a remarkable increase of 4.2-fold upon exogenous feeding of CA in combination with CAT indicating that rapid utilization of exogenously added both CA and CAT stimulated the production of P-I due to synergistic effect. This was also supported by a non-significant change in p-CA content and the decreased transcript level of *C4H* in CA+CAT fed shoots as compared to control. These results further confirmed that both CAT and CA were required for maximum production of P-I in *P. kurroa*. Moreover, the utilization of exogenously supplied both CA and CAT for P-I biosynthesis appeared to induce more endogenous production of CA as demonstrated by 3.8-fold higher CA content in CA+CAT fed shoots as compared to control (Figure 5.2). This statement was supported by the increased expression levels of genes encoding DAHPS and CM, the enzymes likely to increase the flux of shikimate/phenylpropanoid pathway towards enhanced phenylalanine production. However, the expression level of gene encoding PAL showed down-regulation but significant elevation in its enzyme activity indicated the reversal of inhibitory effect on PAL enzyme (Figure 5.2). As a whole, from the results of elucidation of metabolic basis of the P-I production, it was concluded that both CA+CAT stimulated P-I biosynthesis while their individual feeding limited P-I production due to feedback inhibition effect.

The investigation of metabolic basis of P-II biosynthesis on the other hand, faced challenges since it was not produced in *P. kurroa* plants grown *in vitro* [11]. Moreover, the shoots of *P. kurroa* plants grown in natural habitats exhibited only P-I while stolons

contained both P-I and P-II [7]. Thus, to address this issue, we have employed a strategy utilizing natural genetic diversity existing for the production of P-II among *P. kurroa* accessions collected from different geographic locations of North-Western Himalayas, India. The analysis of stolon tissues from different *P. kurroa* accessions revealed prominent increase in P-II content upon reduction in P-I level indicating that both P-I and P-II biosynthesis skewed from a common metabolic node. It is likely since VA, the immediate precursor of P-II, is supposed to be formed from either PA or FA, both derived from shikimate/phenylpropanoid pathway which also produces CA, the immediate biosynthetic precursor of P-I [14, 90].

Therefore, it is crucial to monitor dynamic profiles of intermediate metabolites in shikimate/phenylpropanoid pathway to get deep insight for metabolic switches of P-II biosynthesis. To address this, we have analysed stolon tissues of four *P. kurroa* accessions based on their varying P-II contents ranging from minimum to maximum (1.36 – 2.65%). The results observed in this study revealed a statistically significant increase in VA content among the high P-II content stolon tissues (PKST-3 and PKST-5) as compared to stolons possessing low P-II content (PKST-16 and PKST-18) thereby establishing that VA was associated with P-II biosynthesis. This result is consistent with the proposed hypothesis that VA is the immediate precursor of P-II biosynthesis [14]. It is noteworthy that analysis of CA and p-CA metabolites content in selected stolon tissues revealed the flux direction of shikimate/phenylpropanoid pathway through to the CA step leading to the biosynthesis of p-CA and P-I as CA is located at the branching point between P-I and p-CA production [16]. Interestingly, 87% CA was converted to p-CA in PKST-5 (P-1, 0.08%; P-II, 2.19%), 44.4% in PKST-3 (P-1, 0.17%; P-II, 2.65%), 21.1% in PKST-16 (P-1, 1.05%; P-II, 1.52%) and 8.2% in PKST-18 (P-1, 1.32%; P-II, 1.36%). This implies that with increase in the P-I content, the flux of shikimate/phenylpropanoid pathway limits through to the CA step to p-CA while increase in the P-II content directs the flux of shikimate/phenylpropanoid pathway through to the CA to p-CA leading to the enhanced P-II production in *P. kurroa* (Figure 5.3). This statement is also supported by comparative transcriptome analysis of selected stolon tissues which showed high positive correlation of the gene transcript encoding C4H enzyme (0.60) with P-II content compared to the gene encoding PAL enzyme which showed PCC of 0.28 with P-II content (Figure 4.23). The C4H is an enzyme that catalyzes the conversion of CA to p-CA while PAL catalyzes the conversion of phenylalanine to CA, the immediate precursor

of the P-I biosynthesis [60]. Therefore, based on this analysis, we have hypothesised that CA is the common metabolic node between P-I and P-II biosynthesis in *P. kurroa* rather than 3-dehydroshikimate which serves as the branch point between PA and shikimate production, the metabolites also supposed to be the common nodes for P-I and P-II biosynthesis [16].
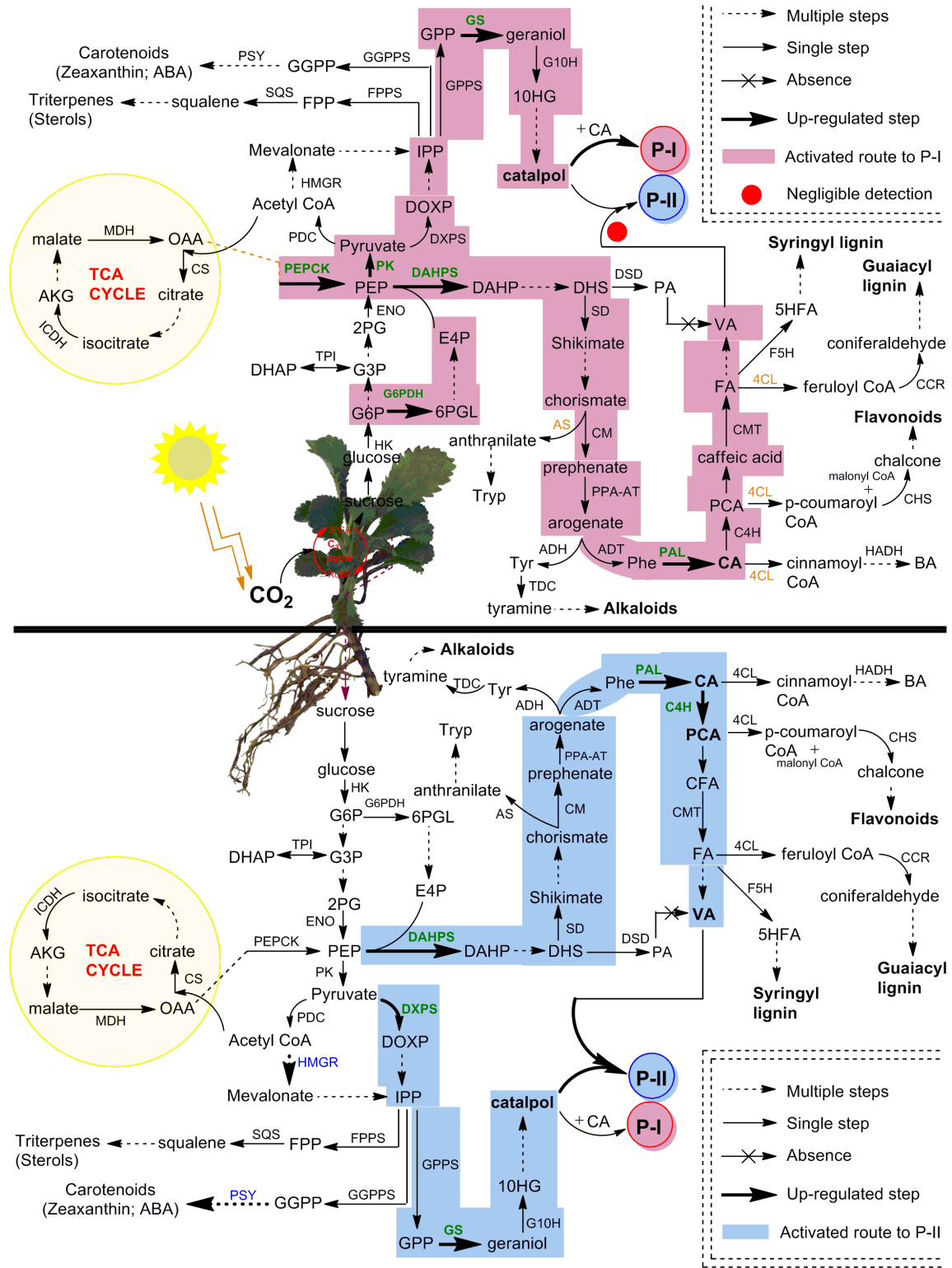
Figure 5.3. Complete framework of metabolic network depicting P-I and P-II biosynthesis in different tissues of *P. kurroa*. The established routes of P-I and P-II production were presented with different colors to highlight the modulations in shoots and stolons of *P. kurroa*. Up-regulated gene expressions are highlighted with bold and green color.

The analysis of FA, however, did not show statistically significant variations among the selected stolon tissues. Albeit, a higher VA content was observed in PKST-3 and PKST-5 (high P-II content stolons) as compared to PKST-16 and PKST-18 (low P-II content stolons). Keeping in view that FA is a canonical intermediate metabolite in the biosynthesis of guaiacyl- and syringyl lignin's in addition to its proposed role in VA production, the results observed in this study might indicate that flux of FA is directed towards both VA and P-II in PKST-3 and PKST-5, whereas maximum flux of FA might deviate to lignin biosynthesis in PKST-16 and PKST-18. This statement is in agreement with correlation map constructed between P-II content and transcripts abundance values (FPKM) which revealed negative correlation of gene encoding caffeic acid-3-O-methyltransferase (CMT) with P-II content (-0.63) followed by a strong positive correlation of CMT through a PCC value of 0.82 with ferulic acid-5-hydroxylase (F5H), an enzyme that catalyzes the conversion of ferulic acid to 5-hydroxy ferulic acid, which represents as a precursor for syringyl lignin biosynthesis [91]. Consequently, it is apparent that up-regulated transcript level of CMT, an enzyme catalyzing the conversion of caffeic acid to ferulic acid accompanied by F5H, might be linked to the activation of lignin biosynthesis in PKST-16 and PKST-18. Trabucco et al. [92] also reported the reduced total lignin content upon down-regulation of gene encoding CMT enzyme in *Brachypodium distachyon*. As a whole, the analysis of stolon tissues with natural variations for P-II content hypothesized that P-II is produced *via.* shikimate/phenylpropanoid pathway through degradation of FA to VA, which finally integrates with catalpol (CAT) to produce P-II in *P. kurroa* (Figure 5.3).

Previous studies have reported that shoots of *P. kurroa* are independent biosynthetic tissues for P-I, a secondary metabolite produced by the combination of CA and CAT [16]. Nevertheless, the current study established stolons of *P. kurroa* as autonomous biosynthetic machinery for P-I and P-II, both sharing a common biosynthetic pathway, it is inspiring to comprehend the negligible amount of P-II biosynthesis in *P. kurroa* shoots.

To address this, the shoot tissues of four *P. kurroa* accessions based on their varying P-I content ranging from minimum to maximum (0.13 – 2.31%) were selected for analysis of p-CA, CA, FA and VA with the aim to investigate the fate of shikimate/phenylpropanoid pathway in *P. kurroa* shoots. The analysis of shoot tissues of four *P. kurroa* accessions for CA and p-CA showed that increased P-I production limits the flux of CA towards p-CA biosynthesis. It is likely since CA shares a common biosynthetic node for P-I and p-CA. In contrast, the analysis of FA revealed slight significant variation between the selected shoots and also showed a high positive correlation by PCC of 0.85 with p-CA. However, *C4H* and chalcone synthase (*CHS*) showed a strong positive correlation with PCC of 0.90 as compared to PCC of 0.23 between *C4H* and *CMT* (Figure 4.23). CHS is an enzyme that catalyzes the formation of naringenin chalcone; the later one serves as a starting metabolite for flavonoids biosynthesis [93]. Therefore, this finding underscores that phenylpropanoid pathway might allocate the flux of p-CA to produce both FA and flavonoids in *P. kurroa* shoots. This statement is in agreement with the finding that silencing of gene encoding hydroxycinnamoyl-CoA shikimate/quinate hydroxycinnamoyl transferase enzyme (HCT) involved in lignin biosynthesis, re-routed the flux of phenylpropanoid pathway into flavonoids through CHS activity [94]. Interestingly, negligible levels of VA were observed in all the selected shoot tissues, thereby implying that P-II biosynthesis arrests in the downstream steps of FA, which possibly limits the VA supply.

Hence, p-CA, FA and PA were exogenously applied along with a mixture of VA and CAT in tissue culture conditions not only to establish the course of P-II biosynthesis but also to produce P-II in *P. kurroa* shoots. The results showed a significant enhancement in VA content in FA fed shoots as compared to shoots without treatment. This observation further ascertained that FA was associated with VA production rather than PA which was previously proposed as the precursor for VA biosynthesis [14, 16]. Moreover, significant enhancement in VA content in VA+CAT fed shoots over untreated control might indicate it's accumulation due to exogenous application. This was also supported by the absence of VA content observed in the MS media left after the collection of VA+CAT fed shoots. Upon analysis of P-II content, minor detection was only observed in VA+CAT fed shoots which indicated that exogenous application of VA+CAT, both immediate precursors of P-II biosynthesis, might stimulate its production in *P. kurroa* shoots. Therefore, different concentrations of VA+CAT were further tested with the aim to observe the progressive

increase of P-II content in *P. kurroa* shoots. Unfortunately, we did not observe significant increment in P-II content among different VA+CAT fed shoots which was possibly due to low activity of a probable acyltransferase catalyzing the esterification of VA and CAT to produce P-II. However, we have not observed the activity of probable acyltransferase as it is not discovered yet. It is striking that P-II was not taken up by the *P. kurroa* plants upon its exogenous introduction in purified form. This was clearly demonstrated from the negligible level of P-II observed in shoots fed with P-II whereas its substantial content was detected in the MS media left after the collection of P-II fed shoots. This finding suggests that *P. kurroa* plants are unable to take P-II in its ready form and subsequently they are dependent on its endogenous production. Therefore, it is a necessity to identify an enzyme catalyzing the conversion of VA and CAT to produce P-II in *P. kurroa*.

CONCLUSION AND FUTURE PROSPECTS

The findings of this research work shed light on metabolic modulations underlying the biosynthesis of Picroside-I and Picroside-II in *P. kurroa*. It offers convincing evidences that independent mechanisms control the biosynthesis of P-I and P-II in shoots and stolons of *P. kurroa*. The intermediates of shikimate/phenylpropanoid pathway produced in stolons guided the flux towards P-II biosynthesis *via.* degradation of FA to produce VA, while deviate from the non-canonical view of P-II biosynthesis in shoot tissues of *P. kurroa*. Moreover, CA is found to be the limiting moiety for P-I biosynthesis. However, supplementing CA along with CAT is found to be activating both shikimate/phenylpropanoid and iridoid pathways for enhanced P-I production whereas their individual application caused feedback inhibition and limited the production of P-I. As a whole in the face of such a complex biosynthetic architecture, one may ask what strategy we should focus on for biosynthetic engineering of P-I in *P. kurroa*. Indeed, we argue that multi-step engineering for augmenting both CA and CAT by exploitation of DAHPS, CM, PAL, GS and G10H catalyzed steps is more appropriate. Finally, we have illustrated the basis of negligible amounts of P-II in shoots that provides impetus for the future investigation of an enzyme catalyzing the conversion of VA and CAT to produce P-II, a task that can rewrite the P-II production in shoot cultures along with P-I in *P. kurroa*.

REFERENCES

[1] V. Kumar, R.S. Chauhan, and C. Tandon, "Biosynthesis and therapeutic implications of iridoid glycosides from Picrorhiza genus: the road ahead," *Journal of Plant Biochemistry and Biotechnology*, vol. 26, no. 1, pp. 1-13, Jan 2017.

[2] Y. Dwivedi, R. Rastogi, N.K. Garg, and B.N. Dhawan, "Picroliv and its components kutkoside and P-I protect liver against galactosamine induced damage in rats," *Pharmacology and Toxicology*, vol. 71, no. 5, pp. 383-387, Nov 1992.

[3] K.L. Joy, and R. Kuttan, "Anti-oxidant activity of selected plant extract," *Amala Research Bulletin*, vol. 15, pp. 68–71, 1995.

[4] W. Dorsch, H. Stuppher, H. Wagner, M. Gropp, S. Demolin, and J. Ring, "Antiasthmatic effect of *Picrorhiza kurrooa*: androsin prevents allergen and PAV induced bronchial obstruction in guinea pig," *International Archives of Allergy and Applied Immunology*, vol. 95, no. 2-3, pp. 128-133, 1991.

[5] K.L. Joy, N.V. Rajeshkumar, G. Kuttan, and R. Kuttan, "Effect of *Picrorrhiza kurroa* extract on transplanted tumours and chemical carcinogenesis in mice," *Journal of Ethnopharmacology*, vol. 71, no. 1-2, pp. 261-266, Jul 2000.

[6] A. Puri, R.P. Saxena, S.P.Y. Guru, D.K. Kulshrestha, K.C. Saxena, and B.N. Dhawan, "Immunostimulant activity of picroliv, the iridoid glycoside fraction of *Picrorhiza kurrooa* and its protective action against *Leishmania donovani* infection in hamsters," *Planta Medica*, vol. 58, no. 6, pp. 528-532, Dec 1992.

[7] S. Pandit, K. Shitiz, H. Sood, and R.S. Chauhan, "Differential biosynthesis and accumulation of picrosides in an endangered medicinal herb *Picrorhiza kurroai*," *Journal of Plant Biochemistry and Biotechnology*, vol. 22, no. 3, pp. 335-342, Jul 2013.

[8] A. Uniyal, S. K. Uniyal, and G.S. Rawat, "Commercial Extraction of *Picrorhiza kurrooa* Royle ex Benth. in the Western Himalaya," *Mountain Research and Development*, vol. 31, no. 3, pp. 201-208, Aug 2011.

[9] M.P. Nayar, and A.R.K. Sastri, "Red data plants of India," *CSIR Publication*, New Delhi, pp. 271, 1990.

[10] K. Shitiz, S. Pandit, R.S. Chauhan, and H. Sood, "Picrosides content in the rhizomes of *Picrorhiza kurroa* Royle ex Benth. traded for herbal drugs in the markets of North India," *International Journal of Medicinal and Aromatic Plants*, vol. 3, no. 2, pp. 226-233, Jun 2013.

[11] H. Sood, and R.S. Chauhan, "Biosynthesis and accumulation of a medicinal compound, Picroside-I, in cultures of *Picrorhiza kurroa* Royle ex Benth," *Plant Cell, Tissue and Organ Culture*, vol. 100, pp. 113, Jan 2010.

[12] N. Sharma, R.S. Chauhan, and H. Sood, "Seaweed extract as a novel elicitor and medium for mass propagation and picroside-I production in an endangered medicinal herb *Picrorhiza kurroa*," *Plant Cell, Tissue and Organ Culture*, vol. 122, no. 1, pp. 57-65, Jul 2015.

[13] N. Sharma, V. Kumar, R.S. Chauhan, and H. Sood, "Modulation of picroside-I biosynthesis in grown elicited shoots of *Picrorhiza kurroa* In Vitro,". *Journal of Plant Growth Regulation*, vol. 35, no. 4, pp. 965-973, Dec 2016.

[14] V. Kumar, H. Sood, M. Sharma, and R.S. Chauhan, "A proposed biosynthetic pathway of picrosides linked through the detection of biochemical intermediates in the endangered medicinal herb *Picrorhiza kurroa*,". *Phytochemical Analysis*, vol. 24, no. 6, pp. 598-602, Nov-Dec 2013.

[15] S. Pandit, K. Shitiz, H. Sood, P.K. Naik, and R.S. Chauhan, "Expression pattern of fifteen genes of non-mevalonate (MEP) and mevalonate (MVA) pathways in different tissues of endangered medicinal herb *Picrorhiza kurroa* with respect to picrosides content," *Molecular Biology Reports*, vol. 40, no. 2, pp. 1053-1063, Feb 2013.

[16] K. Shitiz, N. Sharma, T. Pal, H. Sood, and R.S. Chauhan, "NGS transcriptomes and enzyme inhibitors unravel complexity of picrosides biosynthesis in *Picrorhiza kurroa* Royle ex. Benth," *PLoS ONE*, vol. 10, no. 12, pp. e0144546, Dec 2015.

[17] X. Zhu, M. Gerstein, and M. Snyder, "Getting connected: analysis and principles of biological networks," *Genes and Development*, vol. 21, no. 9, pp. 1010-1024, May 2007.

[18] M.C. Asters, W.P. Williams, A.D. Perkins, J.E. Mylroie, G.L. Windham, and X. Shan, "Relating significance and relations of differentially expressed genes in response to *Aspergillus flavus* infection in maize," *Scientific Reports*, vol. 4, pp. 4815, Apr 2014.

[19] H. Ishihara, T. Obata, R. Sulpice, A.R. Fernie, and M. Stitt, "Quantifying protein synthesis and degradation in Arabidopsis by dynamic 13CO$_2$ labeling and analysis of enrichment in individual amino acids in their free pools and in protein," *Plant Physiology*, vol. 168, no. 1, pp. 74-93, May 2015.

[20] W. Xiong, J.A. Morgan, J. Ungerer, B. Wang, P.C. Maness, and J. Yu, "The plasticity of cyanobacterial metabolism supports direct CO_2 conversion to ethylene," *Nature Plants*, vol. 1, pp. 15053, Apr 2015.

[21] G. Stephanopoulos, "Synthetic biology and metabolic engineering," *ACS Synthetic Biology*, vol. 1, no. 11, pp. 514-525, Nov 2012.

[22] F. Bourgaud, A. Gravot, S. Milesi, and E. Gontier, "Production of plant secondary metabolites: a historical perspective," *Plant Science*, vol. 161, no. 5, pp. 839-851, Oct 2001.

[23] S. Whitmer, C. Canel, D. Hallard, C. Goncalves, and R. Verpoorte, "Influence of precursor availability on alkaloid accumulation by transgenic cell line of *Catharanthus roseus*," *Plant Physiology*, vol. 116, no. 2, pp. 853-857, Feb 1998.

[24] J.A. Morgan, and J.V. Shanks, "Determination of metabolic rate-limitations by precursor feeding in *Catharanthus roseus* hairy root cultures," *Journal of Biotechnology*, vol. 79, no. 2, pp. 137-145, Apr 2000.

[25] P. Gahlan, H.R. Singh, R. Shankar, N. Sharma, A. Kumari, V. Chawla, P.S. Ahuja, and S. Kumar, "De novo sequencing and characterization of *Picrorhiza kurrooa* transcriptome at two temperatures showed major transcriptome adjustments," *BMC Genomics*, vol. 13, pp. 126, Mar 2012.

[26] D.J. Kliebenstein, J. Kroymann, P. Brown, A. Figuth, D. Pedersen, J. Gershenzon, and T. Mitchell-Olds, "Genetic control of natural variation in Arabidopsis glucosinolate accumulation," *Plant Physiology*, vol. 126, no. 2, pp. 811-825, Jun 2001.

[27] S. Li, I.T. Baldwin, and E. Gaquerel, "Navigating natural variation in herbivory-induced secondary metabolism in coyote tobacco populations using MS/MS structural analysis," *Proceedings of the National Academy of Sciences of the United States of America*, vol. 112, no. 30, pp. E4147-E4155, Jul 2015.

[28] P. Muriel, and Y. Rivera-Espinoza, "Beneficial drugs for liver diseases," *Journal of Applied Toxicology*, vol. 28, no. 2, pp. 93-103, Mar 2008.

[29] A. Rambaldi, and C. Gluud, "Colchicine for alcoholic and non-alcoholic liver fibrosis and cirrhosis,' *Cochrane Database of Systematic Reviews*, vol. 3, pp. CD002148, Jul 2001.

[30] K. Shitiz, "Biosynthetic machinery of iridoid glycosides – the major pharmacological components of a medicinal herb *Picrorhiza kurroa* Royle ex Benth," Ph.D. thesis,

Dept. Biotechnology & Bioinformatics, Jaypee University of Information Technology, Solan, H.P., India, 2016.

[31] P. Li, K. Matsunaga, T. Yamakuni, and Y. Ohizumi, "Potentiation of nerve growth factor-action by picrosides I and II, natural iridoids, in PC12D cells," *European Journal of Pharmacology*, vol. 406, no. 2, pp. 203-208, Oct 2000.

[32] P. Li, K. Matsunaga, T. Yamakuni, and Y. Ohizumi, "Picrosides I and II, selective enhancers of the mitogen-activated protein kinase-dependent signalling pathway in the action of neuritogenic substances on PC12D cells," *Life Sciences*, vol. 71, no. 15, pp. 1821-1835, Aug 2002.

[33] D. Rathee, M. Thanki, S. Bhuva, S. Anandjiwala, and R. Agrawal, "Iridoid glycosides-kutkin, picroside-I and kutkoside from *Picrorhiza kurroa* Benth inhibits the invasion and migration of MCF-7 breast cancer cells through the down regulation of matrix metalloproteinases: 1st cancer update," *Arabian Journal of Chemistry*, vol. 6, no. 1, pp. 49-58, Jan 2013.

[34] Y. Guo, X. Xu, Q. Li, Z. Li, and F. Du, "Anti-inflammation effects of picroside 2 in cerebral ischemic injury rats," *Behavioral and Brain Functions*, vol. 6, pp. 43, Jul 2010.

[35] Q. Li, Z. Li, X. Xu, Y. Guo, and F. Du, "Neuroprotective properties of picroside II in a rat model of focal cerebral ischemia," *International Journal of Molecular Sciences*, vol. 11, no. 11, pp. 4580-4590, Nov 2010.

[36] H. Pei, X. Su, L. Zhao, H. Li, Y. Guo, M. Zhang, and H. Xin, "Primary study for the therapeutic dose and time window of picroside II in treating cerebral ischemic injury in rats," *International Journal of Molecular Sciences*, vol. 13, no. 3, pp. 2551-2562, Feb 2012.

[37] L. Zhao, Y. Guo, X. Ji, and M. Zhang, "The neuroprotective effect of picroside II via regulating the expression of myelin basic protein after cerebral ischemia injury in rats," *BMC Neuroscience*, vol. 15, pp. 25, Feb 2014.

[38] G. Liu, L. Zhao, T. Wang, M. Zhang, and H. Pei, "Optimal therapeutic dose and time window of picroside II in cerebral ischemic injury," *Neural Regeneration Research*, vol. 9, no. 15, pp. 1437-1445, Aug 2014.

[39] T. Wang, L. Zhai, Y. Guo, H. Pei, and M. Zhang, "Picroside II has a neuroprotective effect by inhibiting ERK1/2 activation after cerebral ischemic injury in rats," *Clinical and Experimental Pharmacology and Physiology*, vol. 42, no. 9, pp. 93-939, Sep 2015.

[40] H. Gao, and Y.W. Zhou, "Inhibitory effect of picroside II on hepatocyte apoptosis," *Acta Pharmacologica Sinica*, vol. 26, no. 6, pp. 729-736, Jun 2005.

[41] H. Gao, and Y.W. Zhou, "Anti-lipid peroxidation and protection of liver mitochondria against injuries by picroside II," *World Journal of Gastroenterology*, vol. 11, no. 24, pp. 3671-3674, Jun 2005.

[42] F.J. Meng, Z.W. Hou, Y. Li, Y. Yang, and B. Yu, "The protective effect of picroside II against hypoxia/reoxygenation injury in neonatal rat cardiomyocytes," *Pharmaceutical Biology*, vol. 50, no. 10, pp. 1226-1232, Oct 2012.

[43] F.J. Meng, S.M. Jiao, and B. Yu, "Picroside II protects cardiomyocytes from hypoxia/reoxygenation-induced apoptosis by activating the PI3K/Akt and CREB pathways," *International Journal of Molecular Medicine*, Vol. 30, no. 2, pp. 263-270, Aug 2012.

[44] N. Wu, W. Li, W. Shu, and D. Jia, "Protective effect of picroside II on myocardial ischemia reperfusion injury in rats," *Drug Design, Development and Therapy*, vol. 8, pp. 545-554, May 2014.

[45] F.M. Comu, Y. Kilic, A. Ozer, M. Kirisci, A.D. Dursun, T. Tatar, M.H. Zor, H. Kartal, A. Kucuk, H. Boyunaga, and M. Arslan, "Effect of picroside II on erythrocyte deformability and lipid peroxidation in rats subjected to hind limb ischemia reperfusion injury," *Drug Design, Development and Therapy*, vol. 10, pp. 927-931, Mar 2016.

[46] L. Wang, X. Liu, H. Chen, Z. Chen, X. Weng, T. Qiu, L. Liu, "Effect of picroside II on apoptosis induced by renal ischemia/reperfusion injury in rats," *Experimental and Therapeutic Medicine*, vol. 9, no. 3, pp. 817-822, Mar 2015.

[47] F. Geu-Flores, N.H. Sherden, V. Courdavault, V. Burlat, W.S. Glenn, C. Wu, E. Nims, Y. Cui, and S.E. O'Connor, "An alternative route to cyclic terpenes by reductive cyclization in iridoid biosynthesis," *Nature*, vol. 492, no. 7427, pp. 138-142, Dec 2012.

[48] O. Laule, A. Furholz, H.S. Chang, T. Zhu, X. Wang, P.B. Heifetz, W. Gruissem, and M. Lange, Crosstalk between cytosolic and plastidial pathways of isoprenoids biosynthesis in *Arabidopsis thaliana*. *Proceedings of the National Academy of Sciences of the United States of America*, vol. 100, no. 11, pp. 6866-6871, May 2003.

[49] B.M. Lange, T. Rujan, W. Martin, and R. Croteau, "Isoprenoid biosynthesis: the evolution of two ancient and distinct pathways across genomes," *Proceedings of the*

National Academy of Sciences of the United States of America, vol. 97, no. 24, pp. 13172-13177, Nov 2000.

[50] M. Rohmer, M. Knani, P. Simonin, B. Sutter, and H. Sahm, "Isoprenoid biosynthesis in bacteria: a novel pathway for early steps leading to isopentenyl diphosphate," *Biochemical Journal*, vol. 295, no. 2, pp. 517-524, Oct 1993.

[51] H.K. Lichtenthaler, "The 1-deoxy-d-xylulose- 5-phosphate pathway of isoprenoid biosynthesis in plants," *Annual Review of Plant Physiology and Plant Molecular Biology*, vol. 50, pp. 47-65, Jun 1999.

[52] W. Eisenreich, F. Rohdich, and A. Bacher, "Deoxyxylulose phosphate pathway to terpenoids," *Trends in Plant Science*, vol. 6, no. 2, pp. 78-84, Feb 2001.

[53] Y. Iijima, D.R. Gang, E. Fridman, E. Lewinsohn, and E. Pichersky, "Characterization of geraniol synthase from the peltate glands of sweet basil," *Plant Physiology*, vol. 134, no. 1, pp. 370-379, Jan 2004.

[54] G. Collu, N. Unver, A.M. Peltenburg-Looman, R. van der Heijden, R. Verpoorte, and J. Memelink, "Geraniol-10-hydroxylase, a cytochrome P450 enzyme involved in terpenoid indole alkaloid biosynthesis," *FEBS Letters*, vol. 508, no. 2, pp. 215-220, Nov 2001.

[55] R. Krithika, P.L. Srivastava, B. Rani, S.P. Kolet, M. Chopade, M. Soniya, and H.V. Thulasiram, "Characterization of 10-hydroxygeraniol dehydrogenase from *Catharanthus roseus* reveals cascaded enzymatic activity in iridoid biosynthesis," *Scientific Reports*, vol. 5, pp. 8258, Feb 2015.

[56] K. Miettinen, L. Dong, N. Navrot, T. Schneider, V. Burlat, J. Pollier, L. Woittiez, S. van der Krol, R. Lugan, T. Llc, R. Verpoorte, K.M. Oksman-Caldentey, E. Martinoia, H. Bouwmeester, A. Goossens, J. Memelink, and D. Werck-Reichhart, "The seco-iridoid pathway from *Catharanthus roseus*," *Nature Communications*, vol. 5, pp. 3606, Apr 2014.

[57] M.I. Sampaio-Santos, M.A.C. Kaplan, "Biosynthesis significance of iridoids in chemosystematics," *Journal of the Brazilian Chemical Society*, vol. 12, no. 2, pp. 144-153, Mar-Apr 2001.

[58] S. Damtoft, S.R. Jensen, C.U. Jessen, and T.B. Knudsen, "Late stages in the biosynthesis of aucubin in *Scrophularia*," *Phytochemistry*, vol. 33, no. 5, pp. 1089-1093, Jul 1993.

[59] W.W. Bhat, N. Dhar, S. Razdan, S. Rana, R. Mehra, A. Nargotra, R.S. Dhar, N. Ashraf, R. Vishwakarma, and S.K. Lattoo, "Molecular Characterization of UGT94F2

and UGT86C4, two glycosyltransferases from *Picrorhiza kurrooa*: comparative structural insight and evaluation of substrate recognition," *PLoS ONE*, vol. 8, no. 9, pp. e73804, Sep 2013.

[60] F. De Jong, S.J. Hanley, M.H. Beale, and A. Karp, "Characterisation of the willow phenylalanine ammonia-lyase (*PAL*) gene family reveals expression differences compared with poplar," *Phytochemistry*, vol. 117, pp. 90-97, Sep 2015.

[61] H. Singh, P. Gahlan, and S. Kumar, "Cloning and expression analysis of ten genes associated with picrosides biosynthesis in *Picrorhiza kurroa*," *Gene*, vol. 515, no. 2, pp. 320-328, Feb 2013.

[62] J. Zhao, L.C. Davis, and R. Verpoorte, "Elicitor signal transduction leading to production of plant secondary metabolites," *Biotechnology Advances*, vol. 23, no. 4, pp. 283-333, Jun 2005.

[63] A.R. Fernie, P. Geigenberger, and M. Stitt, "Flux an important, but neglected, component of functional genomics," *Current Opinion in Plant Biology*, vol. 8, no. 2, pp. 174-182, Apr 2005.

[64] E. Glawischnig, B.G. Hansen, C.E. Olsen, and B.A. Halkier, "Camalexin is synthesized from indole-3-acetaldoxime, a key branching point between primary and secondary metabolism in Arabidopsis," *Proceedings of the National Academy of Sciences of the United States of America*, vol. 101, no. 21, pp. 8245-8250, May 2004.

[65] J. Boatright, F. Negre, X. Chen, C.M. Kish, B. Wood, G. Peel, I. Orlova, D. Gang, D. Rhodes, and N. Dudareva, "Understanding in vivo benzenoid metabolism in petunia petal tissue," *Plant Physiology*, vol. 135, no. 4, pp. 1993-2011, Aug 2004.

[66] N. Totte´, L. Charon, M. Rohmer, F. Compernolle, I. Baboeuf, and J.M.C. Geuns, "Biosynthesis of the diterpenoid steviol, an *ent*-kaurene derivative from *Stevia rebaudiana* Bertoni, via the methylerythritol phosphate pathway," *Tetrahedron Letters*, vol. 41, no. 33, pp. 6407-6410, Aug 2000.

[67] N.J. Gallage, E.H. Hansen, R. Kannangara, C.E. Olsen, M.S. Motawia, K. Jørgensen, I. Holme, K. Hebelstrup, M. Grisoni, and B.L. Møller, "Vanillin formation from ferulic acid in *Vanilla planifolia* is catalysed by a single enzyme," *Nature Communications*, vol. 5, pp. 4037, Jun 2014.

[68] W. Weckwerth, and O. Fiehn, "Can we discover novel pathways using metabolomic analysis?," *Current Opinion in Biotechnology*, vol. 13, no. 2, pp. 156-160, Apr 2002.

[69] A.G. Fett-Neto, S.J. Melanson, S.A. Nicholson, J.J. Pennington, and F. DiCosmo, "Improved taxol yield by aromatic carboxylic and amino acid feeding to cell cultures

of *Taxus cuspidata*," *Biotechnology and Bioengineering*, vol. 44, no. 8, pp. 967-971, Oct 1994.

[70] L.G. Romagnoli, and D. Knorr, "Effects of ferulic acid treatment on growth and flavour development of cultured *Vanilla planifolia* cells," *Food Biotechnology*, vol. 2, no. 1, pp. 93-104, 1988.

[71] T. Mulder-Krieger, R. Verpoorte, A. Svendse, and J. Scheffer, "Production of essential oils and flavours in plant cell and tissue cultures. A review," *Plant Cell, Tissue and Organ Culture*, vol. 13, no. 2, pp. 85-154, Jan 1988.

[72] K.M. Oksman-Caldentey, and D. Inze, "Plant cell factories in the post-genomic era: new ways to produce designer secondary metabolites," *Trends in Plant Science*, vol. 9, no. 9, pp. 433-440, Sep 2004.

[73] D. Li, S. Heiling, I.T. Baldwin, and E. Gaquerel, "Illuminating a plant's tissue-specific metabolic diversity using computational metabolomics and information theory," *Proceedings of the National Academy of Sciences of the United States of America*, vol. 113, no. 47, pp. E7610-E7618, Nov 2016.

[74] G. Pasquali, D.D. Porto, and A.G. Fett-Neto, "Metabolic engineering of cell cultures versus whole plant complexity in production of bioactive monoterpene indole alkaloids: Recent progress related to old dilemma," *Journal of Bioscience and Bioengineering*, vol. 101, no. 4, pp. 287-296, Apr 2006.

[75] A.L. Schilmiller, E. Pichersky, and R.L. Last, "Taming the hydra of specialized metabolism: how systems biology and comparative approaches are revolutionizing plant biochemistry," *Current Opinion in Plant Biology*, vol. 15, no. 3, pp. 338-344, Jun 2012.

[76] J. Kroymann, "Natural diversity and adaptation in plant secondary metabolism," *Current Opinion in Plant Biology*, vol. 14, no. 3, pp. 246-251, Jun 2011.

[77] J. Ziegler, S. Voigtlander, J. Schmidt, R. Kramell, O. Miersch, C. Ammer, A. Gesell, and T.M. Kutchan, "Comparative transcript and alkaloid profiling in *Papaver* species identifies a short chain dehydrogenase/reductase involved in morphine biosynthesis," *The Plant Journal*, vol. 48, no. 2, pp. 177-192, Oct 2006.

[78] S. Mönchgesang, N. Strehmel, S. Schmidt, L. Westphal, F. Taruttis, E. Müller, S. Herklotz, S. Neumann, and D. Scheel, "Natural variation of root exudates in *Arabidopsis thaliana*-linking metabolomics and genomic data," *Scientific Reports*, vol. 6, pp. 29033, Jul 2016.

[79] T. Murashige, and F. Skoog, "A revised medium for rapid growth and bioassay with tobacco tissue cultures," *Physiologia Plantarum*, vol. 15, no. 3, pp. 473-497, Jul 1962.

[80] P. Mattila, and J. Kumpulainen, "Determination of free and total phenolic acids in plant-derived foods by HPLC with diode-array detection," *Journal of Agricultural and Food Chemistry*, vol. 50, no. 13, pp. 3660-3667, May 2002.

[81] V. Nour, I. Trandafir, and S. Cosmulescu, "HPLC determination of phenolic acids, flavonoids and juglone in walnut leaves," *Journal of Chromatographic Science*, vol. 51, no. 9, pp. 883-890, Oct 2013.

[82] M. Friendly, "Corrgrams: exploratory displays for correlation matrices," *The American Statistician*, vol. 56, no. 4, pp. 316-324, Aug 2002.

[83] J.M. Mutuku, and A. Nose, "Changes in the contents of metabolites and enzyme activities in rice plants responding to *Rhizoctonia solani* Kuhn infection: activation of glycolysis and connection to phenylpropanoid pathway," *Plant and Cell Physiology*, vol. 53, no. 6, pp. 1017-1032, Jun 2012.

[84] C.E. Bita, and T. Gerats, "Plant tolerance to high temperature in a changing environment: scientific fundamentals and production of heat stress-tolerant crops," *Frontiers in Plant Science*, vol. 4, pp. 273, Jul 2013.

[85] V. Doubnerova, and H. Ryslava, "What can enzymes of C4 photosynthesis do for C3 plants under stress?," *Plant Science*, vol. 180, no. 4, pp. 575-583, Apr 2011.

[86] N. Dudareva, S. Andersson, I. Orlova, N. Gatto, M. Reichelt, D. Rhodes, W. Boland, and J. Gershenzon, "The nonmevalonate pathway supports both monoterpene and sesquiterpene formation in snapdragon flowers," *Proceedings of the National Academy of Sciences of the United States of America*, vol. 102, no. 3, pp. 933-938, Jan 2005.

[87] T. Vogt, "Phenylpropanoid Biosynthesis," *Molecular Plant*, vol. 3, no. 1, pp. 2-20, Jan 2010.

[88] C.M. Fraser, and C. Chapple, "The phenylpropanoid pathway in Arabidopsis," *The Arabidopsis Book*, vol. 9, pp. e0152, Dec 2011.

[89] C. Lillo, U.S. Lea, and P. Ruoff, "Nutrient depletion as a key factor for manipulating gene expression and product formation in different branches of the flavonoid pathway," *Plant, Cell and Environment*, vol. 31, no. 5, pp. 587-601, May 2008.

[90] C. Funk, and P.E. Brodelius, "Phenylpropanoid metabolism in suspension cultures of *Vanilla planifolia* Andr. : IV. Induction of vanillic acid formation," *Plant Physiology*, vol. 99, no. 1, pp. 256-262, May 1992.

[91] A. Wagner, Y. Tobimatsu, L. Phillips, H. Flint, B. Geddes, F. Lu, and J. Ralph, "Syringyl lignin production in conifers: Proof of concept in a Pine tracheary element system," *Proceedings of the National Academy of Sciences of the United States of America*, vol. 112, no. 19, pp. 6218-6223, May 2015.

[92] G.M. Trabucco, D.A. Matos, S.J. Lee, A.J. Saathoff, H.D. Priest, T.C. Mockler, G. Sarath, and S.P. Hazen, "Functional characterization of cinnamyl alcohol dehydrogenase and caffeic acid O-methyltransferase in *Brachypodium distachyon*," *BMC Biotechnology*, vol. 13, pp. 61, Jul 2013.

[93] J. Kontturi, R. Osama, X. Deng, H. Bashandy, V.A. Albert, and T.H. Teeri, "Functional characterization and expression of GASCL1 and GASCL2, two anther-specific chalcone synthase like enzymes from *Gerbera hybrida*," *Phytochemistry*, vol. 134, pp. 38-45, Feb 2017.

[94] S. Besseau, L. Hoffmann, P. Geoffroy, C. Lapierre, B. Pollet, and M. Legrand, "Flavonoid accumulation in Arabidopsis repressed in lignin synthesis affects auxin transport and plant growth," *The Plant Cell*, vol. 19, no. 1, pp. 148-162, Jan 2007.

LIST OF PUBLICATIONS

[1] V. Kumar, A. Bansal, and R.S. Chauhan, "Modular design of picroside-II biosynthesis deciphered through NGS transcriptomes and metabolic intermediates analysis in naturally variant chemotypes of a medicinal herb, *Picrorhiza kurroa*," *Frontiers in Plant Science*, vol. 8, pp. 564, April 2017.

[2] V. Kumar, R.S. Chauhan, and C. Tandon, "Biosynthesis and therapeutic implications of Iridoid glycosides from Picrorhiza genus: the road ahead," *Journal of Plant Biochemistry and Biotechnology*, vol. 26, no. 1, pp. 1-13, Jan 2017.

[3] V. Kumar, N. Sharma, H. Sood, R.S. Chauhan, "Exogenous feeding of immediate precursors reveals synergistic effect on picroside-I biosynthesis in shoot cultures of *Picrorhiza kurroa* Royle ex Benth," *Scientific Reports*, vol. 6, pp. 29750, Jul 2016.

[4] V. Kumar, K. Shitiz, R.S. Chauhan, H. Sood, and C. Tandon, "Tracking dynamics of enzyme activities and their gene expression in *Picrorhiza kurroa* with respect to picroside accumulation," *Journal of Plant Biochemistry and Biotechnology*, vol. 25, no. 2, pp. 125-132, Apr 2016.

[5] V. Kumar, N. Sharma, K. Shitiz, T.R. Singh, C. Tandon, H. Sood, and R.S. Chauhan, "An insight into conflux of metabolic traffic leading to picroside-I biosynthesis by tracking molecular time course changes in a medicinal herb, *Picrorhiza kurroa*," *Plant Cell, Tissue and Organ Culture*, vol. 123, no. 2, pp. 435-441, Nov 2015.

[6] V. Kumar, V. Kumar, R.S. Chauhan, H. Sood, and C. Tandon, "Cost effective quantification of picrosides in *Picrorhiza kurroa* by employing response surface methodology using HPLC-UV," *Journal of Plant Biochemistry and Biotechnology*, vol. 24, no. 4, pp. 376-384, Oct 2015.

[7] N. Sharma, V. Kumar, R.S. Chauhan, and H. Sood, "Modulation of picroside-I biosynthesis in grown elicited shoots of *Picrorhiza kurroa* in vitro," Journal of Plant Growth Regulation, vol. 35, no. 4, pp. 965-973, Dec 2016.

CONFERENCES/WORKSHOPS

[1]   V. Kumar, and R.S. Chauhan, Oral Presentation on "Biosynthetic Pathways Discovery for Major Medicinal Compounds in Endangered Medicinal Herbs of North-Western Himalayas" at International conference on "*Biodiversity: Current Scenario and Future Strategies*" sponsored by "State Council for Science, Technology and Environment Himachal Pradesh" held at St. Bede's College, Shimla, October 6-8, 2016.

[2]   V. Kumar, and R.S. Chauhan, Presented a poster on 'Exogenous feeding of cinnamic acid and catalpol directs metabolic flux towards Picroside-I biosynthesis in a medicinal herb, *Picrorhiza kurroa* Royle Ex Benth' at INDO-US Workshop on "Cell Factories", held at IIT Bombay, Mumbai, March 18-20, 2016.

[3]   Participated in an ICMR sponsored National Workshop-cum-Training Programme on "Standardization of Medicinal Plants and their Products", held at Shoolini University, Solan, March 22-24, 2015.

[4]   V. Kumar, R.S. Chauhan, and C. Tandon, Presented a poster on 'Optimization of picrosides extraction from *Picrorhiza kurroa* using HPLC-UV by employing response surface methodology' at 7th Annual Convention of ABAP and International Conference on Plant Biotechnology, Molecular Medicine and Human Health, held at Delhi University (South Campus), New Delhi, October 18-20, 2013.